

https://dspace.org/

An evaluation of the Upper Zone sequence in core NP1 and its regional significance to the northern limb of the Bushveld Igneous Complex

Masunte, Tumelo

2020
https://hdl.handle.net/10539/31074

Downloaded from a DSpace repository. https://dspace.org/



An evaluation of the Upper Zone sequence in core NP1 and its regional significance to the northern limb of the Bushveld Igneous Complex

By:

Tumelo Masunte

1784139

A research report submitted to the Faculty of Science, University of the Witwatersrand, Johannesburg, In partial fulfilment of the requirements for the degree of Master of Science

October 2020

Supervisors: Prof. Judith Kinnaird and Dr. Marina Yudovskaya

Declaration

I, Tumelo Masunte, declare that this thesis is for completion of a MSc. Economic Geology degree at the University of the Witwatersrand, School of Geoscience. This is my own work and assistance was given by my supervisors. It is the first work at this area or specific borehole and was not copied nor has it been submitted before for any qualification at any institution prior to this. The core was logged and sampled at the Council for Geoscience core library.

Signed on: 05 October 2020

By: Tumelo Masunte

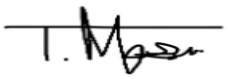

Dedication

This thesis and the MSc. Degree in general is dedicated to my late Father, Lebetla James Masunte. Passed on: 26 November 2018.

Acknowledgements

I would like to thank Professor Judith Kinnaird and Dr Marina Yudovskaya for allowing me an opportunity to work on this project and for their assistance throughout as supervisors. I then acknowledge and thank Mr Sifiso Bucibo from the Council for Geoscience for giving permission to work on and sample the NP1 core from the core library. Mr Majola and Mr Samuel Tshabalala are highly appreciated and acknowledged for thin sections preparation on time. Mr Marlin Patchappa from the School of Geosciences Earth lab played a huge role with regards to XRF (X-ray Fluorescence) whole rock analyses, thank you. I would also like to thank Miss Henriette Ueckermann for her assistance and hospitality at the LA-MC-ICPMS laboratory at the University of Johannesburg. Lastly, I would like to thank SRK Consulting for sponsoring the entire Master's Degree and for the support during the write up of this research report while working.

Abstract

The Bushveld Complex was emplaced by repeated injection of magma ranging in volume from small to large pulses (Eales and Cawthorn, 1996). It consists of five limbs, namely; northern limb, eastern limb, western limb, far western limb as well as south-eastern limb and is variably enriched with ores ranging from chromium and platinum group elements (PGE) to vanadium (Eales and Cawthorn, 1996). The Complex extends north of the Hout River Shear Zone (van der Merve, 1976; Vermark and van der Merve, 1986) that was recently proven at the Waterberg Project area (Huthmann *et al*., 2016; Kinnaird *et al*., 2017).

This research was proposed to further prove the existence of the Bushveld Complex north of the Hout River Shear Zone. The task was to evaluate how the Non Parella sequence (NP1) correlates with the known northern limb (south of the Hout River Shear Zone), the Villa Nora fragment and the Waterberg sequence as well as its affiliation with the Bushveld Upper Zone. Furthermore, Huthmann *et al* (2017) stated that there is a lack of stratigraphic connection between rocks north and rocks south of the Hout River Shear Zone and this research aimed to evaluate this.

The 2500 m deep NP1 borehole was drilled by Rand Mines Ltd in 1991 on the Non Parella farm located north of the Hout River Shear Zone and west of the Waterberg Project area. The entire core was logged as the Upper Zone by the Rand Mines exploration team. To further evaluate the NP1 sequence, core logging and sampling were carried out in April 2017 at the Council for Geoscience core library. Core logging was followed by the petrographic description of thin sections and whole rock XRF analysis undertaken at the University of the Witwatersrand in 2017. Sr isotopic analysis of fresh, unaltered plagioclase grains using laser ablation multi-collector inductively coupled plasma mass spectrometry (LA-MC-ICPMS) was also performed at the University of Johannesburg in June 2018.

The stratigraphy of the NP1 core is made up of Waterberg sedimentary rocks and dolerite sills from surface to a depth of 1312 m below surface. From 1312 m to 2158 m further below surface is the fine-grained to porphyritic gabbronorite package. The lower unit of the NP1 sequence from 2158 m to end of hole at 2500 m consists of magnetite and olivine-rich gabbroic rocks. These olivine-rich gabbroic rocks are olivine-bearing gabbro, plagioclase-phyric (plagio-phyric) olivine gabbro, and olivine gabbro to troctolite, and the section includes a 3.5 m interlayer of mottled anorthosite. The gabbronorite section includes a number of subvertical feldspar-quartz-magnetite veins and feldspar veins while the zone of the transitional contact between gabbronorite and olivine gabbro includes metasedimentary xenoliths.

NP1 whole rock geochemistry does not reveal the upwards Si, Fe, and P enrichment expected for the Bushveld Upper Zone as identified by von Gruenewaldt (1973) in the eastern and western limbs and by Ashwal *et al* (2005) in the northern limb. It rather reveals an opposite trend consistent with the visible increase in magnetite, fayalitic olivine and apatite contents towards the lower part of the NP1 intersection within the gabbroic rocks. The trace and major element compositions of NP1 gabbronorite appeared to be sharing similar characteristics with the compositions of low and high Ti volcanic rocks of the Dullstroom Formation (Buchanan *et al*., 1999) indicating that the NP1 gabbronorite package could belong to the Dullstroom Formation and not the Upper Zone as it was initially logged by the Rand Mines exploration team.

Sr isotope analysis of plagioclase in situ was carried out to verify the NP1 sequence affiliation with the Upper Zone. The initial Sr ratios of plagioclase from NP1 gabbronorite range from 0.7042 to 0.7066 and are not consistent with the Upper Zone signature of 0.7063 to 0.7079 in the northern limb (Mangwegape *et al*., 2016) and 0.7065 to 0.7075 at the Waterberg Project area (Huthmann *et al*., 2017). In contrast, the initial Sr isotope ratios of plagioclase from NP1 olivine-rich gabbroic rocks,

ranging from 0.7064 to 0.7073, are consistent with an origin from the Upper Zone melts. This interpretation is also supported by the elevated while variable abundances of apatite, magnetite, and olivine within the NP1 gabbroic rocks that is consistent with the Upper Zone rock compositions elsewhere in the northern limb and the rest of the Bushveld Complex.

Field relations between the Bushveld Complex and Rooiberg Group whereby the unconformable emplacement of the Rustenburg Layered Suite (RLS) cross-cut the Rooiberg Group, specifically the Damwal and Dullstroom Formations, across the Bushveld Complex (Buchanan *et al*., 2004: Buchanan, 2006) provides more evidence that the NP1 gabbronorite package indeed belong to the Rooiberg Group. Dullstroom Formation rocks form the roof of the RLS in the NP1 sequence. The intrusive relationships between the RLS and its roof are supported by evidence of metamorphism within the NP1 gabbronorite section that include the presence of recrystallised sieve-texture porphyroblasts of clinopyroxene and phlogopite as well as granoblastic texture and metamorphic associations of hornfels.

Considering the analytical results from this research and evidence from literature, the NP1 borehole intersected an earlier unseen top contact (at 2158 m) of the Upper Zone with the metamorphosed rocks of the Dullstroom Formation. This correlation is consistent with the similarities in the mineral assemblages, the similar whole rock geochemical compositions, the identical Sr isotope composition of plagioclase, evidence of metamorphism and the occurrence of sedimentary xenoliths in the up-section of the NP1 core. The NP1 sequence further confirms the existence of the Bushveld extensive magmatic basin north of the Hout River Shear Zone. The absence of magnetitite layers at the NP1 sequence favours a provisional stratigraphic connection rather with the Waterberg Project area (located north of the Hout River Shear Zone) than with the Villa Nora sequence and the northern limb (both located south of the Hout River Shear Zone) supporting an earlier hypothesis on a lack of stratigraphic continuity between RLS sequences north and south of the Hout River Shear Zone (Huthmann *et al*., 2017).

Table of Contents

Declaration i

Dedication ii

Acknowledgements iii

Abstract iv

List of Figures ix

List of Tables xi

Chapter 1 1

Introduction of the Bushveld Complex, background and aim of the project 1

1.1 Introduction of the Bushveld Complex 1

1.1.1 Introduction 1

1.1.2 Marginal Zone 3

1.1.3 Lower Zone 3

1.1.4 Critical Zone 3

1.1.5 Main Zone 3

1.1.6 Upper Zone 3

1.2 Background and aim of the project 4

1.3 Summary and conclusion 4

Chapter 2 5

The Northern limb 5

2.1 Introduction 5

2.2 "Extended northern limb" 5

2.3 Geology of the northern limb 5

2.4 Summary and conclusion 6

Chapter 3 7

The Upper Zone in the northern limb 7

3.1 Introduction 7

3.2 Bellevue 7

3.3 Villa Nora 8

3.3.1 Petrology of drill hole BH-2 and BH-5 from the Villa Nora segment 9

3.4 Waterberg Project area 10

3.5 Summary and conclusion 11

Chapter 4 12

Stratigraphy of NP1 core 12

4.1 Introduction 12

4.2 Method 12

4.3 Results 13
4.3.1 Gabbroic rocks 13
4.3.2 Mottled anorthosite 13
4.3.3 Gabbronorite rocks 14
4.3.4 Monzodiorites 14
4.3.5 Xenoliths 15
4.3.6 Veins 16
4.3.7 NP1 top-most sequence 17
4.4 Discussion and conclusion 17
Chapter 5 18
Petrography of NP1 core 18
5.1 Introduction 18
5.2 Method 18
5.3 Results 19
5.3.1 Olivine-rich gabbroic rocks 19
5.3.2 Mottled anorthosite 20
5.3.3 Olivine-free fine-grained gabbronoritic rocks 21
5.3.4 Monzodiorites 21
5.3.5 Veins 22
5.3.6 Xenoliths 23
5.4 Modal mineralogy versus depth 23
5.5 Discussion and conclusion 24
Chapter 6 26
Whole rock geochemistry 26
6.1 Introduction 26
6.2 Method 26
6.2.1 Sample preparation 26
6.2.2 Instrument 27
6.3 Results 28
6.3.1 Major elements 28
6.3.2 Trace elements 31
6.3.3 Ratios 33
6.4 Discussion and conclusion 34
Chapter 7 35
Sr isotope geochemistry 35
7.1 Introduction 35

7.2 Method 35
7.2.1 Sample preparation 35
7.2.2 Equipment 35
7.3 Results 36
7.4 Discussion and conclusion 37
Chapter 8 38
Discussion and Conclusion 38
8.1 Introduction 38
8.2 Discussion 38
8.2.1 Stratigraphic correlation between the Bushveld Complex and Rooiberg Group 38
8.2.2 Rock composition of the Dullstroom Formation 40
8.2.3 Whole rock geochemistry of the Dullstroom Formation 40
8.2.4 Sr Isotopes of the Bushveld Complex, Waterberg Project and Dullstroom Formation 42
8.2.5 A comparison of the NP1 Results with those of the northern limb, the Waterberg Project and the Dullstroom Formation 44
8.3 Conclusion 49
8.4 Limitations 51
8.5 Recommendations 51
List of References 52
Appendices 56
Appendix A: Hand specimen descriptions of the samples from core NP1 used in this thesis 56
Appendix B: Petrography and modal mineralogy of selected samples from core NP1 69
Appendix C: NP1 Whole rock geochemistry results 86
Appendix D: NP1 Binary plots of SiO_2 against other major elements 90
Appendix E: NP1 Binary plots of MgO against other major elements 93
Appendix F: NP1 Sr and Rb isotope results 96
Appendix G: Low and High Ti Dullstroom Formation rocks major element data from literature (Buchanan *et al*., 1999) 101
Appendix H: Low and High Ti Dullstroom Formation rocks trace element data from literature (Buchanan *et al*., 1999) 102

List of Figures

Figure 1.1: Geological map of the Bushveld Complex showing various limbs (modified from Roelofse, 2010) 1
Figure 1.2: Stratigraphic and isotope summary showing the mineralogy variation, isotope compositions and the location of major unconformities of the Bushveld Complex (Kruger, 2005) 2
Figure 1.3: Local map showing Non Parella farm location respective to the northern lobe, Villa Nora segment and the Waterberg Project area which is represented by "Drill Holes" (modified from Huthmann *et al*., 2016) 4
Figure 2.1: Map showing the geology of the northern limb (Kinnaird *et al*., 2017) 6
Figure 3.1: Bellevue drill core stratigraphy log (Ashwal *et al*., 2005) 8
Figure 3.2: Diagrammatic section through the No.2 Olivine-apatite magnetitite on the Turflaagte farm coloured in pink (Grobler and Whitfield, 1970) 9
Figure 3.3: Stratigraphy of the Waterberg Project area (Kinnaird *et al*., 2017) 11
Figure 4.1: Stratigraphy of the NP1 sequence, from 1070 m to 2500 m 12
Figure 4.2: Photographs of gabbroic rocks, (a) Plagio-phyric olivine gabbro, (b) Olivine gabbro / olivine gabbro to troctolite 13
Figure 4.3: Mottled anorthosite, (a) Mottled anorthosite sample in core NP1 from a depth of 2376 m, (b) Mottled anorthosite interval, surrounded by a red rectangle, occurring in-between olivine gabbro 14
Figure 4.4: Photographs of gabbronorite rocks in NP1 core, (a) Olivine-free fine-grained gabbronorite cross-cut by coarse-grained feldspar-quartz-magnetite vein in the middle core sample, (b) Olivine-free fine-grained gabbronorite with phlogopite phenocrysts 14
Figure 4.5: Monzodiorite rocks within core NP1, (a) An interval of monzodiorite rocks within the core at approximately 2061 to 2066 m, (b) Sample showing a contact (in red) between monzodiorite on the left and fine-grained gabbronorite on the right 15
Figure 4.6: Xenoliths in NP1 core, (a) quartz-feldspathic xenolith, (b) Top-view of quartz-feldspathic xenolith, (c) shale to hornfels xenolith 15
Figure 4.7: Photographs of veins occurring in the NP1 core, (a) & (b) Coarse-grained feldspar-magnetite veins, (c) Plagioclase vein, (d) Granitic vein, (e) Coarse-grained feldspar-quartz-magnetite vein, (f) Feldspar vein, marked with a cross (X) 16
Figure 4.8: Photographs of the upper part of the NP1 core, (a) Contact between chill zone and Waterberg sedimentary rocks marked in red, (b) Waterberg Red Beds 17
Figure 5.1: Olympus BX41 petrographic microscope at the petrography laboratory, University of the Witwatersrand School of Geoscience, 2017 18
Figure 5.2: Modal percentage estimation scale guide, produced by Caracle Creek International Consulting Inc. 19
Figure 5.3: Photographs of olivine-rich gabbroic rocks in core NP1, (a) Olivine-bearing gabbro showing olivine, plagioclase and clinopyroxene, (b) Plagio-phyric olivine gabbro, (c) Olivine gabbro showing large elongated apatite crystals, (d) Olivine gabbro to troctolite showing subophitic texture. All images in crossed polarised light (XPL) 20
Figure 5.4: Photographs of mottled anorthosite in core NP1, (a) Sample 2374.9 showing plagioclase, magnetite and olivine, (b) Sample 2377.8 showing plagioclase and clinopyroxene. All images in XPL20
Figure 5.5: Photographs of olivine-free fine-grained gabbronorite rocks in core NP1, (a) Sample 1356.3 showing altered plagioclase crystals, (b) Sample 1541.5 showing phlogopite phenocrysts. All images in XPL 21

Figure 5.6: Photographs of samples representing monzodiorite rocks in core NP1, (a) Sample 2043, (b) Sample 2076.8 showing granophyre. All images in XPL 21
Figure 5.7: Photographs of veins in core NP1, (a) and (b) Coarse-grained feldspar-magnetite vein, (c) Coarse-grained feldspar-quartz-magnetite vein showing plagioclase crystals with lamellar twinning, (d) Feldspar vein showing hornblende crystals. All images in XPL 22
Figure 5.8: Photographs of xenoliths in core NP1, (a) Metamorphosed quartz-feldspathic xenolith, (b) Hornfels showing foliation. All images in XPL 23
Figure 5.9: Modal mineralogy against depth through core NP1 24
Figure 5.10: Modal composition of some NP1 gabbronorite and gabbroic samples plotted on the IUGS classification diagram for mafic and ultramafic rocks (modified after La Maitre, 2002) 25
Figure 6.1: Axiox max XRF machine (The analytical X-ray company, 2009) 27
Figure 6.2: Whole rock major elements against depth through core NP1, with plagioclase-magnetite veins and quartz-feldspathic xenoliths represented by green and blue horizontal lines respectively 29
Figure 6.3: Binary plots of SiO_2 vs other major elements [xenoliths = Quartz-feldspathic xenoliths, veins = Plagioclase-magnetite veins], (a) SiO_2 vs Fe_2O_3, (b) SiO_2 vs TiO_2, (c) SiO_2 vs P_2O_5 30
Figure 6.4: Binary plots of MgO vs other major elements [xenoliths = Quartz-feldspathic xenoliths, veins = Plagioclase-magnetite veins], (a) MgO vs Fe_2O_3, (b) MgO vs TiO_2, (c) MgO vs P_2O_5 ,(d) MgO vs Al_2O_3 30
Figure 6.5: Whole rock trace elements against depth through core NP1, with plagioclase-magnetite veins and quartz-feldspathic xenoliths represented by the green and blue horizontal lines respectively 32
Figure 6.6: Binary plots of Cr vs other trace elements [xenoliths = Quartz-feldspathic xenoliths, veins = Plagioclase-magnetite veins], (a) Cr vs Co, (b) Cr vs Ni, (c) Cr vs V, (d) Cr vs Pb 33
Figure 6.7: Element ratios against depth in core NP1 34
Figure 7.1: Laser Ablation Multi-collector ICPMS (LA-MC-ICPMS Laboratory, University of Johannesburg, 2018) 36
Figure 7.2: NP1 initial $^{87}Sr/^{86}Sr$ against depth 37
Figure 8.1: Generalised stratigraphic column of the Rooiberg Group as proposed by Schweitzer *et al* (1995). Adapted from Cheney and Twist (1991), Council for Geosciences, (1978), Eriksson *et al* (1994), and Schweitzer *et al* (1995). Scale in metres shows approximate thickness of units (from Buchanan *et al*., 1999) 38
Figure 8.2: Diagrams showing the emplacement of the Rustenburg Layered Suite , (a) Schematic north-south section in the Loskop Dam area showing the relationship between the Rooiberg Group, the underlying Pretoria Group (Transvaal Supergroup), and the intrusions o the Rustenburg and Lebowa Granite Suite. Modified after SACS (1980), Walraven (1982), Harmer and Sharpe (1985) and Schweitzer *et al* (1995) (from Lenhardt and Eriksson, 2012), (b) Reconstructed emplacement level of the Rustenburg Layered Suite (in green) for the eastern portion of the Bushveld Complex using the lithological and geochemical characteristics of the volcanic rocks of the Rooiberg Group (modified from Schweitzer *et al*., 1995) 39
Figure 8.3: Geological map showing locations of the Loskop dam and Stofberg area (modified from Roelofse, 2010) 40
Figure 8.4: Generalised geological map of the south-eastern portion of the Bushveld Complex after the Council for Geoscience (1978). Sampling locations for the analysed material are concentrated in areas 1 and 2 (from Buchanan *et al*., 1999) 41
Figure 8.5: Dullstroom Formation major elements plots, (a) Classification system for Dullstroom Formation volcanic rocks based on SiO_2 (wt. %) vs $Na_2O + K_2O$ (wt. %) after Le Bas *et al* (1986). (b) SiO_2 (wt. %) vs TiO_2 (wt. %) and, (c) Al_2O_3 (wt. %) vs P_2O_5 (wt. %) for volcanic units of the Dullstroom

Formation. High Ti rocks represented by asterisks, low Ti (filled diamonds), and high Mg felsic represented by filled triangles (all Figures from Buchanan *et al*., 1999) 41
Figure 8.6: Geological map showing the locations of borehole BV-1 and MO-1 (cropped from Roelofse, 2010) 42
Figure 8.7: Geology of the northern limb of the Bushveld Complex, (a) Map showing the Waterberg Project location. HRSZ = Hout River Shear Zone, PYF = Planknek-Ysterberg Fault, TML = Thabazimbi-Murchison Lineament. (b) Stratigraphy of the Waterberg Project area (from Kinnaird *et al*., 2017) .. 43
Figure 8.8: NP1 stratigraphy plotted against olivine, apatite and magnetite modal mineralogy which shows an increase in concentration of these minerals from 2158 m to the base of the core (2 500 m) 45
Figure 8.9: Thin section image of a metamorphosed quartz-feldspathic xenolith showing a granoblastic texture, sample 1844.4 45
Figure 8.10: Major element comparison plots of NP1 gabbronorite, Upper Zone olivine-rich gabbro, mottled anorthosite and monzodiorite against low and high Ti Dullstroom rocks, (a) SiO_2 vs (Na_2O + K_2O), (b) SiO_2 vs MgO, (c) SiO_2 vs Fe_2O_3, (d) SiO_2 vs P_2O_5 47
Figure 8.11: Trace element comparison plots of NP1 gabbronorite, Upper Zone olivine-rich gabbro, mottled anorthosite and monzodiorite against low and high Ti Dullstroom rocks, (a) Cr vs Co, (b) Cr vs Ni, (c) Cr vs V 47
Figure 8.12: NP1 initial $^{87}Sr/^{86}Sr$ against depth in comparison with the initial Sr ratio ranges of Dullstroom Formation represented by a green arrow (0.7052-0.7083, Buchanan *et al*., 2004), Waterberg Project Upper Zone represented by an orange arrow (0.7065-0.7075, Huthmann *et al*., 2017) and northern limb Upper Zone represented by a blue arrow (0.7065-0.7079, Mangwegape *et al*., 2016) 48
Figure 8.13: NP1 stratigraphic diagram illustrating a contact between Dullstroom Formation rocks and the Bushveld Upper Zone 50

List of Tables

Table 1.1: Summary of the RLS U-Pb age dating results (Zeh *et al*., 2015) 2
Table 5.1: Modal composition of some gabbronorites and gabbroic NP1 samples 25
Table 6.1: Major element concentration ranges within NP1 gabbronorite and olivine-rich gabbroic rocks 28
Table 6.2: Trace element concentration ranges within NP1 gabbronorites and olivine-rich gabbroic rocks 31
Table C.1: Trace element data 86
Table C.2: Major element data 88
Table G.1: High Ti Dullstroom Formation rocks major element compositions determined by XRF and INAA (Instrumental Neutron Activation Analysis) (Buchanan *et al*., 1999) 101
Table G.2: Low Ti and high Mg Dullstroom Formation rocks major element determined by XRF and INAA (Instrumental Neutron Activation Analysis) (Buchanan *et al*., 1999) 101
Table H.1: High Ti Dullstroom Formation rocks trace element compositions determined by XRF and INAA (Instrumental Neutron Activation Analysis) (Buchanan *et al*., 1999) 102
Table H.2: Low Ti and high Mg Dullstroom Formation rocks trace element determined by XRF and INAA (Instrumental Neutron Activation Analysis) (Buchanan *et al*., 1999) 103

Chapter 1

Introduction of the Bushveld Complex, background and aim of the project

1.1 Introduction of the Bushveld Complex

1.1.1 Introduction

The Bushveld Complex intruded the sedimentary sequence of the Transvaal Supergroup and was emplaced by repeated injection of magma ranging in volume from small to large pulses (Eales and Cawthorn, 1996). This emplacement by repeated injection of magma is supported by breaks in initial Sr isotopic ratio (Kruger, 1994), as well as textures showing evidence of partial resorption of earlier crystallising phases (Eales and Cawthorn, 1996). The Complex consists of five limbs, namely; northern, eastern, western, far western and south-eastern/Bethal limbs (Figure 1.1; Roelofse, 2010).The Complex is variably ore-enriched ranging from chromium in the Lower and Critical Zones, platinum group elements (PGE) in the Critical Zone and vanadium in the Upper Zone (Eales and Cawthorn, 1996).

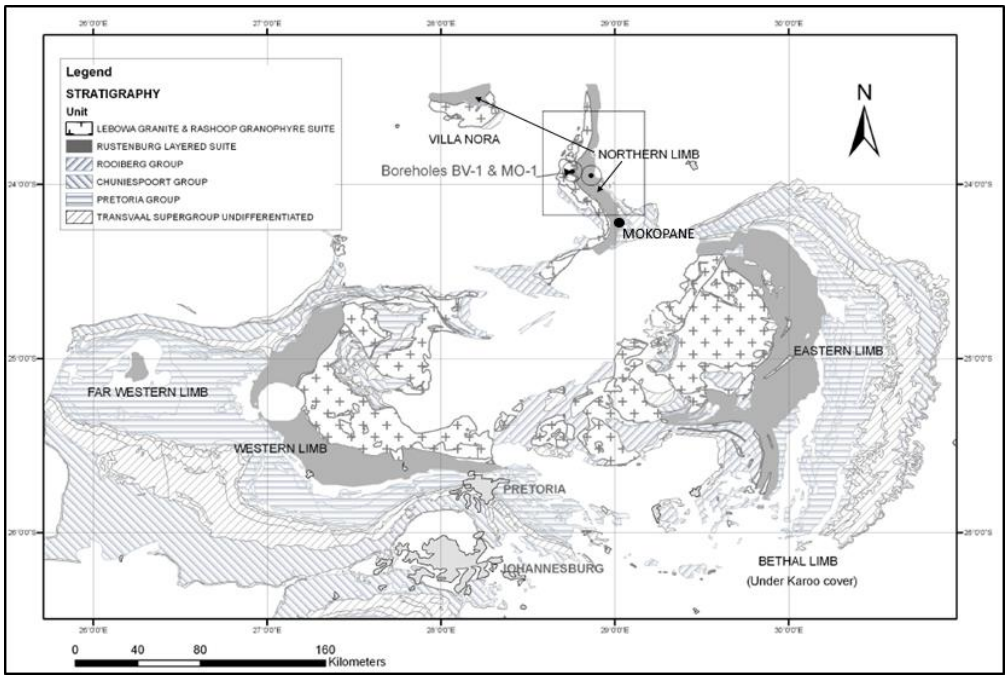

Figure 1.1: Geological map of the Bushveld Complex showing various limbs (modified from Roelofse, 2010)

van der Merwe (1978) indicated that the Bushveld Complex occupies an area of approximately 66 000 km ^{2}. However, with further research in the most recent years, Finn *et al* (2015) identified that the layered mafic rocks of the Complex cover an aerial extent of about 90 000 km^2 with lithologies ranging between the extremes of dunite and pyroxenite to anorthosite and pure oxide layers. The South African Committee for Stratigraphy (SACS) recommended that the Bushveld Complex be subdivided into the following lithostratigraphic units: Lebowa Granite Suite, Rashoop Granophyre Suite, and Rustenburg Layered Suite (van der Merwe, 1978). The Rustenburg Layered Suite (RLS) has an age of 2.06 Ga, and its chronological framework is represented in Table 1.1 by eight samples from the eastern limb and one sample from the western limb (Zeh *et al.*, 2015). Kruger (2005) showed the generalised stratigraphic sections of the Bushveld Complex (Figure 1.2) namely; Lower, Critical, Main and Upper Zones, together with initial Sr isotope compositions. The Marginal Zone is not included in the diagram.

Table 1.1: Summary of the RLS U-Pb age dating results (Zeh *et al*., 2015)

Sample	RLS Unit	Rock	Weight mean $^{207}Pb/^{206}Pb$ age (Ma)
Upper Zone			
MH1	Upper Zone	Mgt-rich ferro-gabbro	2055.81
Lower Main Zone			
GC	Lower Main Zone	Mottled anorthosite	2055.01
Upper Critical Zone			
PGMT	Merensky Reef	Pegmatoidal pyroxenite	2055.09
FW-PX	Upper Critical Zone	Pyroxenite	2054.89
UG2K	Upper Critical Zone	Pegmatoidal pyroxenite	2055.32
Lower Critical Zone			
JGL	Lower Critical Zone	Cr-bearing pyroxenite	2055.40
CH-12-1	Lower Critical Zone	Cr-rich pyroxenite	2055.65
Marginal Zone			
CH12-3	Marginal Zone	Norite (chill zone)	2055.68
CH12-26	Marginal Zone	Pyroxenite (chill zone)	2055.91

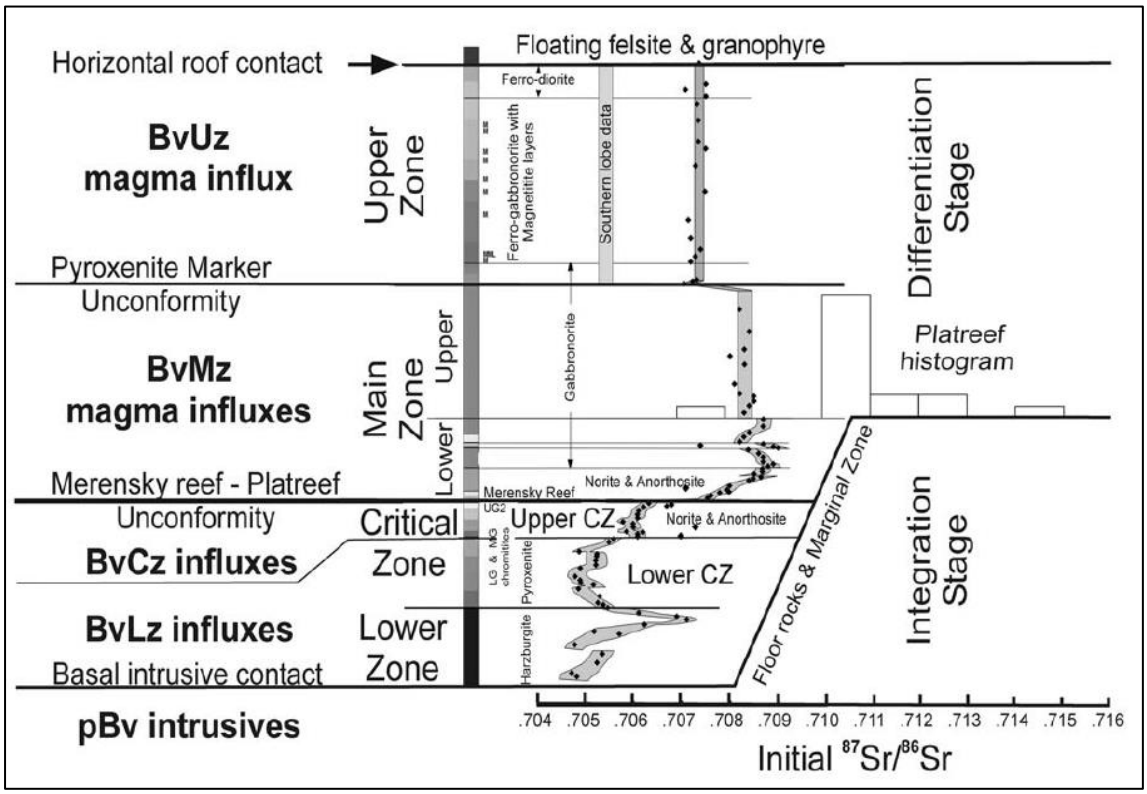

Figure 1.2: Stratigraphic and isotope summary showing the mineralogy variation, isotope compositions and the location of major unconformities of the Bushveld Complex (Kruger, 2005)

1.1.2 Marginal Zone

The Marginal Zone is dominated by layered and unlayered basic rocks found towards the margin of the Rustenburg Layered Suite (van der Merwe, 1978). These are noritic rocks that may represent composite sills or distal facies of evolved magmas from within the chamber. The sequence is up to 800 m thick and the noritic rocks of the Marginal Zone encircle most of the Bushveld Complex (Eales and Cawthorn, 1996).

1.1.3 Lower Zone

Layered rocks in the Lower Zone occur below a position in the sequence where chromite becomes a major cumulus phase (van der Merwe, 1978). Chromitite layers from the Lower Zone are only known from the northern limb (Vermaak and von Gruenewaldt, 1986). Teigler (1990) described an 800 m thick core of Lower Zone from Union Section Mines in the western limb as an olivine-and orthopyroxene-rich sequence with accessory chromite and variable amounts of intercumulus plagioclase, biotite, and clinopyroxene. In the eastern limb, Cameron (1978) divided the Lower Zone into basal feldspathic pyroxenite, with minor harzburgite, lower pyroxenite, harzburgite, and upper pyroxenite.

1.1.4 Critical Zone

At the base of the Critical Zone, there is an increase in the amount of intercumulus plagioclase as well as the appearance of layers whereby chromite is a major cumulus phase (van der Merwe, 1978). The Lower and Upper Critical Zones of the main eastern and western limbs hold the largest deposits of chromite in the world (Vermaak and von Gruenewaldt, 1986). The Lower Group (LG) of chromitite layers occur within the pyroxenite unit of the Lower Critical Zone, while the Upper Group (UG) of chromitite layers occur within the anorthositic to noritic Upper Critical Zone (Vermaak and von Gruenewaldt, 1986). The Middle Group (MG) of chromitite layers occur at the pyroxenite-anorthosite intersection between the LG and UG. The UG2 chromitite layer and Merensky Reef in the Upper Critical Zone contain significant amounts of PGE (Vermaak and von Gruenewaldt, 1986).

1.1.5 Main Zone

The boundary between the Critical Zone and Main Zone is difficult to determine by relying on mineralogy only. The boundary has been taken at the top of the giant mottled anorthosite, capping the Bastard cyclic unit (von Gruenewaldt, 1973; Mitchell, 1990). The Main Zone mainly comprise norite and gabbronorite and has a vast lithological diversity of cumulates devoid of olivine with chromian spinel, augite, pigeonite and anorthosites (main mottled and upper mottled anorthosites). The upper mottled anorthosite is not identified in the western limb (Eales and Cawthorn, 1996).

von Gruenewaldt (1973) subdivided the Main Zone into subzone A, B, and C In the eastern limb. Subzone B, in the centre, consists of pigeonite and separates subzone A and C with primary orthopyroxene-bearing gabbronorite. Mitchell (1990) separated the Lower Main Zone and the Upper Main Zone by a pyroxenite marker, which was indicative of primary pigeonite being replaced by primary orthopyroxene. Close to this level, a break in the Sr isotopic ratio is identified (Mitchell, 1990).

1.1.6 Upper Zone

Molyneux (1970) and von Gruenewaldt (1973) took the base of the Upper Zone at the appearance of magnetite as a major cumulus phase in the sequence. The appearance of magnetite and magnetitite layers provided an ideal base for mapping the boundary between the Main Zone and the Upper Zone in the northern limb (Eales and Cawthorn, 1996) and it differentiates the Upper Zone from the other Zones of the Rustenburg Layered Suite. The South African Committee for Stratigraphy (1980) subdivided the lithology of the Upper Zone into subzone A, made up of magnetite gabbro, ferrogabbro, and anorthosite, subzone B comprising ferrian olivine at the base followed by anorthosite

and magnetite ferrogabbro and subzone C consisting of cumulus apatite at the base. In the eastern limb, Molyneux (1970) subdivided the Upper Zone into four units, subzone A, B, C, and D, with the topmost subzone D consisting of ferrodiorite.

1.2 Background and aim of the project

The northern limb extends from the Ysterberg Planknek Fault to the Hout River Shear Zone (van der Merwe, 1976; Vermaak and van der Merwe, 1986; Kinnaird, 2005b). Since it has been confirmed that the Bushveld lithologies continue north of the Hout River Shear Zone (Kinnaird *et al*., 2017), this project aimed to evaluate how the NP1 sequence correlates with the Bellevue, Villa Nora and Waterberg sequences and its affiliation with the general stratigraphy of the Upper Zone elsewhere within the Bushveld Complex. The findings will therefore contribute to better understand the stratigraphy of the area. Core logging, petrographical description, whole rock geochemistry and initial Sr isotope analysis of plagioclase grains were carried out on the NP1 core, drilled by Rand Mines Ltd in 1991 at Non Parella farm (Figure 1.3; modified from Huthmann *et al*., 2016).

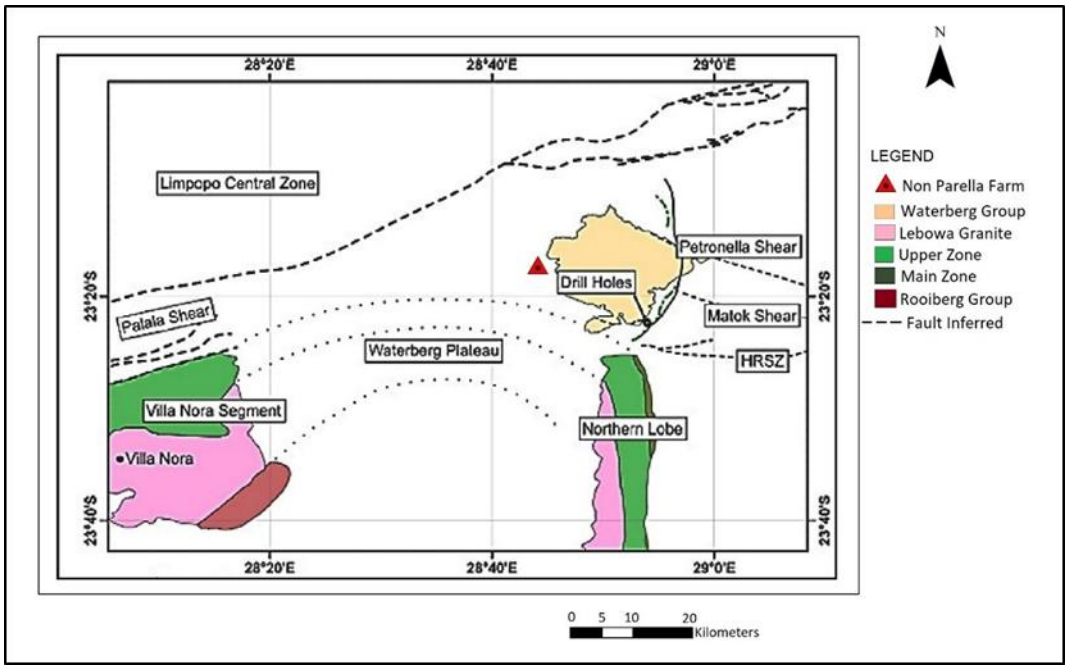

Figure 1.3: Local map showing Non Parella farm location respective to the northern lobe, Villa Nora segment and the Waterberg Project area which is represented by "Drill Holes" (modified from Huthmann *et al*., 2016)

1.3 Summary and conclusion

The entire NP1 core was logged as the Upper Zone by the Rand Mines exploration team. Detailed core logging, petrographical analysis, whole rock geochemistry and Sr isotope analysis were undertaken as part of this research to confirm the stratigraphy of the NP1 core and its affiliation to the Upper Zone of the northern limb, Villa Nora sequence and Waterberg sequence. As a result, this project focused on the Upper Zone north of the northern limb and the Hout River Shear Zone.

Chapter 2

The Northern limb

2.1 Introduction

The northern limb of the Bushveld Complex is exposed over a strike length of approximately 100 km from an estimated 30 km southwest of Mokopane town to 25 km north of Gilead (Figure 1.1). The total areal extent of the layered mafic cumulate rocks on the northern limb was estimated at 7 275 km^2 (van der Merwe, 1978). Some workers, such as Finn *et al* (2015) and Huthmann *et al* (2016) included a 320 km^2 exposure of layered mafic rocks, "extended northern limb", north of the Hout River Shear Zone as part of the northern limb. Structurally, the northern limb is separated from the rest of the Bushveld Complex by the east-northeast, west-southwest (ENE-WSW) trending Thabazimbi-Murchison Lineament (TML). The TML is a major tectonic boundary in South Africa formed by the collision of the Pietersburg and Kaapvaal terranes around 2.7 Ga (Kinnaird and McDonald, 2005). It may have behaved as a dyke-like feeder for the magmas or as a barrier between the northern limb and the rest of the Bushveld, during the intrusion of the Bushveld Complex at 2.06 Ga, allowing the northern limb to develop separately (Kinnaird and McDonald, 2005).

2.2 "Extended northern limb"

The Bushveld Complex covers an estimated areal extent of approximately 65 000 km^2 (Eales and Cawthorn, 1996). However, recent geophysical studies (Finn *et al*., 2015) and drilling projects by Platinum Group Metals Ltd (PTM Ltd) revealed the possibility that the intersected ultramafic-mafic rocks, extending for approximately 24 km north of the Hout River Shear Zone, belong to the Bushveld Complex and could increase the total area to approximately greater than 90 000 km^2. This succession has been proven to have a Bushveld Intrusion age of 2.06 Ga (Huthmann *et al.,*2016) and consists of a basal ultramafic sequence, troctolite-gabbronorite-anorthosite sequence and the Upper Zone (Kinnaird *et al*., 2017).

2.3 Geology of the northern limb

An important feature of the northern limb is the transgressive nature of the ultramafic-mafic sequence across successively older basement rocks towards the north, a point recognised by Hall (1932). Northwards from Mokopane, Bushveld rocks rest upon successively older strata of the Pretoria Group, followed by Banded Iron Formation (BIF) and dolomites of the Chuniespoort Group, and eventually onto Archaean Granitic basement rocks (Van der Merwe, 1976; Cawthorn *et al*., 1985). Some key elements of the stratigraphy within the Bushveld Complex such as the pyroxenite marker and the whole of the Lower Critical Zone that can be identified and traced across the western and eastern limbs, are absent in the northern limb (McDonald *et al*., 2017). Similarly, the northern limb has its unique stratigraphic markers such as the thick zone of troctolite and olivine gabbronorite in the Main Zone, which is not recognised in the eastern and western limbs (McDonald *et al.*, 2017).

With regards to the stratigraphy of the northern limb, van der Merwe (1976) regarded the Lower Zone to be restricted to satellite bodies cutting Archean granite. However, Yudovskaya *et al* (2013) confirmed the existence of an 800 m thick Lower Zone beneath the Platreef. This ultramafic sequence consists of dunite-harzburgite-pyroxenite cycles with sporadic chromite seams and contains one of the most magnesian-rich olivine compositions identified in the entire Bushveld Complex, with a magnesium number of 91 (Yudovskaya *et al*., 2013).

The Platreef is the major mineralised horizon in the northern limb (Lee, 1996) and the stratigraphic equivalent of the Critical Zone in other limbs (Yudovskaya *et al*., 2017). It is a composite body of geochemically distinct mafic-ultramafic sills, dominantly of feldspathic pyroxenites, which are variably

mineralised in PGE, nickel, and copper between footwall and Main Zone (Kinnaird *et al*., 2005a). The Platreef may be more than 500 m thick in areas where interlayers of metasedimentary rocks of the older Transvaal are incorporated (Yudovskaya *et al*., 2017).

The Main Zone of the northern limb is 2200 m thick and overlies the Platreef (van der Merwe, 1978). The lithology of the Main Zone is dominated by pyroxenites, anorthosite, and gabbronorites with lesser norites, especially towards the base. van der Merwe (1978) mapped a greater than 100 m thick sequence of troctolites for about 35 km along strike. This distinctive sequence occurs 1100 m from the base and is unique to the northern limb (van der Merwe, 1978).

The Upper Zone is transgressive, resting on the Main Zone in the south but on the Archean footwall in the far north of the exposed northern limb (Figure 2.1; Kinnaird *et al*., 2017). The appearance of magnetite and apatite distinguish the Upper Zone from the Main Zone (Kinnaird *et al*., 2017). The 1188 m thick Bellevue drill core is dominated by magnetite-rich olivine gabbro and olivine ferrodiorite, with minor gabbro/norite, plagioclase-magnetite cumulates, magnetite, pyroxenite, and anorthosite (Ashwal *et al*., 2005).

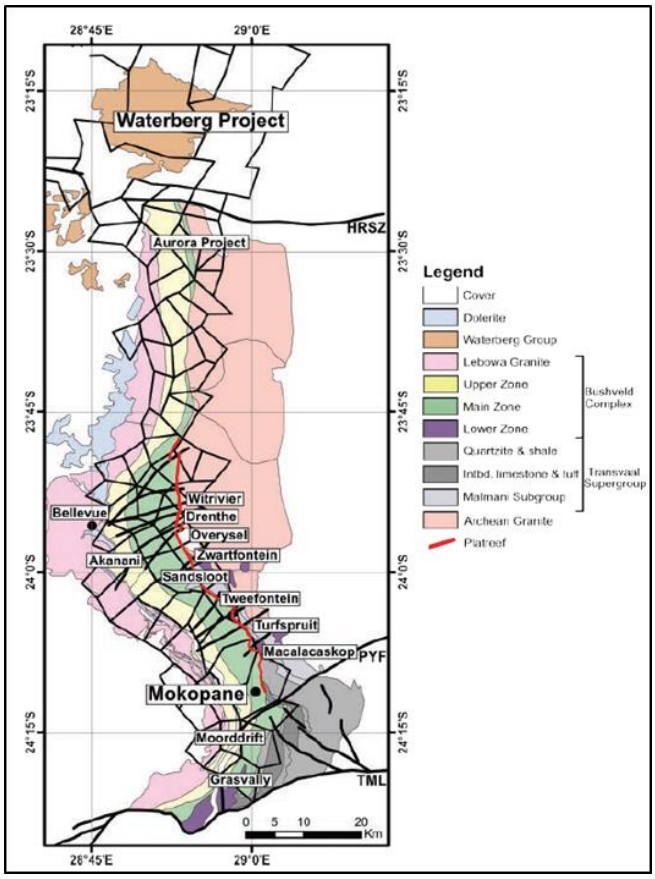

Figure 2.1: Map showing the geology of the northern limb (Kinnaird *et al*., 2017)

2.4 Summary and conclusion

The northern limb of the Bushveld Complex is a different entity to the other limbs. Its separation from the rest of the Bushveld Complex by the Thabazimbi-Murchison Lineament (TML), the presence of the "extended northern limb" and its lithological differences makes it unique in comparison to other limbs. With regards to the lithological sequence, the Upper Zone is identified by the appearance of magnetite and apatite, and this is discussed further in the next chapter.

Chapter 3

The Upper Zone in the northern limb

3.1 Introduction

In the northern limb, the Upper Zone is transgressive and rests on the Main Zone in the south but rests on the Archean footwall in the far north of the exposed northern limb (Kinnaird *et al*., 2017). Majority of the research on the Upper Zone was done by von Gruenewaldt and co-authors (e.g. Molyneux, 1974). von Gruenewaldt (1973) indicated the base of the Upper Zone to be characterised by the appearance of cumulus magnetite and magnetitite layers in some areas. The Upper Zone is approximately 2 km thick and comprise anorthosite and leucogabbro, with variable amounts of pyroxenes and olivine, magnetite and apatite, as well as ilmenite (Eales and Cawthorn, 1996).

According to Eales and Cawthorn (1996), the Upper Zone has three subzones. Subzone A is made up of magnetite gabbro, ferrogabbro, and anorthosite; subzone B consists of troctolite, anorthosite and magnetite ferrogabbro; and subzone C comprises cumulus apatite at the base. von Gruenewaldt (1973) and Molyneux (1974) subdivided the Upper Zone into four subzones, with the topmost D zone consisting of ferrodiorite.

There is accessible data from research carried out on the petrology and lithologies, with emphasis on the Upper Zone, from three different areas namely; Bellevue (Ashwal *et al*., 2005), Waterberg (Kinnaird *et al*., 2017) and Villa Nora sequence (Grobler and Whitfield 1969).These findings formed a basis which was compared against the NP1 drill hole data.

3.2 Bellevue

Ashwal *et al* (2005) provided a detailed study of the geophysical and mineralogical data from the 2950 m Bellevue drill core (BV-1). The borehole intersected the entire Upper Zone and approximately half of the Main Zone of the northern limb (BV-1 location, Figure 1.1). The uppermost 83.55 m of the drill core is composed of granitic roof rocks, which are very likely to be part of the suite of intrusive granitoids that immediately post-dates the emplacement of the Rustenburg Layered Suite. Granitoids occur occasionally throughout the drill core as veins as thin as 2 cm to sill bodies of up to 56 m thick. A prominent dolerite sill (72.17 m thick) at a depth of 161.97 m occurs near the top of the sequence, with chilled margins on both contacts. These dolerite rocks were of Waterberg age (1.6 to 1.9 Ga) (van der Merwe, 1978), however, Huthmann *et al* (2016) dated the dolerite sills to be 1125+/-5 Ma. Xenoliths of metasediments, possibly derived from the underlying Transvaal Supergroup, are present sporadically throughout the core (Ashwal *et al*., 2005).

The Upper Zone of the Bellevue drill core is approximately 1188 m thick (corrected a mean dip of 17.5 degrees). Uppermost rocks are magnetite-rich olivine ferrodiorites, representing the most fractionated Bushveld lithology (Ashwal *et al*., 2005). The most abundant rock types are magnetite gabbro (41.1%) and olivine ferrodiorite (21.4%), with lesser gabbro/norite, plagioclase-magnetite cumulates and pyroxenite (Ashwal *et al*., 2005). The Upper Zone of this core has 32 layers of magnetite or magnetite-enriched rocks, ranging in thickness between 7 cm and 13 m which were correlated with the other 20 magnetite layers identified in the northern limb elsewhere (van der Merwe, 1978). Anorthosite horizons range in thickness between 5 cm and 29 m and the anorthosite rocks are abundant in a 110 m thick zone at a depth of 1070 m to 1180 m, which is approximately 400 m above the Upper Zone-Main Zone boundary (Ashwal *et al*., 2005).

The Upper Zone-Main Zone boundary becomes obvious as a distinct change in magnetite content at a depth of 1575.8 m (Figure 3.1; Ashwal *et al*., 2005). Over 1370 m of the Main Zone rocks occur in the Bellevue core and the most abundant lithologies are gabbronoritic rocks (59.9% including gabbros and norites), lesser anorthosite (15.5%), leucogabbro/leuconorite (9.7%) as well as an assortment of other mafic cumulates. Anorthosite layers in this Main Zone range between 10 cm and 31.6 m in thickness (Ashwal *et al*., 2005).

The bottom 204.4 m of the drill core constitutes part of a distinctive and unusual olivine-bearing or troctolitic horizon that was mapped for approximately 35 km of strike length in the northern limb (van der Merwe, 1978). This troctolitic unit along with other rocks of the Main Zone appear to be transgressed by Upper Zone lithologies in the region between latitudes 23°50' south and 23°40' south. Olivine does not occur within the Main Zone rocks of the eastern and western limbs (Ashwal *et al*., 2005).

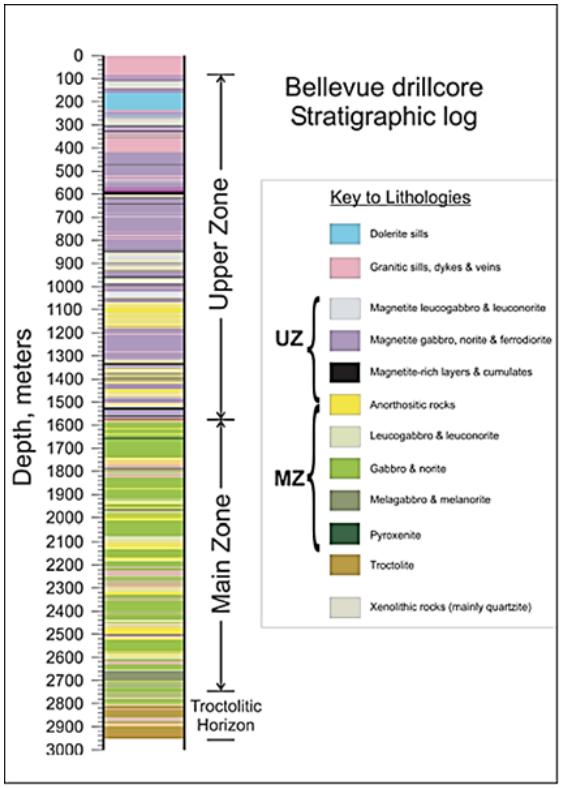

Figure 3.1: Bellevue drill core stratigraphy log (Ashwal *et al*., 2005)

3.3 Villa Nora

The Villa Nora segment was regarded as an extension of the northern limb (Grobler and Whitfield, 1970). This mafic portion of the Bushveld Complex strikes east-west over an estimated 32.2 km, with a width of roughly 12.8 km in the east diminishing to approximately 6.4 km west of the Palala river (Grobler and Whitfield, 1970). Olivine-apatite magnetites and related rocks at the Villa Nora segment were examined and the mineralogical and geochemical information correlated the area with the Upper Zone of the Bushveld Complex (Grobler and Whitfield, 1970).

Throughout the exploration period in the area, the most important types of magnetitites found include olivine-apatite magnetitite, apatite-magnetitite, feldspar-apatite magnetitite, and feldspathic magnetitite (Grobler and Whitfield, 1970). These magnetitite layers are generally concordant with the

layering of host rocks and occasionally discordant (Grobler and Whitfield, 1970). In the southernmost part of the investigated area, there is an occurrence of apatite mineralisation without associated magnetite as well as apatite-free magnetite (Grobler and Whitfield, 1970). Generally, the rocks of the Upper Zone of the Villa Nora segment are thought to be late-stage products of a normal trend of iron-enrichment of tholeiitic magma (Grobler and Whitfield, 1970).

Two vertical diamond drill holes BH-2 and BH-5, which are 64.6 m and 95.1 m in length respectively, were drilled on the Turflaagte farm. The holes intersected a typical apatite-magnetite body and provided fresh material of No.2 magnetitite and its footwall rocks (Figure 3.2; Grobler and Whitfield, 1970). Material from BH-2 and BH-5 is extensively weathered up to about 2.7 m below the surface, therefore very little is known about the rocks above No.2 magnetite (Grobler and Whitfield, 1970).

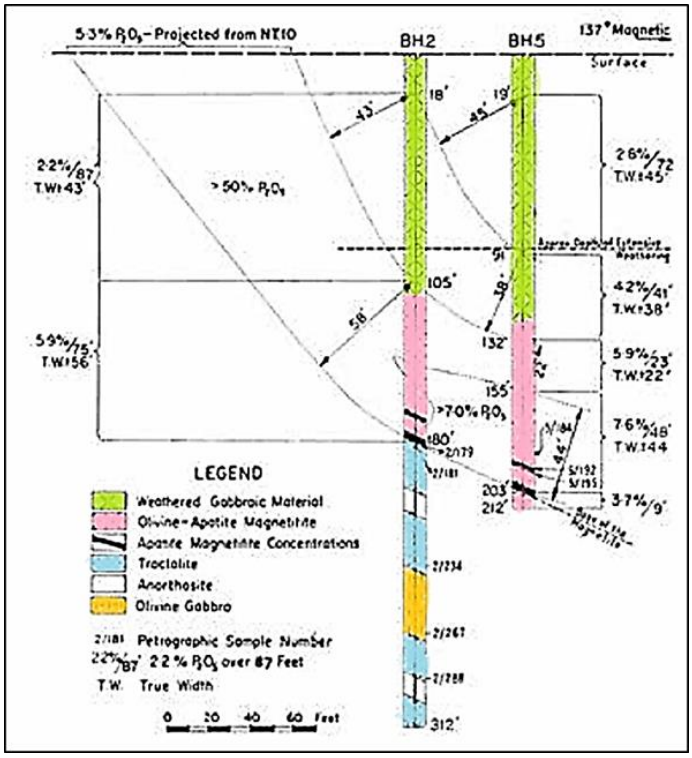

Figure 3.2: Diagrammatic section through the No.2 Olivine-apatite magnetitite on the Turflaagte farm coloured in pink (Grobler and Whitfield, 1970)

3.3.1 Petrology of drill hole BH-2 and BH-5 from the Villa Nora segment

A brief petrographic description of major rock types encountered from drill hole BH-2 and BH-5 on the Turflaagte farm at the Villa Nora segment by Grobler and Whitfield (1970) is given. This will form a basis for comparison with observations from the NP1 core.

a) Magnetitites: Olivine-apatite magnetitite (No.2 magnetitite) is distinctly layered in some places but the bulk of this rock type is more massive, consisting of euhedral crystals of clear apatite (less or equal to 2 mm) and subhedral grains of brown fresh olivine cemented by an interstitial mass of magnetite-ilmenite (Grobler and Whitfield, 1970). Apatite-magnetitite, a minor but distinct rock type, occurs as thin bands within olivine-apatite and feldspar-apatite magnetitites. Feldspar-apatite magnetitites are strongly layered, consisting of subhedral laths of plagioclase and grains of apatite and interstitial magnetite and plagioclase (Grobler and Whitfield, 1970).

b) Troctolite: Four clear bands of troctolitic rocks are occur below No.2 magnetitite with the thickest band being 7 m. These rocks show compositional variation grading from leucotroctolite into impure anorthosite or through augite troctolite into olivine gabbro (Grobler and Whitfield, 1970).

c) Olivine gabbro: Occurs as one distinct layer of approximately 6.7 m in thickness below the No.2 magnetitite, and as a rock in which few last metres of BH-2 were drilled (Grobler and Whitfield, 1970).

d) Magnetite gabbro: Well layered with platy plagioclase grains and olivine as well as biotite as accessory minerals. It is made up of large amounts of interstitial clinopyroxene with a resultant decrease in magnetite and apatite content (Grobler and Whitfield, 1970).

e) Anorthosite: Two prominent layers of impure anorthosite (approximately 3 m thick each) and both enclosed by troctolite, occur within the basal rocks beneath the No.2 magnetitite. The anorthosite is highly altered in this area (Grobler and Whitfield, 1970).

f) Leuconorite, Leucogabbro: This forms the main mass of the complex and is very similar in appearance to material found in the Main Zone. In hand specimen, leucogabbro is very similar to leuconorite, consisting of plagioclase laths, orthopyroxene, some interstitial clinopyroxene with accessory amounts of olivine and greenish amphibole (Grobler and Whitfield, 1970).

In general, the Upper Zone is characterised by the incoming of magnetite, iron-rich olivine and apatite as important cumulus phases (Grobler and Whitfield, 1970). Similarly, the composition of the iron-rich olivine and plagioclase indicate a position well into the Upper Zone of the Bushveld Complex (Grobler and Whitfield, 1970).

3.4 Waterberg Project area

The Waterberg Project is focused on a greater than 3.5 km x 24 km lobate intrusion north of the Hout River Shear Zone (Figure 1.3). This intrusion consists of a layered package of gabbros, gabbronorites, norites, anorthosite with troctolites, harzburgite, dunite, and orthopyroxene towards the base (Kinnaird *et al*., 2017). U/Pb zircon age dating of the ultramafic-mafic succession gives intrusion ages of 2059 +/- 3 and 2053 +/- 5 Ma, which therefore suggest that the Waterberg and Bushveld Complex intrusions are of the same age (Kinnaird *et al*., 2017).

The stratigraphy of the Waterberg Project area is subdivided into three main parts, namely; the basal ultramafic sequence, the troctolite-gabbronorite-anorthosite (TGA) sequence and the Upper Zone (Figure 3.3; Kinnaird *et al*., 2017). Overlying the Upper Zone are doleritic sills and Waterberg Group sediments (Kinnaird *et al*., 2017).

The basal ultramafic sequence is less than 100 m thick and has two components; lower pyroxenite unit and overlying harzburgite unit (Kinnaird *et al*., 2017). Pyroxenites, interpreted as crystallised from the initial magma to intrude the area, are interfingered with gabbronorite sills (Kinnaird *et al*., 2017). The harzburgite sequence, locally pegmatoidal towards the base, has lesser olivine-bearing gabbronorite, olivine-bearing norite, feldspathic harzburgite, pyroxenite, and feldspathic pyroxenite. PGE are associated with chalcopyrite-pentlandite-pyrrhotite mineralisation (Kinnaird *et al*., 2017).

The TGA sequence is up to 850 m thick, with a troctolite unit at the base and varies upwards from melatroctolite and rare dunite to olivine norite and leucotroctolite (Kinnaird *et al*., 2017). The gabbronorite unit consists of gabbronorite, altered orthopyroxene, subordinate clinopyroxene and inverted pigeonite. A mineralised T-zone occurs towards the top of the TGA in the southern part of the project area (Kinnaird *et al*., 2017).

The Upper Zone is dominated by magnetite gabbro and gabbronorite with ferrogabbro at the top in some of the holes (Kinnaird *et al*., 2017). In the southwest close to the Hout River Shear Zone, the Upper Zone may be approximately 350 m thick, however it thins northwards and becomes completely absent in the north-central parts of the project area but reappears in the far north where it is 70 – 500 m thick (Kinnaird *et al*., 2017). The uppermost portions of the Upper Zone are characterised by brick-red alteration and a highly sheared contact zone (Kinnaird *et al*., 2017). Where the Upper Zone is missing, either TGA troctolite or pyroxenite of the basal ultramafic sequence is in contact with the overlying Waterberg sedimentary rocks (Kinnaird *et al*., 2017). It has been identified that the Upper Zone in the Waterberg area has no magnetitite layers (Kinnaird *et al*., 2017).

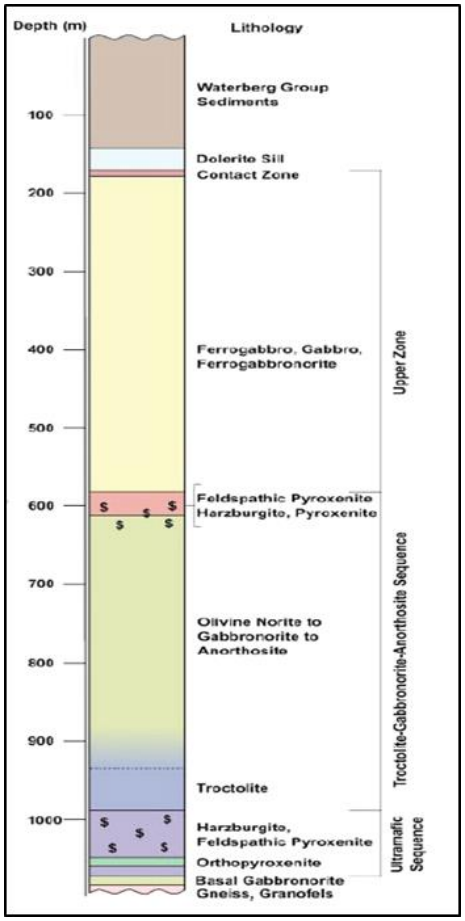

Figure 3.3: Stratigraphy of the Waterberg Project area (Kinnaird *et al*., 2017)

3.5 Summary and conclusion

Within the above three mentioned Upper Zone sequences, Bellevue, Villa Nora and the Waterberg area, common lithologies include magnetite-rich rocks, gabbroic rocks, troctolitic rocks and magnetitite layers (magnetitite layers do not occur at the Waterberg Project area). Regarding the NP1 sequence, core logging and other methodologies were undertaken to determine the various rock types and their compositions.

Chapter 4

Stratigraphy of NP1 core

4.1 Introduction

During core Logging procedure of the NP1 sequence, different rock types were identified, which includes Waterberg sedimentary rocks, gabbronorite, gabbro, mottled anorthosite, monzodiorite, and xenoliths. Various cross-cutting veins such as coarse-grained feldspar-magnetite veins and plagioclase veins were identified. This chapter aims to provide a petrological description of the NP1 core and indicate the depths at which the different rock types were intersected.

4.2 Method

The 2500 m NP1 core is kept at the Council for Geoscience core library in Pretoria, and a five-day visit was undertaken in April 2017 to complete the logging and sampling. Approximately 1430 m (1070 m – 2500 m) was logged as most of the Waterberg sedimentary rocks were excluded from the logging exercise. From surface to a depth of 1070 m, the core consists of Waterberg sedimentary rocks and dolerite sills. The core logging method is useful in identifying rock types as well as changes in lithology with depth. At the completion of this process, the lithological succession of the NP1 core was compared to the Upper Zone elsewhere in the northern limb (Bellevue), Waterberg Project area and the Villa Nora segment. The NP1 log is shown in Figure 4.1 and individual hand specimen descriptions are presented in Appendix A.

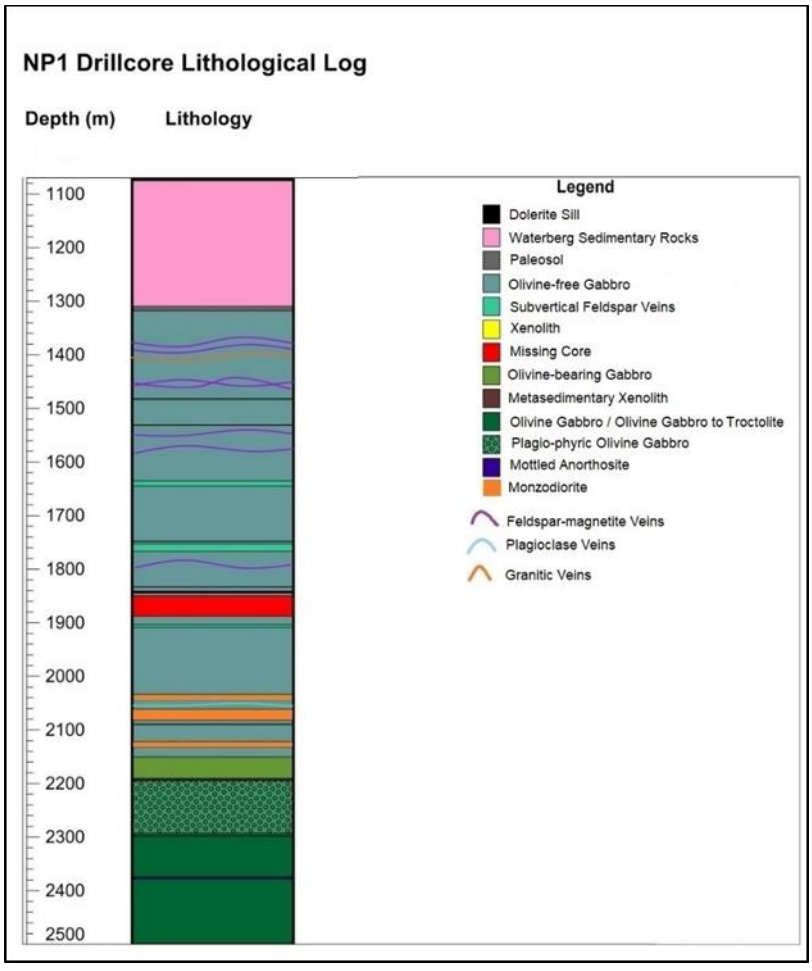

Figure 4.1: Stratigraphy of the NP1 sequence, from 1070 m to 2500 m

4.3 Results

The lithologies are described and presented in stratigraphic order from the base to top of the core.

4.3.1 Gabbroic rocks

Gabbroic rocks dominate the lower part of the NP1 core and have been subdivided into four types namely; olivine-bearing gabbro, plagioclase-phyric (plagio-phyric) olivine gabbro, olivine gabbro and olivine gabbro to troctolite. Olivine was first identified within gabbroic rocks during core logging at a depth of 2158 m, which marks the occurrence of olivine-bearing gabbro up to 2190.5 m. However, above 2158 m depth, olivine was identified within quartz-feldspar veins and xenoliths. Olivine from 2158 m to the base of the core was identified to be Fe-rich (fayalitic olivine), based on an increase in Fe_2O_3 from whole rock geochemical analysis (see Figure 6.2). Plagioclase phenocrysts are visually identified from a depth of 2194.5 m, indicating the plagio-phyric olivine gabbro intervals (Figure 4.2a) from 2194.5 m to 2292.5 m and from 2297 m to 2298 m. Olivine abundance increases towards the base of the core. Based on petrography (chapter 5) and better identification and modal mineralogy of olivine, it was confirmed that the olivine gabbro and olivine gabbro to troctolite packages (Figure 4.2b) occur within the intervals of 2298 m to 2374.5 m and 2378 m to 2500 m respectively. For the sake of consistency, the gabbroic rocks package will be collectively referred to as olivine-rich gabbroic rocks throughout the report. This olivine-rich gabrroic rocks package was found to be very magnetic when tested with a magnetic pencil and fine-grained disseminated magnetite grains were identified.

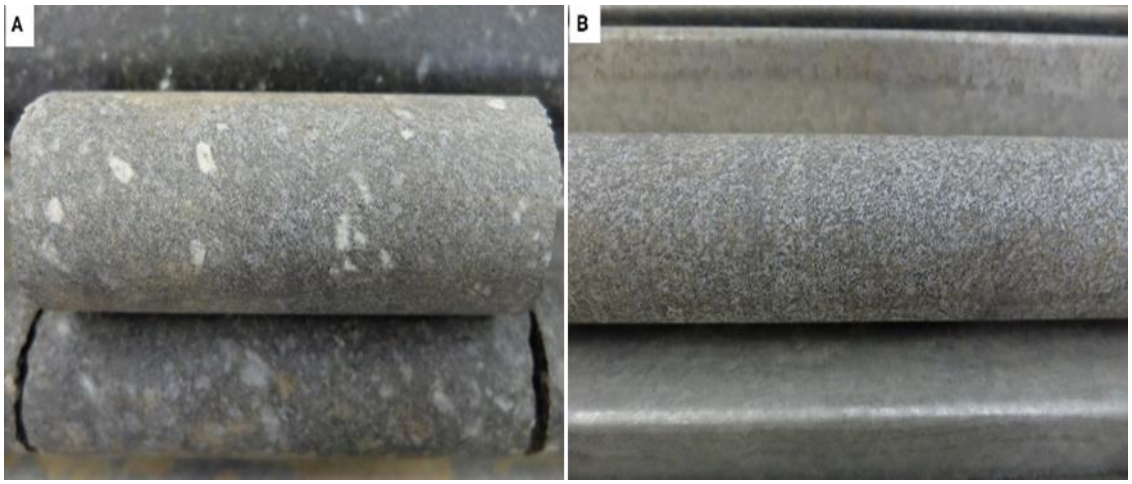

Figure 4.2: Photographs of gabbroic rocks, (a) Plagio-phyric olivine gabbro, (b) Olivine gabbro / olivine gabbro to troctolite

4.3.2 Mottled anorthosite

Mottled anorthosite (Figure 4.3a and b) occurs for an approximate 3.5 m thickness from a depth of 2374.5 m to 2378 m. This coarse-grained mottled anorthosite interval occurs in between the magnetite and olivine-rich gabbroic rocks and its composition comprises plagioclase (dominating the rock type composition), mottles of clinopyroxene, magnetite, and phlogopite.

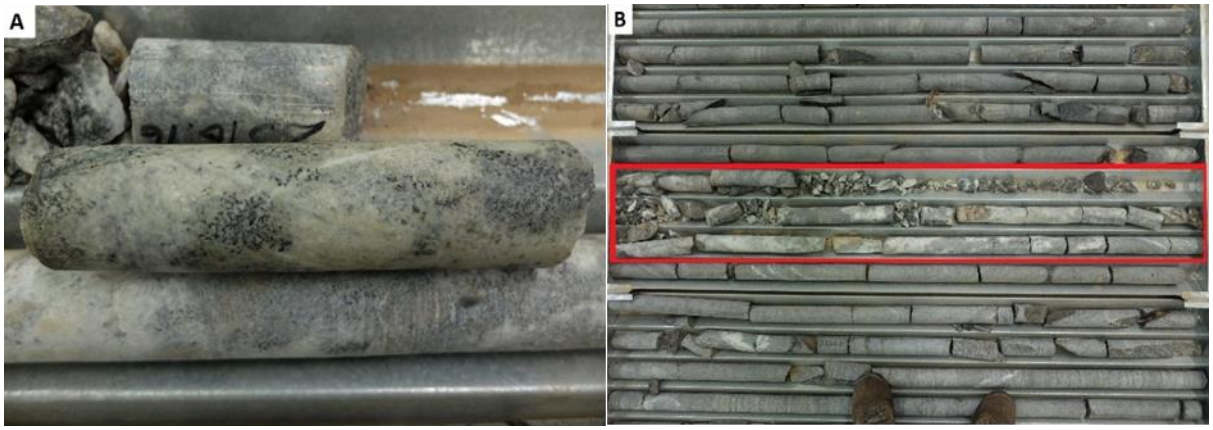

Figure 4.3: Mottled anorthosite, (a) Mottled anorthosite sample in core NP1 from a depth of 2376 m, (b) Mottled anorthosite interval, surrounded by a red rectangle, occurring in-between olivine gabbro

4.3.3 Gabbronorite rocks

Olivine-free fine-grained gabbronoritic rocks occur at a depth of 1318 m to 1481.3 m, beneath the hematitised paleosol, and also in multiple layers ranging in thickness within an interval from 1483.5 m to 2150.5 m (see Figure 4.1). The package is made up of olivine-free, non-magnetic fine-grained gabbronorite with cross-cutting coarse-grained feldspar-quartz-magnetite veins (Figure 4.4a) and terminates in the sequence at 2150.5 m. At some intervals, the olivine-free gabbronoritic rocks are characterised by abundant phlogopite phenocrysts (Figure 4.4b).

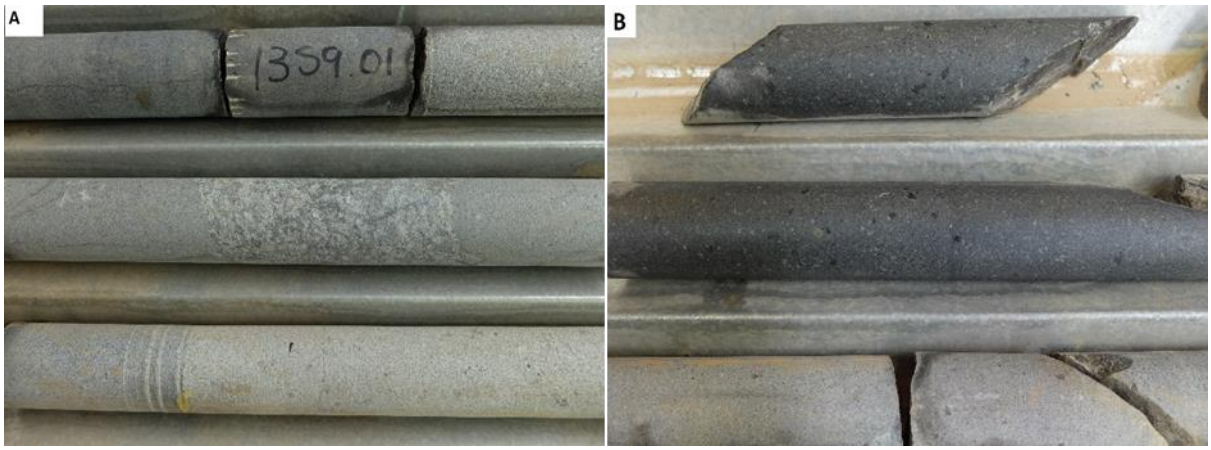

Figure 4.4: Photographs of gabbronorite rocks in NP1 core, (a) Olivine-free fine-grained gabbronorite cross-cut by coarse-grained feldspar-quartz-magnetite vein in the middle core sample, (b) Olivine-free fine-grained gabbronorite with phlogopite phenocrysts

4.3.4 Monzodiorites

The rock type in the interval of 2043 m to 2155 m (Figure 4.5a) was initially described as leucogabbro during core logging. However, with further analyses, XRF whole rock geochemical results indicated a SiO_2 content of 63 – 72 wt.% (chapter 6) and the presence of olivine was identified within thin sections from this interval (chapter 5). The rocks were later classified as monzodiorite. These rocks are coarse-grained and occur within the olivine-free fine-grained gabbronorite sequence. The difference in grain size and colour can be seen in Figure 4.5b showing a contact between the monzodiorite and fine-grained gabbronorite.

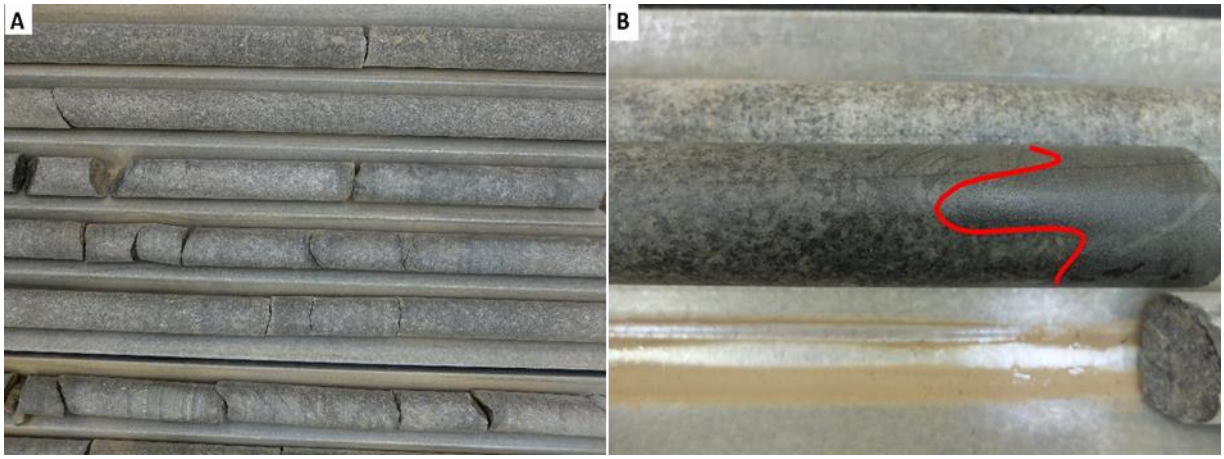

Figure 4.5: Monzodiorite rocks within core NP1, (a) An interval of monzodiorite rocks within the core at approximately 2061 to 2066 m, (b) Sample showing a contact (in red) between monzodiorite on the left and fine-grained gabbronorite on the right

4.3.5 Xenoliths

The NP1 core has two types of xenoliths; quartz-feldspathic xenoliths (Figure 4.6a and b) and shale to hornfels xenoliths (Figure 4.6c). Quartz-feldspathic xenoliths are medium-grained and occur from a depth of 1842.2 m to 1843.1 m and 1843.8 to 1844.5 m. Shale to hornfels xenoliths are fine-grained, with disseminated mica and occur from a depth of 2190.5 m to 2190.7 m and 2191.7 m to 2193.9 m. On the NP1 log (Figure 4.1) quartz-feldspathic xenoliths are represented by “xenolith” while shale to hornfels xenoliths are represented by “metasedimentary xenolith”.



Figure 4.6: Xenoliths in NP1 core, (a) quartz-feldspathic xenolith, (b) Top-view of quartz-feldspathic xenolith, (c) shale to hornfels xenolith

4.3.6 Veins

Several subvertical veins occur throughout the NP1 core. These veins include coarse-grained feldspar-magnetite veins (Figure 4.7a and b), which are the most dominant within the fine-grained gabbronorite section and were first logged at a depth of 1180.5 m. Plagioclase veins (Figure 4.7c) and light pink coloured granitic veins (Figure 4.7d) were also identified. A variety of small to large undulating coarse-grained feldspar-magnetite veins occur within the fine-grained gabbronorite package, from a depth of 1318 m to approximately 1900 m. In addition to these veins, subvertical coarse-grained feldspar-quartz-magnetite veins (Figure 4.7e) and feldspar veins (with variable proportions of quartz, magnetite, and hornblende, with accessory zircon and apatite) cross-cut the gabbronoritic rocks. Feldspar veins (Figure 4.7f) occur in multiple layers ranging in thickness within the interval of 1481.3 m to 1908.5 m.

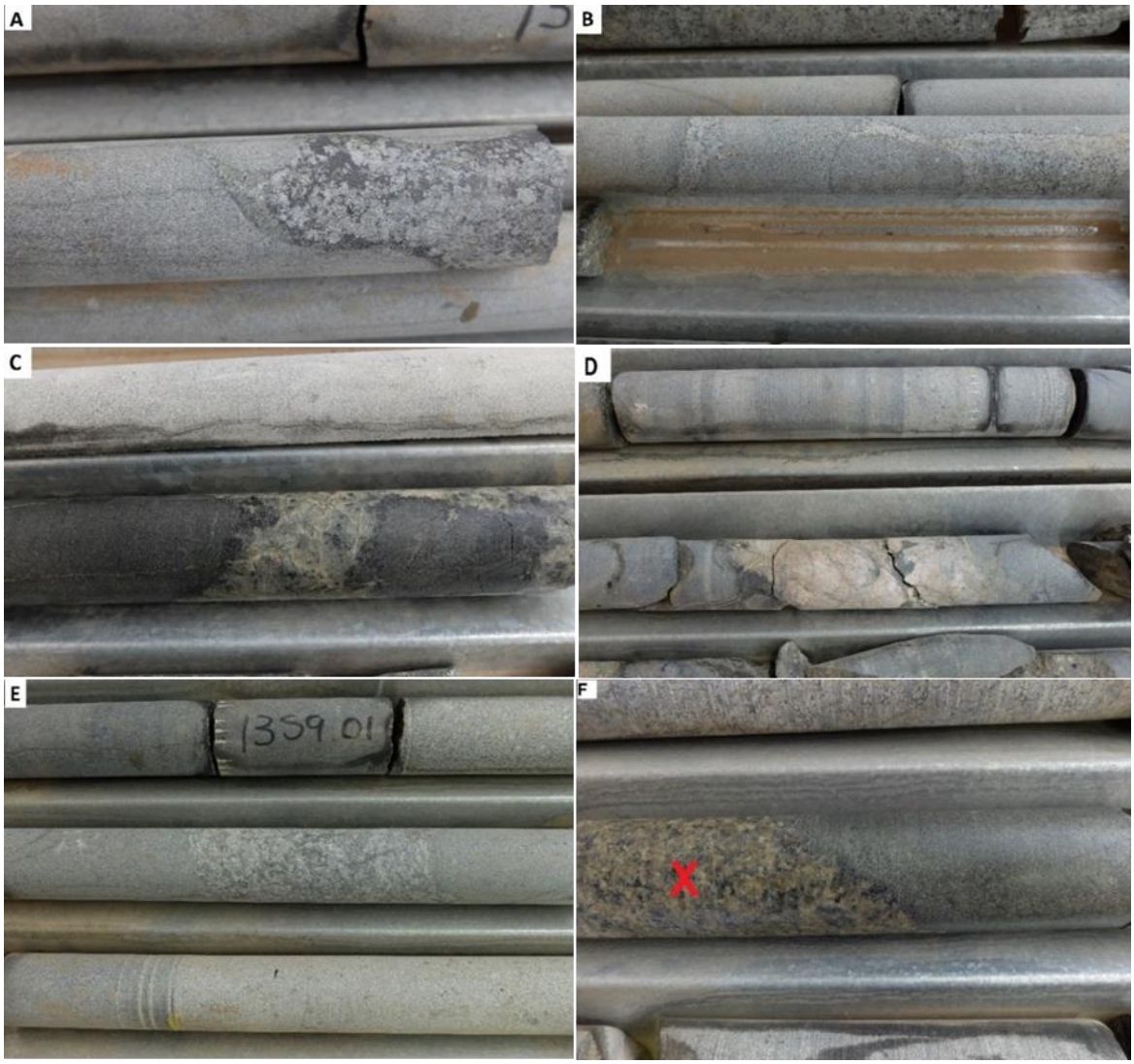

Figure 4.7: Photographs of veins occurring in the NP1 core, (a) & (b) Coarse-grained feldspar-magnetite veins, (c) Plagioclase vein, (d) Granitic vein, (e) Coarse-grained feldspar-quartz-magnetite vein, (f) Feldspar vein, marked with a cross (X)

4.3.7 NP1 top-most sequence

The top part of the NP1 core (from 1070 m) is a dolerite sill with approximately 5 m total thickness of the lower chill zone. From a depth of 1075.28 m, Waterberg sedimentary rocks extend downwards to a depth of 1309.4 m (Figure 4.8a and b). The Waterberg sedimentary rocks are underlain by a tectonic clay and hematitised mafic rock, represented by "paleosol" on the NP1 log in Figure 4.1.



Figure 4.8: Photographs of the upper part of the NP1 core, (a) Contact between chill zone and Waterberg sedimentary rocks marked in red, (b) Waterberg Red Beds

4.4 Discussion and conclusion

There are three main facies identified through NP1 core, a topmost sequence of Waterberg sedimentary rocks with intrusive dolerite sills, a middle sequence of olivine-free gabbronorites and a basal sequence of olivine-bearing (+ magnetite) gabbroic lithologies. The NP1 core does not have any magnetitite layers, but several undulating coarse-grained feldspar-magnetite veins as well as some disseminated magnetite. Magnetite decreases in concentration in the upper part of the sequence from 2158 m upwards. Olivine concentration decreases upwards and that is not consistent with the recognised olivine enrichment in the upper part of the Upper Zone elsewhere in the Bushveld (von Gruenewaldt, 1973). This suggests that the upper part of the NP1 sequence, the gabbronorite section, may not be a component of the Upper Zone. To attain further insight as to whether the NP1 core can be correlated with the Bushveld Upper Zone, a more detailed petrographic analysis was carried out in the next chapter.

Chapter 5

Petrography of NP1 core

5.1 Introduction

The core logging procedure resulted in gathering initial data on the NP1 drill core to identify rock types found in the sequence. To increase data confidence, thin sections were prepared to identify minerals which could not be identified with a naked eye. Sample numbers shown in the results section 5.3 are representative of the depth (in metres) at which the core was sampled. This chapter aims to present petrographic images, modal mineralogy, grain size and texture information of some samples representing different NP1 rock types. More detailed petrographic data is presented in Appendix B. Below are definitions of some rock types identified through the NP1 core.

Gabbro: A plutonic, mafic igneous rock composed of plagioclase feldspar, clinopyroxene, and some olivine. Hornblende, biotite, and magnetite may be accessory minerals (Streckeisen, 1976).

Anorthosite: A coarse-grained igneous rock made up of more than 90% plagioclase feldspar (Streckeisen, 1976).

Hornfels: Fine to medium-grained metamorphic rock that is formed by contact metamorphism along the edges of hot igneous intrusions that cross-cut the country rock (Cairncross, 2004).

5.2 Method

Some minerals could not be identified in hand specimen and 48 thin sections were prepared to assist in the identification of the mineralogy of the NP1 sequence using a petrographic microscope (Figure 5.1). Sample images represent the majority of minerals identified in a specific thin section. The design of the microscope camera magnifies only a certain area of the thin section and not the entire sample, as evident through some of the sample representative images produced. This therefore explains some minerals being identified in thin sections and mentioned in the description but do not appear in the sample representative image in section 5.3 and Appendix B.



Figure 5.1: Olympus BX41 petrographic microscope at the petrography laboratory, University of the Witwatersrand School of Geoscience, 2017

5.3 Results

The modal abundances of thin sections were estimated using the modal percentage scale (Figure 5.2) as a guide, created by Caracle Creek International Consulting Inc.

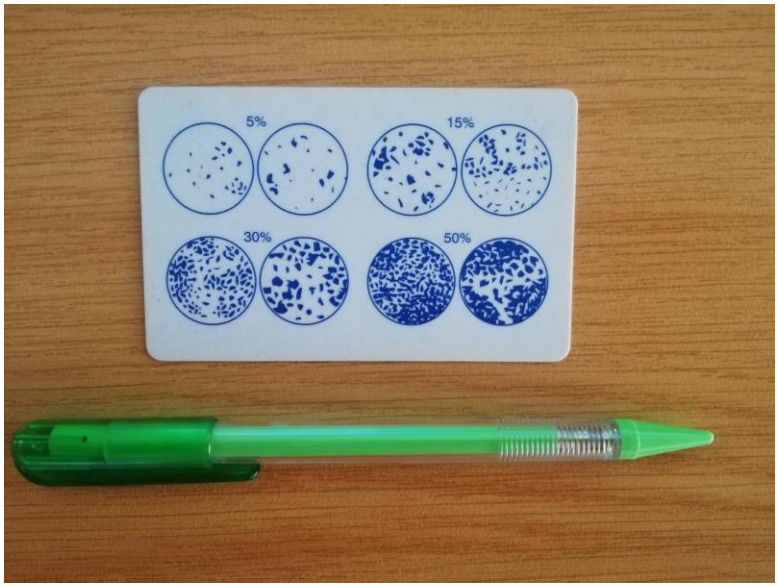

Figure 5.2: Modal percentage estimation scale guide, produced by Caracle Creek International Consulting Inc.

5.3.1 Olivine-rich gabbroic rocks

The olivine-rich gabbroic rocks occur from 2158 m to 2500 m. These gabbroic rocks include olivine-bearing gabbro, plagio-phyric olivine gabbro, olivine gabbro and olivine gabbro to troctolite, occurring successively downhole. During core logging, olivine grains were inferred to be iron-rich (fayalitic olivine) based on their golden brown colour and this was confirmed by high Fe_2O_3 content from XRF analysis (chapter 6). Olivine-bearing gabbro (Figure 5.3a), plagio-phyric olivine gabbro (Figure 5.3b), olivine gabbro (Figure 5.3c) and olivine gabbro to troctolite (Figure 5.3d) have 19%, 20%, 24%, and 30% olivine content respectively which increases downhole. The coarse-grained olivine-bearing gabbro, represented by sample 2177.2, is made up of 65% plagioclase and 10% interstitial magnetite as major minerals in addition to olivine. The minor mineral is 5% clinopyroxene and 1% accessory apatite was also identified. The coarse-grained plagio-phyric olivine gabbro, sample 2220, consists of 39% plagioclase, 20% olivine, 15% clinopyroxene, 15% magnetite, 6% apatite, 4% orthopyroxene and 1% zircon. In addition to the olivine percentage (24%), 31% plagioclase, 22% magnetite, 10% clinopyroxene, 8% apatite and 5% orthopyroxene make up the total modal mineralogy of the olivine gabbro, sample 2300.5, with intergranular to equigranular texture. The olivine gabbro to troctolite, sample 2496.1, has the highest olivine content (30%) of all the rock types in NP1 core. Other minerals making up the sample are 42% plagioclase, 15% magnetite, 8% clinopyroxene, and 5% apatite. The subophitic texture in the sample shows plagioclase laths enclosed by clinopyroxene and olivine crystals. The plagioclase laths display lineation.

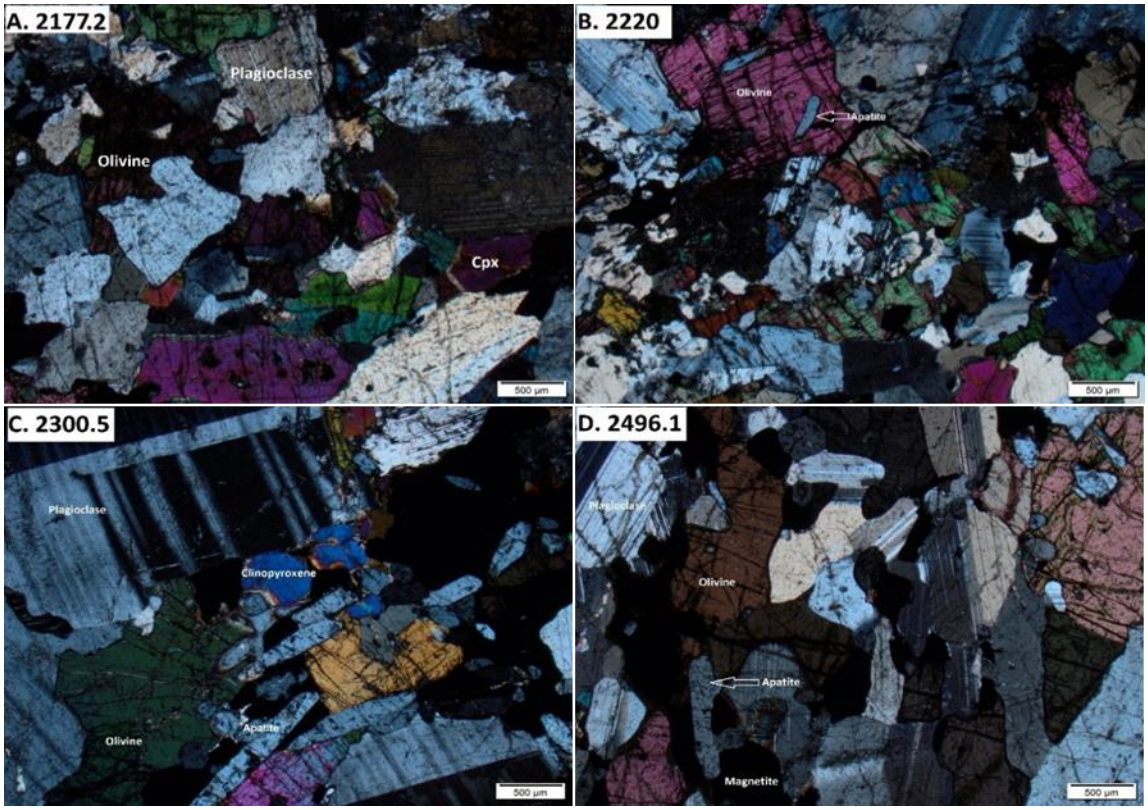

Figure 5.3: Photographs of olivine-rich gabbroic rocks in core NP1, (a) Olivine-bearing gabbro showing olivine, plagioclase and clinopyroxene, (b) Plagio-phyric olivine gabbro, (c) Olivine gabbro showing large elongated apatite crystals, (d) Olivine gabbro to troctolite showing subophitic texture. All images in crossed polarised light (XPL)

5.3.2 Mottled anorthosite

In the Bushveld Complex, the term "anorthosite" is used more loosely to include very plagioclase-rich light coloured rocks. The NP1 mottled anorthosite is dominated by plagioclase with a percentage varying from 58% in sample 2374.9 (Figure 5.4a) to 70% in sample 2377.8 (Figure 5.4b). The coarse-grained plagioclase laths in both samples show lamellar twinning. The mottles in sample 2374.9 are made up of 15% olivine , 2% clinopyroxene and 5% orthopyroxene while mottles in sample 2377.8 are made up of 15% clinopyroxene and 5% orthopyroxene. The magnetite percentage in sample 2377.8 is 5% and 20% in sample 2374.9. Both samples show an equigranular texture.

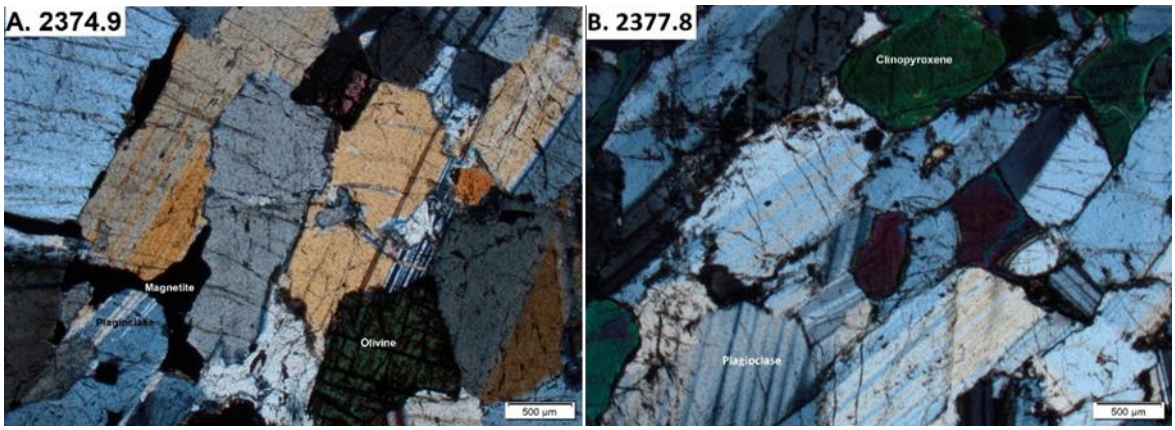

Figure 5.4: Photographs of mottled anorthosite in core NP1, (a) Sample 2374.9 showing plagioclase, magnetite and olivine, (b) Sample 2377.8 showing plagioclase and clinopyroxene. All images in XPL

5.3.3 Olivine-free fine-grained gabbronoritic rocks

The olivine-free fine-grained gabbronorite package is represented by sample 1356.3 and 1541.5. Sample 1356.3 (Figure 5.5a) consists of 48% plagioclase, 16% clinopyroxene and 16% orthopyroxene as major minerals. Minor minerals are 9% magnetite, 9% phlogopite and accessory 2% apatite. The sample has an intergranular texture and some plagioclase crystals show minor to major levels of alteration. Sample 1541.5 (Figure 5.5b) is made up of the same minerals as sample 1356.3, however, phlogopite crystals in 1541.5 are phenocrysts in comparison to those in sample 1356.3. Fifty percent (50%) plagioclase, 20% clinopyroxene and 20% orthopyroxene are major minerals in sample 1541.5. Minor minerals include 6% phlogopite, 3% opaques and accessory 1% apatite.

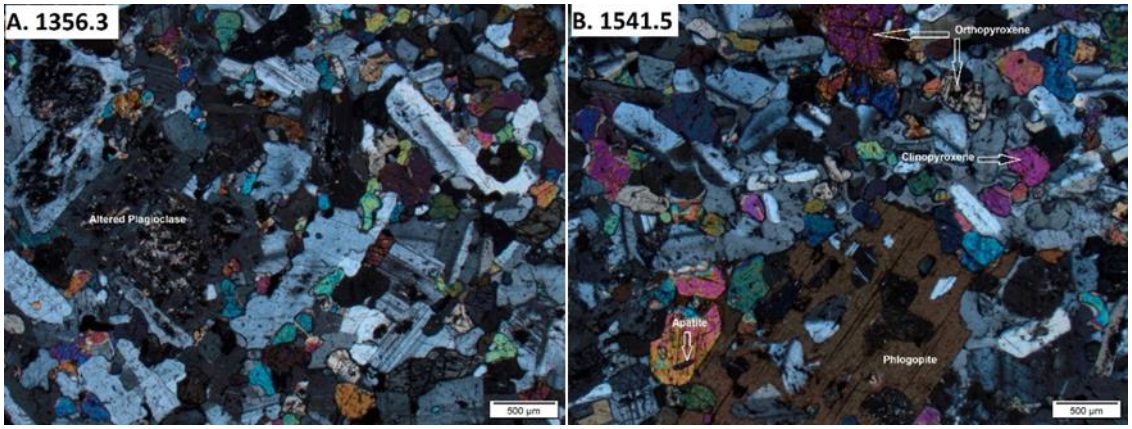

Figure 5.5: Photographs of olivine-free fine-grained gabbronorite rocks in core NP1, (a) Sample 1356.3 showing altered plagioclase crystals, (b) Sample 1541.5 showing phlogopite phenocrysts. All images in XPL

5.3.4 Monzodiorites

Sample 2043 (Figure 5.6a) is made up of alkali feldspar (40%), plagioclase (15%), olivine (15%), magnetite (10%), quartz (10%), clinopyroxene (8%), and zircon (2%). Sample 2076.8 (Figure 5.6b) comprises alkali feldspar (45%), quartz (20%) and olivine (15%) as major minerals. Plagioclase (8%), clinopyroxene (6%), and interstitial magnetite (5%) are minor minerals and the 1% zircon as an accessory mineral. Both samples show granophyric texture.

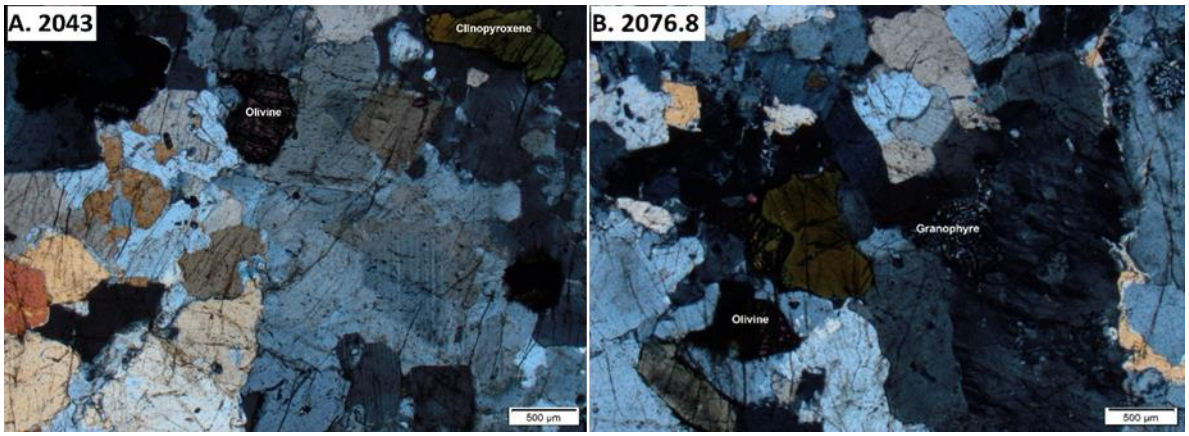

Figure 5.6: Photographs of samples representing monzodiorite rocks in core NP1, (a) Sample 2043, (b) Sample 2076.8 showing granophyre. All images in XPL

5.3.5 Veins

Veins were sampled from three main occurring veins out of the five vein types in NP1 core. The sampled veins are coarse-grained feldspar-magnetite veins, coarse-grained feldspar-quartz-magnetite veins and feldspar veins only. Sample 1385.3 and 1401.5 (Figure 5.7a and b respectively) both represent coarse-grained feldspar-magnetite veins. Sample 1385.3 is dominated by 35% interstitial magnetite, 25% plagioclase and 25% orthopyroxene. Minor minerals include 7% zircon, 5% alkali feldspar and 3% apatite. Sample 1401.5 is made up of 36% magnetite and 35% plagioclase as major minerals, as well as 8% alkali feldspar, 6% phlogopite, 5% zircon, 4% clinopyroxene, 4% orthopyroxene and 2 % apatite as minor minerals. Both samples, 1385.3 and 1401.5, have an equigranular texture with perthitic feldspar.

Sample 1318.35 (Figure 5.7c) represents coarse-grained feldspar-quartz-magnetite veins. The sample is dominated by coarse-grained plagioclase crystals which constitute 40% of total modal mineralogy. Other minerals within the sample include 15% alkali feldspar, 15% quartz, 15% magnetite, 5% phlogopite, 4% zircon, 3% clinopyroxene and 3% apatite. Sample 1481.5 (Figure 5.7d) represents feldspar veins, consisting of anhedral crystals, 40% plagioclase, 15% magnetite, 15% phlogopite, 10% alkali feldspar, 6% quartz, 5% orthopyroxene, 5% hornblende, 3% zircon and 1% apatite.

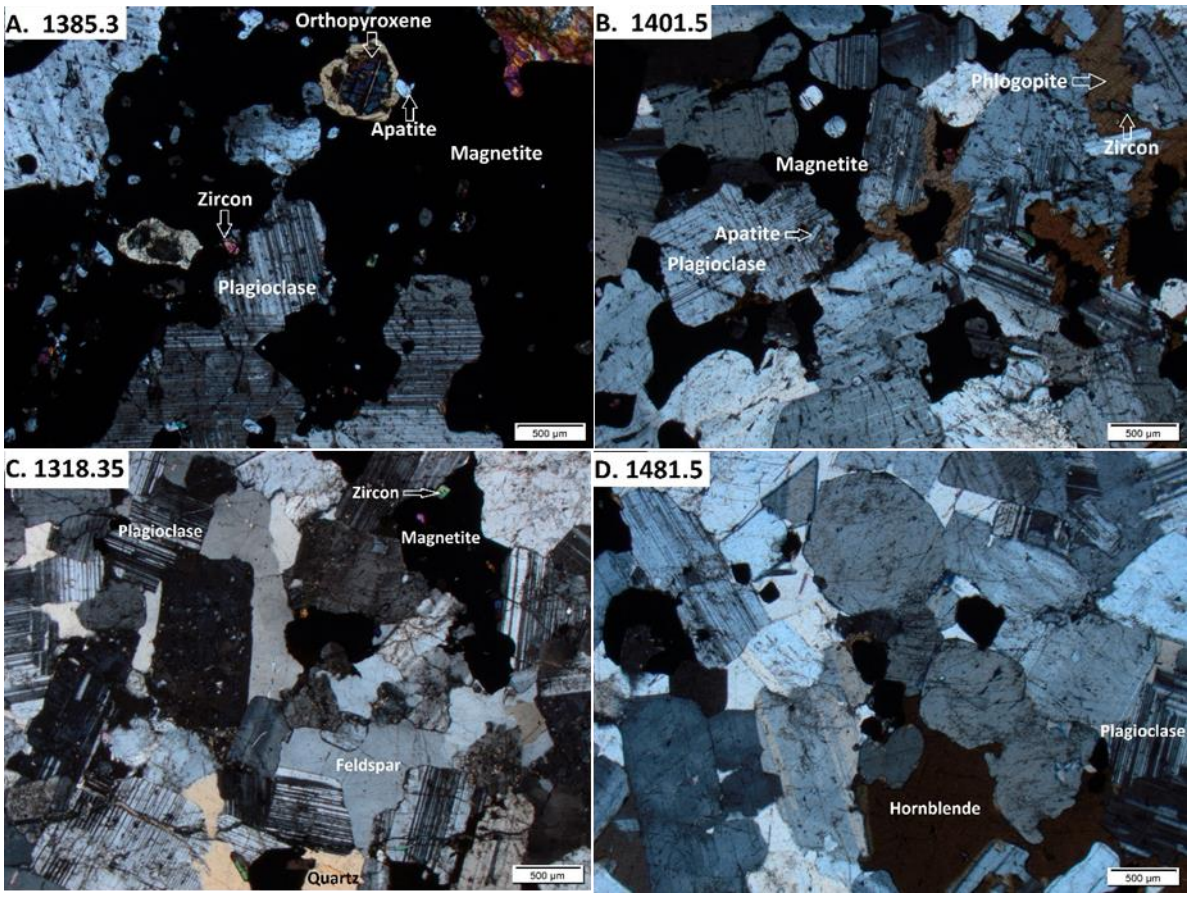

Figure 5.7: Photographs of veins in core NP1, (a) and (b) Coarse-grained feldspar-magnetite vein, (c) Coarse-grained feldspar-quartz-magnetite vein showing plagioclase crystals with lamellar twinning, (d) Feldspar vein showing hornblende crystals. All images in XPL

5.3.6 Xenoliths

Xenoliths occurring within the NP1 core are quartz-feldspathic xenoliths as well as shale to hornfels xenoliths. Sample 1842.5 (Figure 5.8a) is a quartz-feldspathic xenolith which is coarse-grained and dominated by 55% alkali feldspar, followed by 35% quartz and 10% plagioclase. The sample has a granophyric texture. Sample 2193.2 (Figure 5.8b), shale to hornfels xenolith, shows foliation which is suggested to be related to metamorphism. The modal mineralogy is made up of 40% iron oxides, 25% clinopyroxene, 20% alkali feldspar, 10% orthopyroxene and 5 % minor phlogopite.

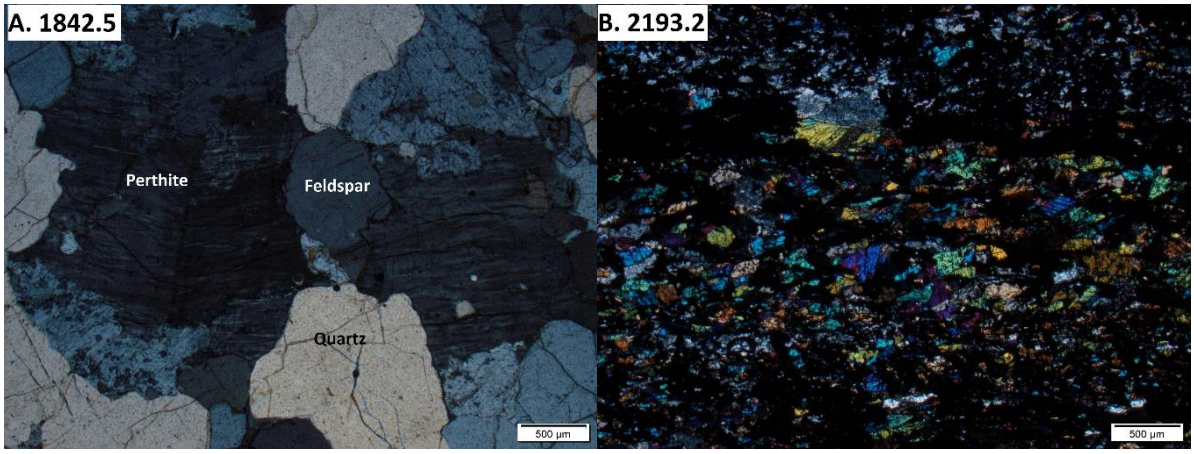

Figure 5.8: Photographs of xenoliths in core NP1, (a) Metamorphosed quartz-feldspathic xenolith, (b) Hornfels showing foliation. All images in XPL

5.4 Modal mineralogy versus depth

Modal mineralogy presented in Appendix B is plotted against depth in Figure 5.9. The figure shows mineral variation and quantity of key minerals at certain depths from where the core was sampled. The "others" category on the diagram represents a combined percentage of quartz, phlogopite, hornblende, zircon and opaques (including iron oxides). Plagioclase, clinopyroxene, and orthopyroxene are all present in gabbronoritic rocks, while gabbroic rocks are primarily made up of plagioclase and clinopyroxene. Monzodiorites and feldspar veins are dominated by plagioclase and alkali feldspars. Magnetite is more abundant in coarse-grained feldspar-magnetite veins; however, it is also common within the olivine-rich gabbroic rocks. Olivine abundance increases with depth from olivine-free gabbro to olivine gabbro to troctolite rocks downhole. Whilst apatite is minor within the olivine-free gabbronorite package, it reaches its highest concentration in the lower olivine-rich gabbroic rocks.

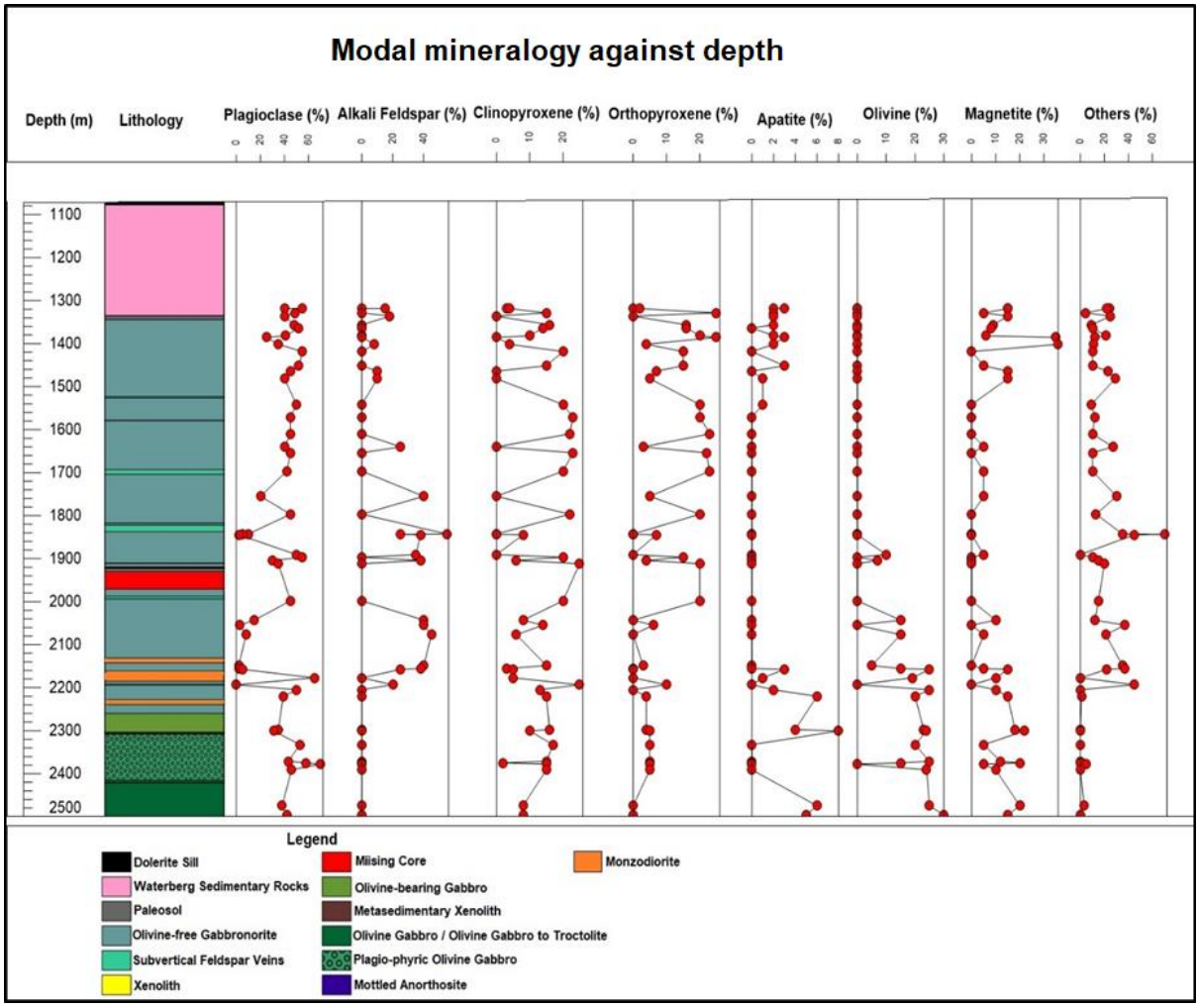

Figure 5.9: Modal mineralogy against depth through core NP1

5.5 Discussion and conclusion

The petrographic observations made it possible to identify minerals which could not be identified with a naked eye, such as apatite. Determining the modal mineralogy of olivine is some samples made it possible to distinguish between olivine gabbro and troctolite. These observations assisted in getting a better understanding of the stratigraphy of the NP1 core.

The modal mineralogy data has been used to clearly distinguish between gabbronoritic and gabbroic rocks of the NP1 core. Le Maitre (2002) classified gabbronorite to consist of plagioclase and almost equal amounts of clinopyroxene and orthopyroxene, and gabbro to primarily be made up of plagioclase and clinopyroxene. The modal compositions of two gabbronorite samples and two gabbroic rocks samples, used for illustration, are tabulated in Table 5.1 and plotted on the IUGS classification diagram for mafic and ultramafic rocks in Figure 5.10 (modified after La Maitre, 2002).

Table 5.1: Modal composition of some gabbronorites and gabbroic NP1 samples

Minerals	1356.3 [Gabbronorite]	1541.5 [Gabbronorite]	2300.5 [Olivine gabbro]	2496.1 [Olivine gabbro to Troctolite]
Plagioclase	48	50	31	42
Clinopyroxene	16	20	10	8
Orthopyroxene	16	20	5	-
Alkali Feldspar	-	-	-	-
Olivine	-	-	24	30
Magnetite	9	-	22	15
Apatite	2	1	8	5
Phlogopite	9	6	-	-
Opaques	-	3	-	-

*The values in this table are in %

*Total % per sample = 100

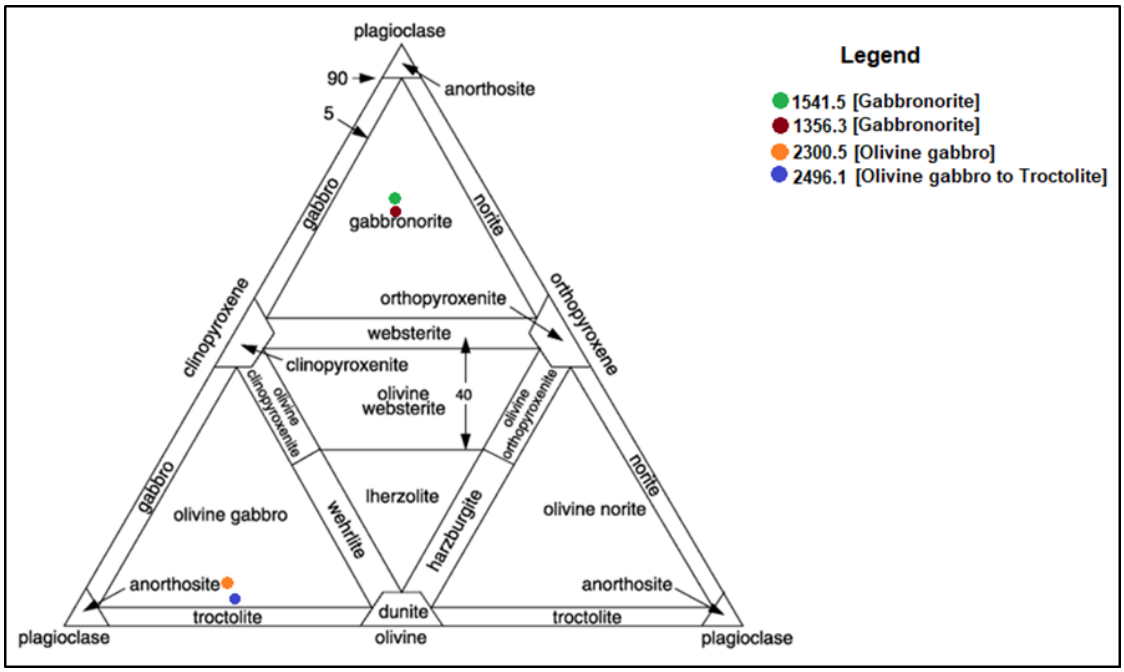

Figure 5.10: Modal composition of some NP1 gabbronorite and gabbroic samples plotted on the IUGS classification diagram for mafic and ultramafic rocks (modified after La Maitre, 2002)

The olivine-rich gabbroic rocks section below the 2158 m depth (contact) to the end of hole at 2500 m have similar characteristics to the Upper Zone of the Bushveld Complex as described in the eastern and western limbs by von Gruenewaldt (1973). These rocks are rich in fayalitic olivine, magnetite and apatite and display lineation typical for Upper Zone cumulates, which are formed by the preferential orientation of elongated plagioclase crystals. The upper part of the NP1 sequence is not similar to any Bushveld sequence due to very low to non-occurrence of olivine and apatite in the olivine-free fine-grained gabbronorite rocks. The presence of phlogopite phenocrysts in gabbronorites is mineralogical evidence that the gabbronorites are not typical Upper Zone rocks. These phlogopite phenocrysts, as hydrous minerals, could be evidence of fluids related to possible metamorphism of the gabbronorites sequence.

Chapter 6

Whole rock geochemistry

6.1 Introduction

Whole rock geochemical analysis was carried out after petrographical analysis to obtain more data on the NP1 core. Forty (40) samples were analysed for major and trace elements. This chapter aims to present the whole rock geochemistry results and highlight the geochemical compositional variations of different rock types.

6.2 Method

Forty (40) samples were prepared (crushed and milled) for whole rock geochemical analysis using X-ray Fluorescence Spectrometry. The process was achieved by using pressed pellets and fusion disks for trace and major element analysis respectively, which resulted in acquiring more data on the NP1 core thus increasing data confidence. This process was performed in the Earth Lab at the University of the Witwatersrand, Johannesburg, South Africa.

6.2.1 Sample preparation

6.2.1.1 Pressed pellets

Sample preparation of pressed pellets involves grinding a sample to very fine particle size, followed by using a binder (Mowiol) to glue the sample together. Once the sample has been glued, the material is pressed in a pellet die using a hydraulic sample press. The pressure should be 10 tons to fully compress the sample so that no void spaces remain in the pellet.

6.2.1.2 Fusion disks

Below are the steps taken to prepare fusion disks.

I. Place all clean Pt crucibles and porcelain loss on ignition (LOI) dishes in the furnace at 1020°C for half an hour to remove any organic residue.

II. Once clean and cool place approximately 1 g of each sample into each LOI dish. Recording both the LOI dish ID number and the weight of the loss on ignition (LOI) dish before and after addition on the weight chart on the laptop. Ignite at 1020°C for 40 minutes. Once complete remove from the furnace and allow to cool in a desiccator.

III. Weigh approximately 1.75 g of flux (Spectroflux 105) into each Pt crucible. Recording both the Pt crucible ID number and the weight of the Pt crucible before and after addition on the weight chart on the laptop. Ignite at 1020°C for 40 minutes. Once complete remove from the furnace and allow to cool in a desiccator.

IV. Switch on the hot plate in the furnace room (must be on for a minimum of 1 hour.

V. Once both the LOI and the Pt crucibles are cool measure and record the after-ignition weights of the LOI dishes to determine the loss on ignition of the samples. Similarly, measure and record the after-ignition weights of the Pt crucibles to obtain the actual flux weights.

VI. Using the Pt crucible ID and LOI dishes ID number to match the samples (see weighing sheet). Measure approximately 0.34 g of pre-ignited sample into each corresponding Pt crucible. Record the weight of the Pt after the addition. Ignite at 1020°C for 50 minutes. Once complete remove from the furnace and allow to cool in a desiccator. Once cool if there are solid particles still present in the fused mixture reignite for an additional half an hour.

VII. Weigh and record the Pt crucibles and return to the furnace at 1020°C.

VIII. Individually pour and press the fusion beads on the hot plate. Make sure to lay the Pt crucibles in the same order as the beads are poured. Should any beads contain bubbles or solid material, break and re-pour.

IX. Once all samples are poured and the Pt crucibles are cool, map the crucible IDs so that the beads can be labelled the following day.

X. Allow the beads to sit for 90 minutes on the hot plate, then switch off the hot plate and allow it to anneal overnight.

XI. Clean the Pt crucibles in dilute HCl for 90 minutes on the hotplate and allow cooling overnight.

XII. Transfer the remaining ignited material from the LOI dishes to vials and store for future use. Clean the LOI dishes.

6.2.2 Instrument

The instrument used for whole rock analysis is known as Axios max from Panalytical (Figure 6.1). Major elements are analysed from fusion disks with a program called Super Q, while trace elements are analysed from pressed pellets with a program called ProTrace. The lower detection limit for the trace method is 0.01 ppm for all elements analysed.



Figure 6.1: Axiox max XRF machine (The analytical X-ray company, 2009)

6.3 Results

The analysed samples were taken from gabbronoritic rocks, olivine-rich gabbroic rocks, monzodiorites, mottled anorthosite, plagioclase-magnetite veins, and quartz-feldspathic xenoliths. Major and trace element data for all 40 samples is presented in Appendix C.

6.3.1 Major elements

Table 6.1 shows ranges of some major element concentrations within the two NP1 main packages, olivine-free gabbronorites (1318.35 m to 2158 m) and olivine-rich gabbroic rocks (2158 m to 2500 m).

Table 6.1: Major element concentration ranges within NP1 gabbronorite and olivine-rich gabbroic rocks

Major elements	**Gabbronorite concentration ranges in wt.%**	**Olivine-rich gabbroic rocks concentration ranges in wt.%**
SiO_2	52.10 – 54.51	34.66 – 49.57
Fe_2O_3	5.12 – 13.28	18.69 – 37.06
P_2O_5	0.05 – 0.45	0.22 – 2.12
TiO_2	0.34 – 1.19	1.19 – 5.53
MgO	0.06 – 6.46	0.85 – 3.11

Figure 6.2 shows core NP1 whole rock major element concentrations against depth. From Table 6.1, gabbronorites contain greater SiO_2 within a limited range, whereas olivine-rich gabbros contain lower amounts of SiO_2 at a broader range. Monzodiorites have SiO_2 concentrations of 65.52 wt.% and 63.06 wt.% while quartz-feldspathic xenoliths have 80.93 wt.% and 72.17 wt.% SiO_2 concentrations. Fe_2O_3 concentrations represent total Fe reported from magnetite as well as Fe from fayalitic olivine, resulting in higher Fe_2O_3 ranges in magnetite and olivine-rich gabbroic rocks in comparison to lower concentration ranges within the non-magnetic olivine-free gabbronorite package. The magnetite abundance in olivine-rich gabbroic rocks is responsible for higher TiO_2 concentrations as well.

From petrography (chapter 5), the olivine-rich gabbroic rocks showed greater modal abundance of apatite compared to gabbronorite rocks, hence a higher P_2O_5 range within the olivine-rich gabbroic rocks. Mg is a major component in many mafic rock-forming minerals such as forsteritic (Mg-rich) olivine and pyroxenes (Salminen *et al*., 2005). In NP1 mafic rocks, Mg concentrations are derived from pyroxenes. From NP1 petrography, gabbronorite consists of both clinopyroxenes and orthopyroxenes, while gabbro consists of clinopyroxene and Mg-poor fayalitic olivine, as a result NP1 gabbronorite rocks recorded higher MgO concentrations due to greater modal abundance of pyroxene as compared to gabbroic rocks. Al_2O_3 recorded the highest concentration of 24.31 wt.% at 2377.8 m in mottled anorthosite because of the greater modal abundances of plagioclase in these rocks. This therefore indicates how modal mineralogy of the analysed samples controls the whole rock major element compositions.

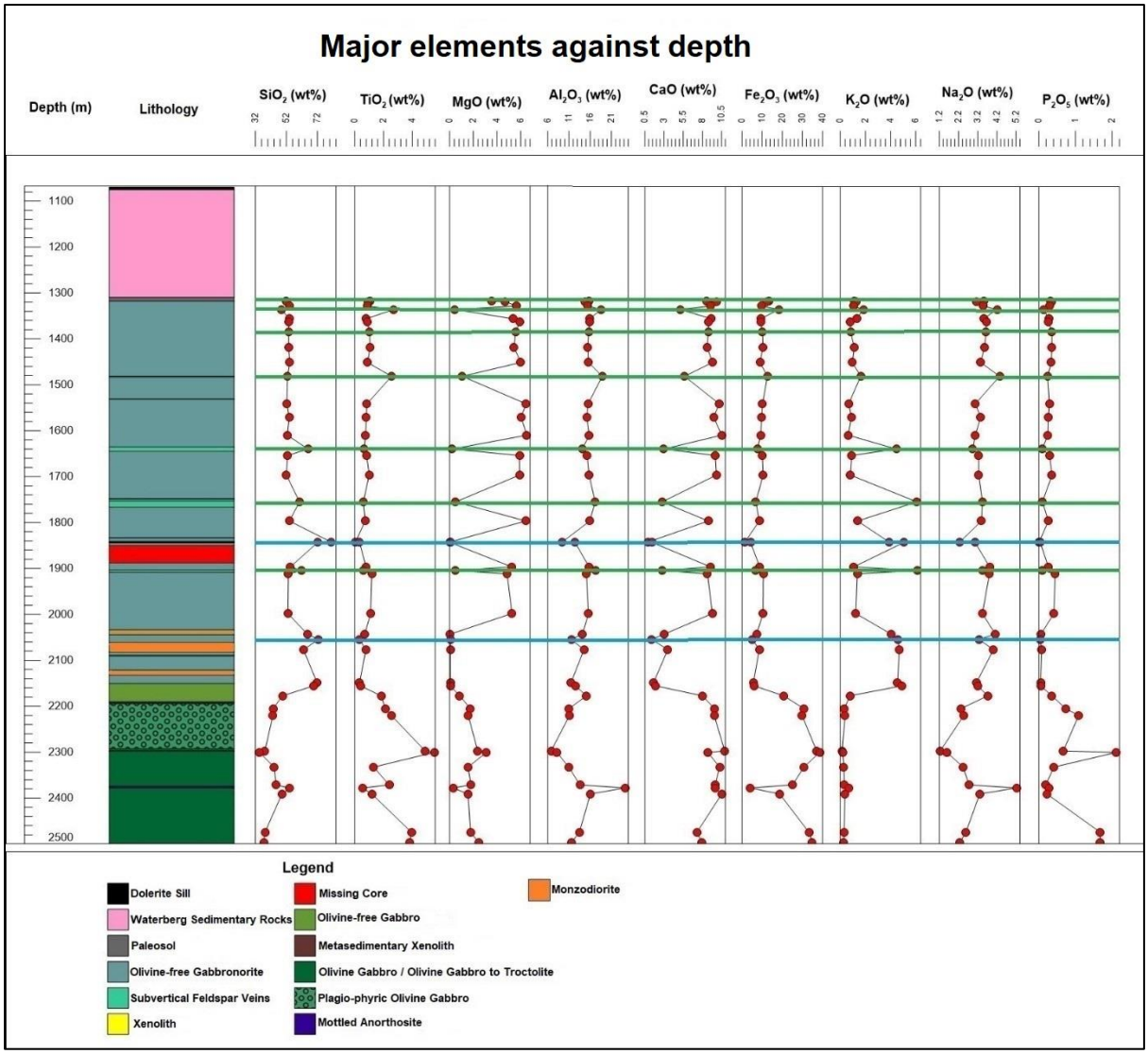

Figure 6.2: Whole rock major elements against depth through core NP1, with plagioclase-magnetite veins and quartz-feldspathic xenoliths represented by green and blue horizontal lines respectively

Two sets of binary diagrams were plotted, with one set representing SiO_2 plotted against other major elements (Figure 6.3) and the second set of diagrams represents MgO being plotted against other major elements (Figure 6.4). These diagrams were plotted to visually clarify the enrichment or depletion of certain major elements and their correlation in certain NP1 rocks. Xenoliths represented in these diagrams are quartz-feldspathic xenoliths and vein types are plagioclase-magnetite veins. SiO_2 and MgO against Fe_2O_3, TiO_2, and P_2O_5 plots show that olivine-rich gabbroic rocks are enriched in these elements in comparison to other NP1 rock types. All SiO_2 diagrams show monzodiorites and quartz-feldspathic xenoliths to be more enriched in SiO_2 as compared to other rock types. MgO against Fe_2O_3, TiO_2, and P_2O_5 diagrams indicate that olivine-free gabbronorites recorded higher MgO concentrations. MgO against Al_2O_3 (Figure 6.4d) shows the highest Al_2O_3 concentration recorded from mottled anorthosite followed by plagioclase-magnetite veins.

Additional binary plots are found in Appendix D and Appendix E.

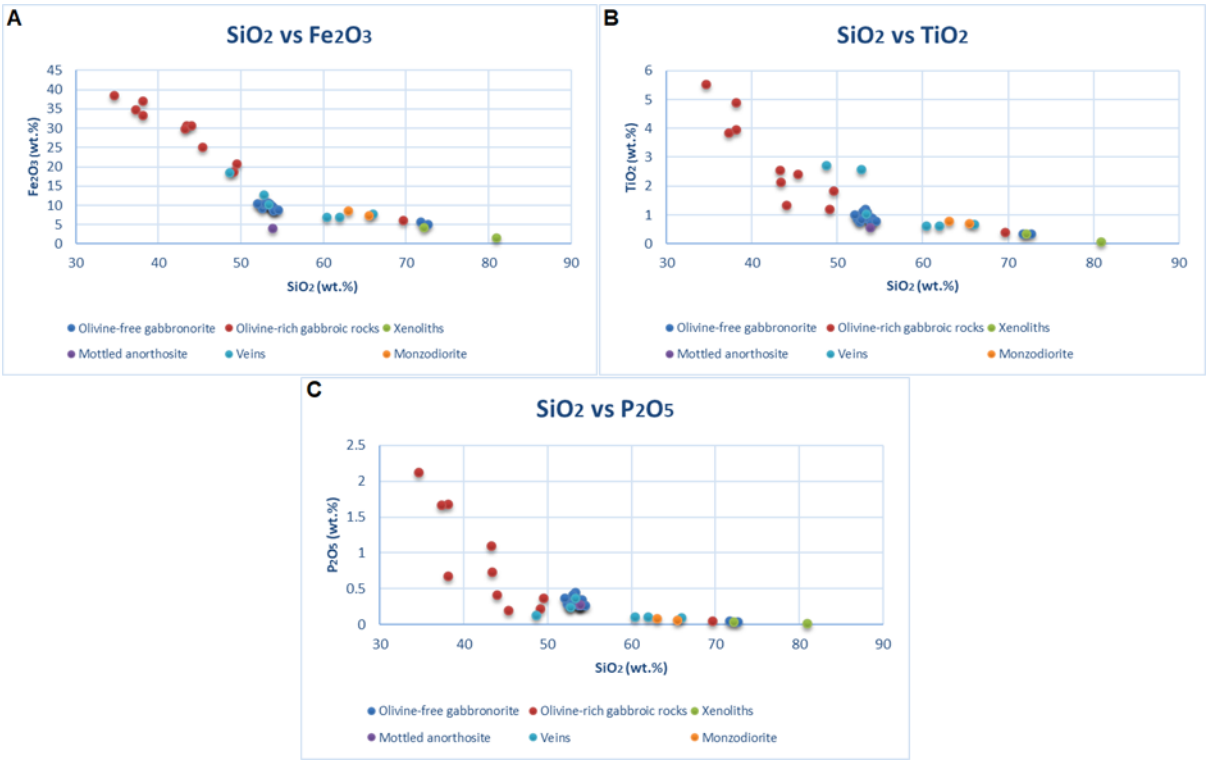

Figure 6.3: Binary plots of SiO_2 vs other major elements [xenoliths = Quartz-feldspathic xenoliths, veins = Plagioclase-magnetite veins], (a) SiO_2 vs Fe_2O_3, (b) SiO_2 vs TiO_2, (c) SiO_2 vs P_2O_5

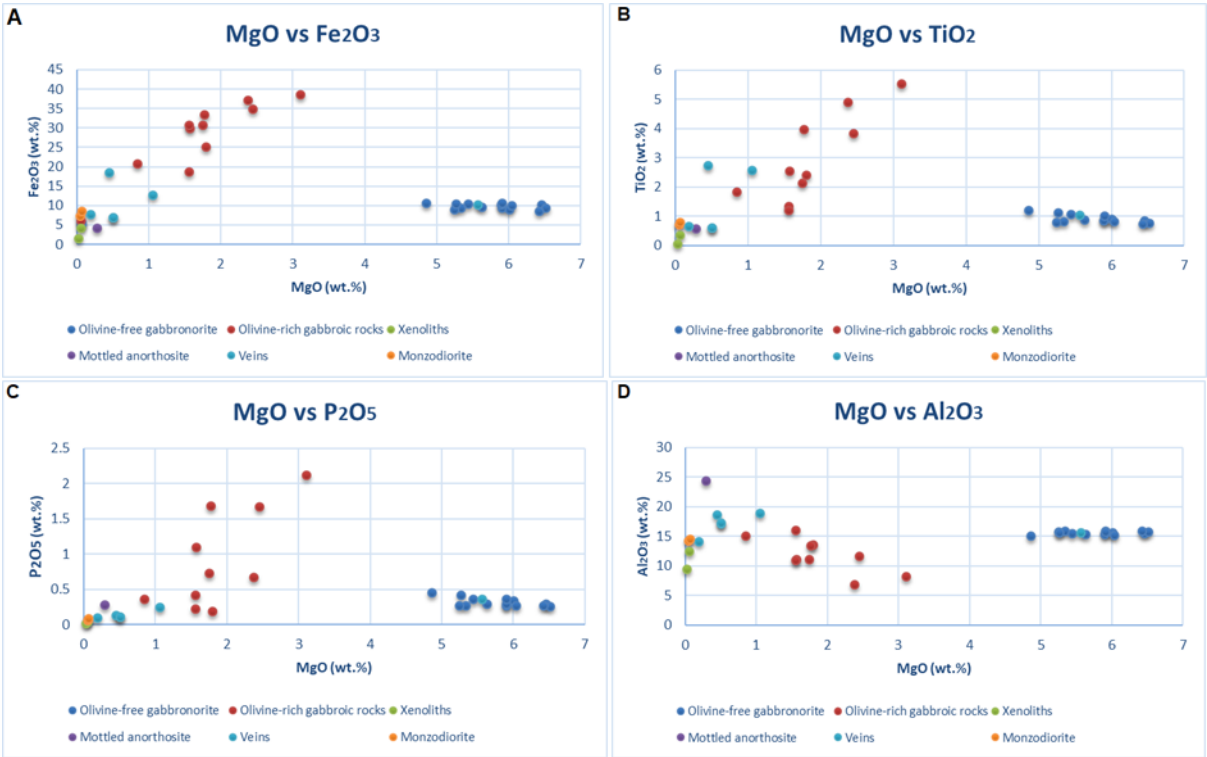

Figure 6.4: Binary plots of MgO vs other major elements [xenoliths = Quartz-feldspathic xenoliths, veins = Plagioclase-magnetite veins], (a) MgO vs Fe_2O_3, (b) MgO vs TiO_2, (c) MgO vs P_2O_5 ,(d) MgO vs Al_2O_3

6.3.2 Trace elements

Table 6.2 shows ranges of some trace elements within olivine-free gabbronorites and olivine-rich gabbroic rocks. The rationale for only representing Cr, Co, Ni and V is to illustrate that similar to major elements, modal mineralogy of the analysed samples controls the whole rock trace element compositions.

Table 6.2: Trace element concentration ranges within NP1 gabbronorites and olivine-rich gabbroic rocks

Trace elements	**Gabbronorite concentration ranges in ppm**	**Olivine-rich gabbroic rocks concentration ranges in ppm**
Cr	52.13 – 221.12	0.75 – 50.63
Ni	28.36 – 105.53	0.32 – 25.13
Co	25.35 – 41.26	0.11 – 23.25
V	120.61 – 179.12	Below detection limit

Figure 6.5 shows NP1 trace elements concentrations against depth. In igneous rocks, Cr is enriched in pyroxenes, amphiboles, spinels and micas (Salminen *et al*., 2005). The source of Cr in NP1 rocks is pyroxenes, hence gabbronorites contains higher Cr concentration as compared to olivine-rich gabbroic rocks as a result of its greater pyroxene content. Salminen *et al* (2005) described Co to be present as an accessory element in pyroxenes, olivine, amphiboles and micas in igneous rocks. Co concentration in NP1 is mainly derived from pyroxenes. This therefore explains the greater Co concentrations in gabbronorites as compared to gabbroic rocks.

Olivine, orthopyroxene and spinel are sources of Ni in igneous rocks (Salminen *et al*., 2005). In NP1 rocks, orthopyroxene is the main Ni enriched mineral. Gabbros comprise a small amount of orthopyroxene (chapter 5) while gabbronorites are made up equal amounts of both orthopyroxenes and clinopyroxenes. As a result, Ni shows greater concentrations in gabbronorites as compared to gabbroic rocks. The abundance of Ni in igneous rocks correlate with that of Co and Cr (Salminen *et al*., 2005).

V is present as a trace element in magnetite, apatite, pyroxenes, micas, and amphiboles (Salminen *et al*., 2005). Concentrations of V in NP1 olivine-rich gabbroic rocks are below the detection limit but detected in gabbronorites. Pb occurs at trace element levels in K-feldspars, plagioclase, micas, zircon, and magnetite (Salminen *et al*., 2005). NP1 plagioclase-magnetite veins have a Pb concentration range of 8.75 ppm to 20.2 ppm. Quartz-feldspathic xenoliths recorded Pb concentrations of 14.78 ppm and 13.97 ppm, while Pb concentrations in monzodiorites were detected to be 21.07 ppm and 14.77 ppm.

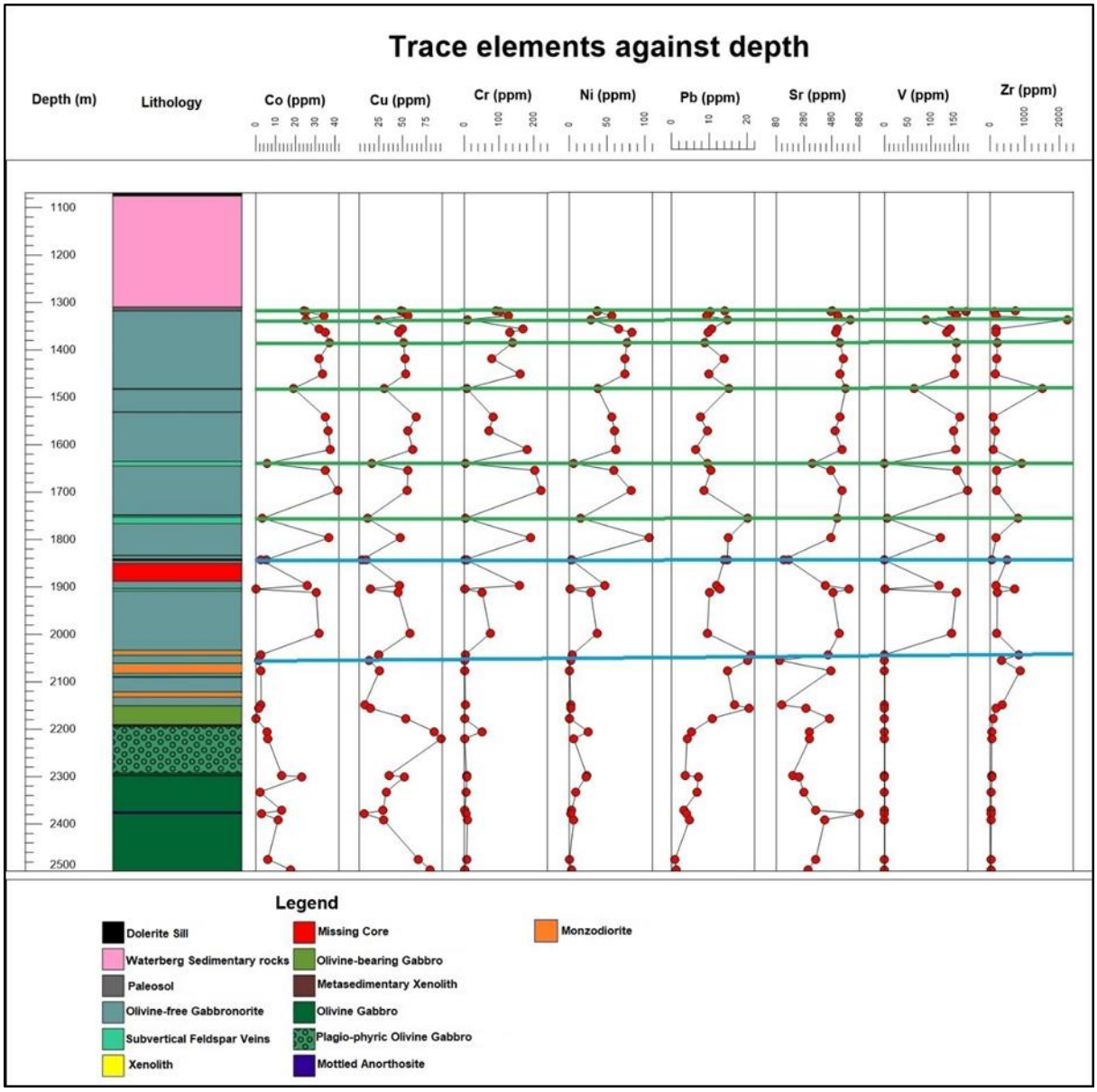

Figure 6.5: Whole rock trace elements against depth through core NP1, with plagioclase-magnetite veins and quartz-feldspathic xenoliths represented by the green and blue horizontal lines respectively

Cr against other trace elements binary diagrams are shown in Figure 6.6. Similar to major elements, these diagrams are plotted to visually clarify the enrichment or depletion of certain trace elements in various NP1 rocks. Xenoliths represented in the plots are quartz-feldspathic xenoliths and represented veins are plagioclase-magnetite veins. Figure 6.6a, b and c show Co, Ni, Cr, and V concentration to be higher in gabbronorites and lower in olivine-rich gabbroic rocks. Cr vs Pb (Figure 6.6d) shows monzodiorites, plagioclase-magnetite veins, and quartz-feldspathic xenoliths to be more enriched in Pb in general.

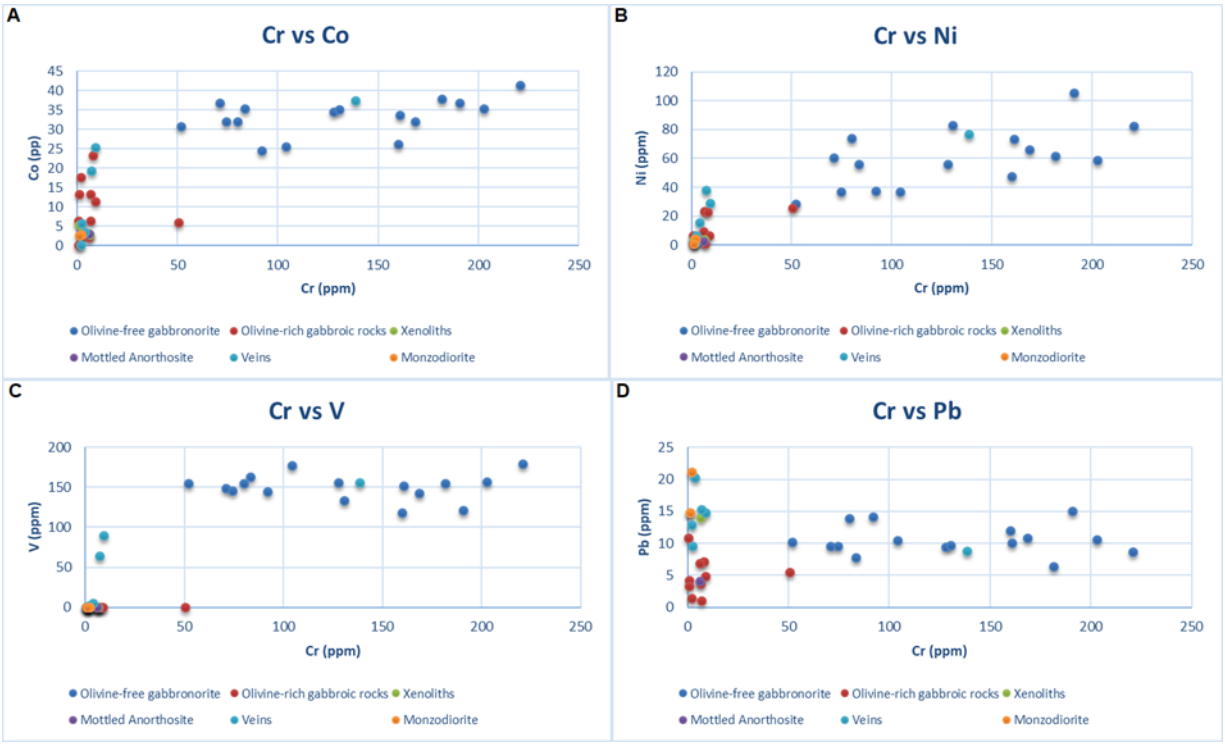

Figure 6.6: Binary plots of Cr vs other trace elements [xenoliths = Quartz-feldspathic xenoliths, veins = Plagioclase-magnetite veins], (a) Cr vs Co, (b) Cr vs Ni, (c) Cr vs V, (d) Cr vs Pb

6.3.3 Ratios

The $CaO:Al_2O_3$ ratio can be used to compare the enrichment of clinopyroxene to plagioclase. Pure plagioclase has a $CaO:Al_2O_3$ ratio of 0.6, and any significant deviation from 0.6 suggests the presence of clinopyroxene (Kinnaird, 2005a). The ratio is approximately 0.6 for most samples within gabbronorites and deviates from 0.6 within the olivine-rich gabbroic rocks (Figure 6.7). This deviation indicates the presence of clinopyroxene in greater concentrations as compared to orthopyroxenes in gabbroic rocks.

The Al_2O_3:FeO+MgO ratio varies with changing pyroxene to plagioclase proportions (Kinnaird, 2005a) and sudden changes may indicate whether more than one magma was involved in forming the NP1 sequence. The ratio results in Figure 6.7 show sudden changes due to an increase in Al_2O_3 concentration associated with feldspars at 1842.5 m (7.64 wt.%) where there is quartz-feldspathic xenolith and at 2177.8 m (6.78 wt.%) in mottled anorthosite. The sudden ratio change at 1842.5 m indicates an introduction of a different magma, which is very likely considering that it is a quartz-feldspathic xenolith. However, mottled anorthosite was formed from the same magma as the associated NP1 gabbroic rocks and gabbronorites and the ratio change reflects an increased alumina concentration in the anorthosite.

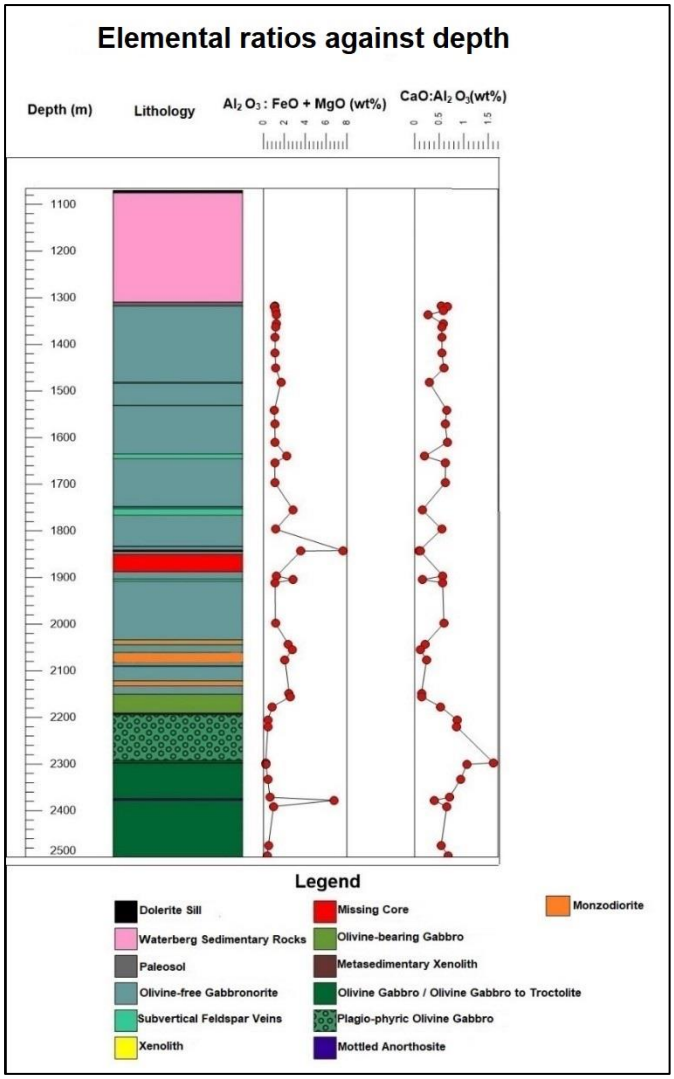

Figure 6.7: Element ratios against depth in core NP1

6.4 Discussion and conclusion

Whole rock geochemical analysis increased data confidence in the petrographic classification of the rock types and showed elemental variations through the NP1 core. Gabbronorites are more enriched in SiO_2, Co, Cr, Ni and V compared to olivine-rich gabbroic rocks which are more enriched in Fe and P compared to gabbronorites. This illustrates how modal mineralogy controls the major and trace element compositions. Elemental ratio data indicated that more than one magma was involved in the formation of NP1 rocks with quartz-feldspathic xenoliths being formed from a different magma to the gabbroic rocks and gabbronorites. Isotope geochemistry data interpretation in the next chapter will provide more data confidence on further interpretation of NP1 core.

Chapter 7

Sr isotope geochemistry

7.1 Introduction

Twenty-one (21) samples with fresh, unaltered plagioclase were selected for in situ Sr isotope analysis using laser ablation multi-collector ICPMS. The results are presented in Appendix F and were compared with the Sr isotope data of the northern limb Upper Zone and of the Waterberg Project area from Mangwegape *et al* (2016) and Huthmann *et al* (2017) respectively. This comparison was used to further elucidate the relationship between lithologies of the NP1 sequence and the Bushveld Upper Zone. The aim of this chapter is to present and interpret the Sr isotope data for plagioclase from the NP1 sequence.

7.2 Method

Initial Sr isotopic ratios were calculated based on the results from the laser ablation multi-collector ICPMS (Figure 7.1). The results were collected from analysing fresh, unaltered plagioclase grains from 21 polished thin sections at the University of Johannesburg, South Africa. The suitable plagioclase grains were selected under optical microscope and mapped on printed photos prior to analysis. A total of 143 analyses were done, with the number of analyses per thin section ranging from a minimum of 5 to a maximum of 11. The table in Appendix F shows total number of analyses per sample.

7.2.1 Sample preparation

Sample preparation involved soaking thin sections in an ultra-sonic buffer to clean the surface and remove loose particles. An in-house plagioclase glass and USGS reference glass BHV02G were used as secondary standards for accuracy evaluation. The standards were measured at regular intervals and treated as unknowns and yielded desired results.

7.2.2 Equipment

Samples were placed on the stage, put in the laser ablation system and exposed to helium and argon gas. The argon gas carrying positive ions is transported to the Plasma unit where ions are separated according to their mass/charge ratio by the mass filter. The Nu Plasma is equipped with 16 Faraday detectors and five ion counters allowing all isotopes of interest to be measured simultaneously. Background signal was collected on mass prior to ablations and subtracted from the signal to account for background correction. With regards to calculating mass bias correction for Sr, ^{86}Sr and ^{88}Sr were used based on invariant ratio of 0.1194, and the $^{87}Rb/^{85}Rb$ mass bias and laser induced fractionation was calculated by adjustment relative to Sr by adjustment to obtains the correct ratios for USGS reference glass BHV02G.

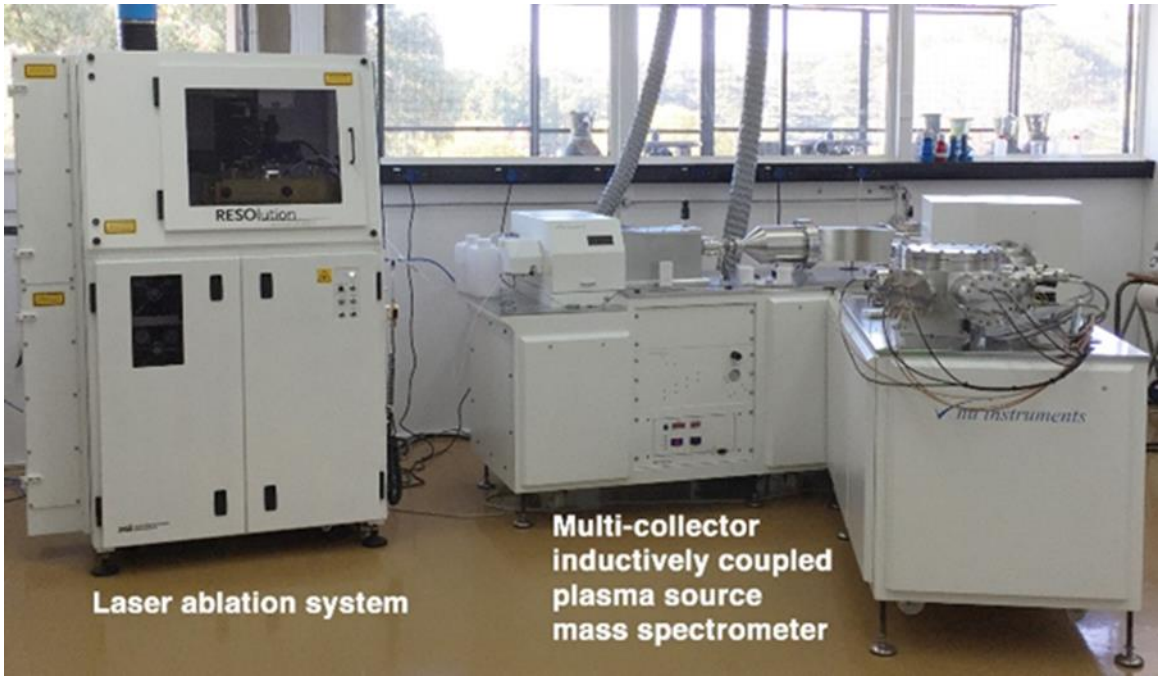

Figure 7.1: Laser Ablation Multi-collector ICPMS (LA-MC-ICPMS Laboratory, University of Johannesburg, 2018)

7.3 Results

Initial $^{87}Sr/^{86}Sr$ ratios were calculated for an age of 2.05 Ga (Zeh *et al*., 2015) using a decay constant of $11{:}393x10^{-11}$ y^{-1} (Nebel *et al*., 2011). Figure 7.2 represents initial Sr ratio results plotted against depth to indicate isotopic signature throughout the NP1 sequence. From a depth of 1318 m to 1451 m (gabbronorites), the initial $^{87}Sr/^{86}Sr$ ratio range from 0.7045 – 0.7063. From 1570 m to 1796 m (gabbronorites), initial Sr ratio range from 0.7042 – 0.7055. The quartz-feldspar-plagioclase veins at 1904.5 indicate a wide initial $^{87}Sr/^{86}Sr$ ratio range from 0.7052 – 0.7072, average 07061. At 1998 m within gabbronorites, a narrow initial $^{87}Sr/^{86}Sr$ ratio range is identified from 0.7052 – 0.7059. The olivine-rich gabbroic rocks package has an initial $^{87}Sr/^{86}Sr$ ratio range from 0.7064 – 0.7073 (average 0.7070), from a depth of 2177 m to 2496 m. The total initial $^{87}Sr/^{86}Sr$ ratio range for gabbronorites is between 0.7042 – 0.7066, with an average of 0.7052.

Analytical uncertainties were calculated as 2 standard deviations of measurements and are in the range of 0.000068 – 0.000161 from 1318 m to 1451 m. From 1570 m to 1796 m, the uncertainty range between 0.000078 – 0.000163, from 1896 m to 1911 m it ranges between 0.000085 – 0.000191. From 2177 m to 2496 m the analytical uncertainty ranges between 0.000097 to 0.000188.

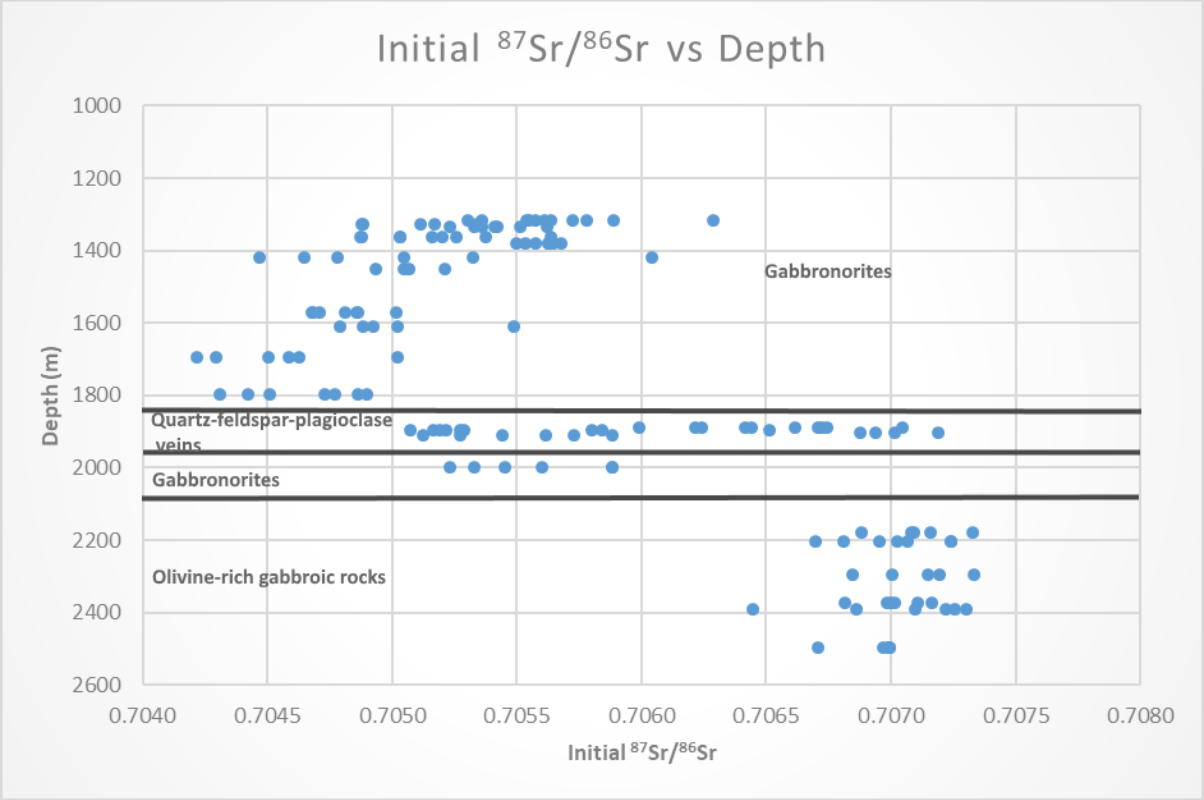

Figure 7.2: NP1 initial $^{87}Sr/^{86}Sr$ against depth

7.4 Discussion and conclusion

The NP1 gabbronorite package has a plagioclase initial $^{87}Sr/^{86}Sr$ ratio range of 0.7042 – 0.7063. The section of quartz-feldspar-plagioclase veins indicates a wide range from 0.7051 – 0.7072. Olivine-rich gabbroic rocks show a homogeneous initial $^{87}Sr/^{86}Sr$ ratio range from 0.7064 – 0.7073. The low initial $^{87}Sr/^{86}Sr$ isotope values of the gabbronorites (ca. 0.7042) are less radiogenic than typical Upper Zone values (0.7063 – 0.7079, in the northern limb as determined by Mangwegape *et al.*, 2016). Mangwegape *et al* (2016) reported initial Sr isotope data for plagioclase. It is inferred that the less radiogenic Sr isotope values in NP1 gabbronorites has been produced by the modifying effects of fluids related to metamorphism. Field relations between the Bushveld Complex and Dullstroom Formation discussed in chapter 8, section 8.2.1, are evidence that the up-section of NP1 core (gabbronorite package) has been metamorphosed.

The initial Sr isotope ratio range of NP1 olivine-rich gabbroic rocks is between 0.7064 – 0.7073. This range correlates with Sr isotope data from the Upper Zone for the Bellevue (BV-1) and Moordekopje (MO-1) cores analysed by Mangwegape *et al* (2016) which ranges from 0.7063 - 0.7079. The initial $^{87}Sr/^{86}Sr$ ratio range of NP1 olivine-rich gabbroic rocks also correlates with the Waterberg Project far northern limb Upper Zone with an initial $^{87}Sr/^{86}Sr$ ratio range of 0.7063 – 0.7075 analysed by Huthmann *et al* (2017). The analysed plagioclase crystals of the Waterberg Project Upper Zone are from magnetite-bearing gabbros and gabbronorites (Huthmann *et al.*, 2017).

A more detailed data comparison of NP1 core with the Bushveld northern limb, Waterberg Project and Dullstroom Formation is presented in the next chapter, using classified rock types, petrography, whole rock geochemistry data as well as Sr isotope data.

Chapter 8

Discussion and Conclusion

8.1 Introduction

To further understand and put into perspective the stratigraphic connection between the NP1 drill core, the Bushveld Complex and the Dullstroom Formation, the discussion and comparisons of petrographic observations, whole rock major and trace element geochemistry as well as initial Sr isotopic results are emphasised in this part of the report. This chapter also aims to provide a synopsis on the relationship between the NP1 sequence, the Bushveld Complex in the northern limb, the Waterberg Project and the Dullstroom Formation of the Rooiberg Group.

8.2 Discussion

8.2.1 Stratigraphic correlation between the Bushveld Complex and Rooiberg Group

The Rooiberg Group is made up of four formations, namely; Dullstroom, Damwal, Kwaggasnek and Schrikklof Formations (Schweitzer *et al*., 1995). Some authors interpreted the Rooiberg volcanics as a result of comets and asteroids impact (e.g. Rhodes, 1975; lston, 1992) and others as a result of subduction zone magmatism (Buchanan *et al*., 1999). Figure 8.1 shows the stratigraphy of the Rooiberg Group.

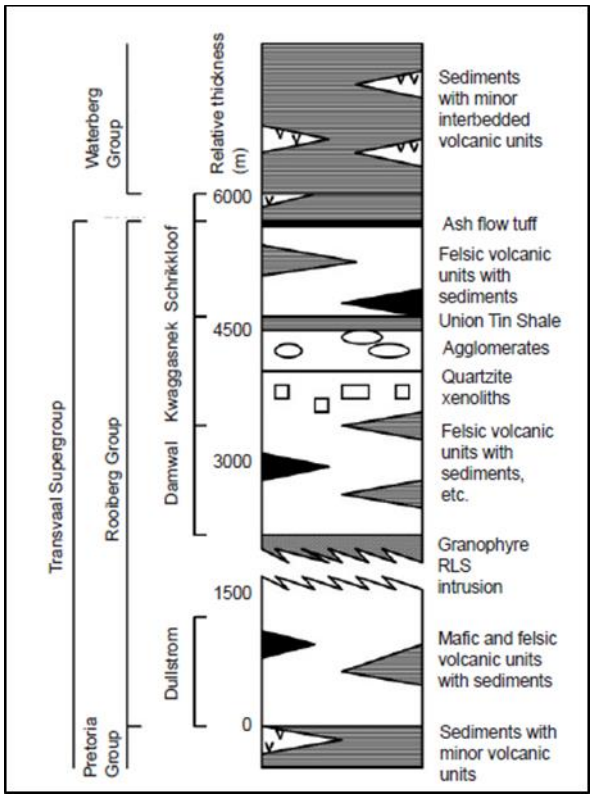

Figure 8.1: Generalised stratigraphic column of the Rooiberg Group as proposed by Schweitzer *et al* (1995). Adapted from Cheney and Twist (1991), Council for Geosciences, (1978), Eriksson *et al* (1994), and Schweitzer *et al* (1995). Scale in metres shows approximate thickness of units (from Buchanan *et al*., 1999)

The emplacement of the Rustenburg Layered Suite (RLS) was not entirely conformable and it is located stratigraphically higher in the northern part of the Bushveld Complex compared to the southern part (Buchanan *et al*., 2004). The RLS thermally metamorphosed the lower two formations (Dullstroom and Damwal) of the Rooiberg Group and the Lebowa Granite Suite (LGS) metasomatically altered the

entire group, particularly in the north western part (Buchanan, 2006). The South African Committee for Stratigraphy (1988) classified the Dullstroom Formation as occurring below the level of intrusion of the RLS and consisting of roughly 80 flows of predominantly basaltic andesite composition with minor basalt, dacite, and rhyolitic units (Harmer and Farrow, 1995). The Rooiberg acid eruptives form the roof of the RLS in the Loskop Dam area and in the south eastern part of the Bushveld Complex (Harmer and Farrow, 1995).

The RLS cuts across the Pretoria Group in the south eastern part of the Bushveld Complex. At the Loskop dam area, the RLS splits the Dullstroom Formation into upper and lower Dullstroom Formation as shown in Figure 8.2a (Lenhardt and Eriksson, 2012; Harmer and Farrow, 1995). At the same south eastern part of the Bushveld Complex, the RLS splits the Damwal Formation at the Stofberg area (Figure 8.2b, Lenhardt and Eriksson, 2012). Figure 8.3 shows locations of the Loskop dam and Stofberg area circled in black. The emplacement of the RLS at different stratigraphic levels as illustrated in Figure 8.2 a and b confirms that it was not entirely conformable. For the NP1 sequence, it is suggested that the RLS (Upper Zone) intruded the Dullstroom Formation rocks which form the immediate roof of the RLS in the area.

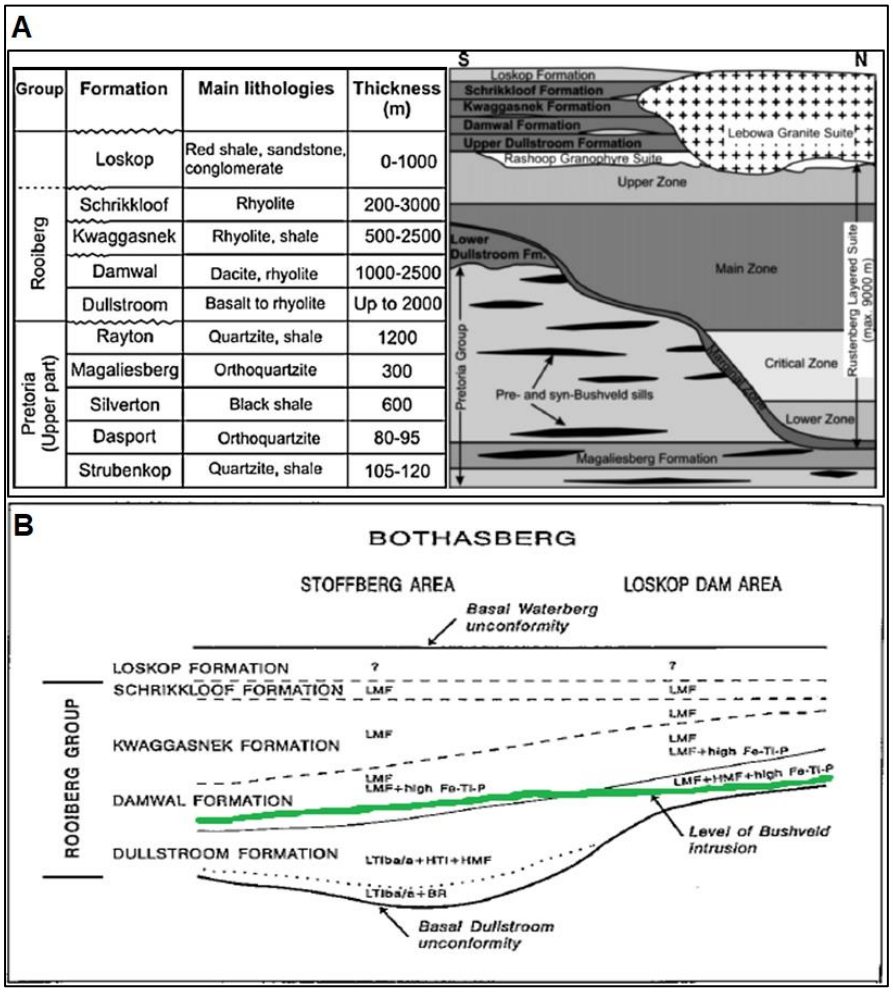

Figure 8.2: Diagrams showing the emplacement of the Rustenburg Layered Suite , (a) Schematic north-south section in the Loskop Dam area showing the relationship between the Rooiberg Group, the underlying Pretoria Group (Transvaal Supergroup), and the intrusions o the Rustenburg and Lebowa Granite Suite. Modified after SACS (1980), Walraven (1982), Harmer and Sharpe (1985) and Schweitzer *et al* (1995) (from Lenhardt and Eriksson, 2012), (b) Reconstructed emplacement level of the Rustenburg Layered Suite (in green) for the eastern portion of the Bushveld Complex using the lithological and geochemical characteristics of the volcanic rocks of the Rooiberg Group (modified from Schweitzer *et al*., 1995)

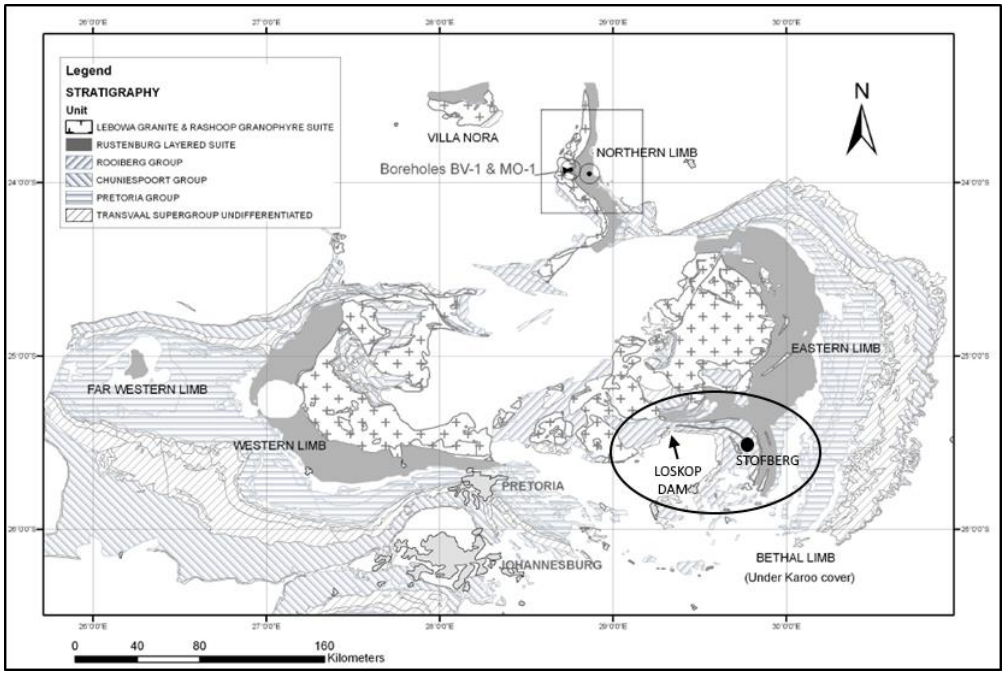

Figure 8.3: Geological map showing locations of the Loskop dam and Stofberg area (modified from Roelofse, 2010)

8.2.2 Rock composition of the Dullstroom Formation

The Dullstroom Formation is mostly completely exposed in the south eastern part of the Bushveld Complex (Schweitzer *et al*., 1999). The Formation represents an approximately 1-2 km thick laterally extensive sequence that is made up of basaltic to andesitic volcanic flows interbedded with subordinate felsic volcanic units and thick sedimentary strata (Schweitzer *et al*., 1999). Lenhardt and Eriksson (2012) described the Dullstroom Formation volcanic rocks to be basaltic to rhyolitic in composition. These rocks are moderately metamorphosed and consist of a fine-grained groundmass with variable minor proportions of phenocrysts, porphyroblasts, and zoned amygdales (Buchanan *et al*., 2004).

8.2.3 Whole rock geochemistry of the Dullstroom Formation

Buchanan *et al* (1999) sampled the Dullstroom Formation strata in two areas of the south eastern Bushveld Complex (Figure 8.4, area 1 and 2; Buchanan *et al*., 1999). A total of 24 samples were analysed by XRF, of which 3 samples represent sedimentary units and the remaining 21 samples are volcanic rocks. Dacites and rhyolites of the Upper Dullstroom Formation throughout the Kwaggasnek Formation were derived from low Ti melts by assimilation and fractional crystallisation in a crustal magma chamber. The high Ti suite of volcanic rocks represents a petrogenetically unrelated sequence (Buchanan *et al*., 1999).

Figure 8.5a (Buchanan *et al*., 1999) shows the compositional contrast between the low Ti and high Ti suites. The low Ti Dullstroom Formation classification based on SiO_2 vs Na_2O+K_2O show SiO_2 range between 53-57 wt.% and Na_2O+K_2O range between 3-4 wt.% whereas high Ti Dullstroom Formation SiO_2 ranges between 56-60 wt.% and Na_2O+K_2O between 4-6 wt.%. The low Ti Dullstroom Formation rocks are of basaltic to basaltic-andesite composition while the high Ti Dullstroom Formation rocks are of basaltic andesite to andesite composition (Buchanan *et al*., 1999). Other compositional differences are plotted in Figure 8.5b (SiO_2 vs TiO_2) and Figure 8.5c (Al_2O_3 vs P_2O_5). On average, the Al_2O_3 concentrations are higher while TiO_2 and P_2O_5 concentrations are lower for low Ti volcanic rocks than those of high Ti volcanic rocks (Buchanan *et al*., 1999).

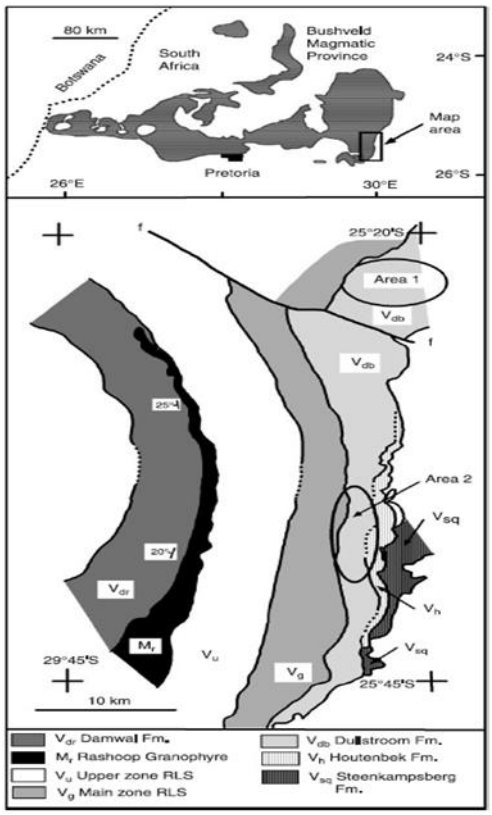

Figure 8.4: Generalised geological map of the south-eastern portion of the Bushveld Complex after the Council for Geoscience (1978). Sampling locations for the analysed material are concentrated in areas 1 and 2 (from Buchanan *et al*., 1999)

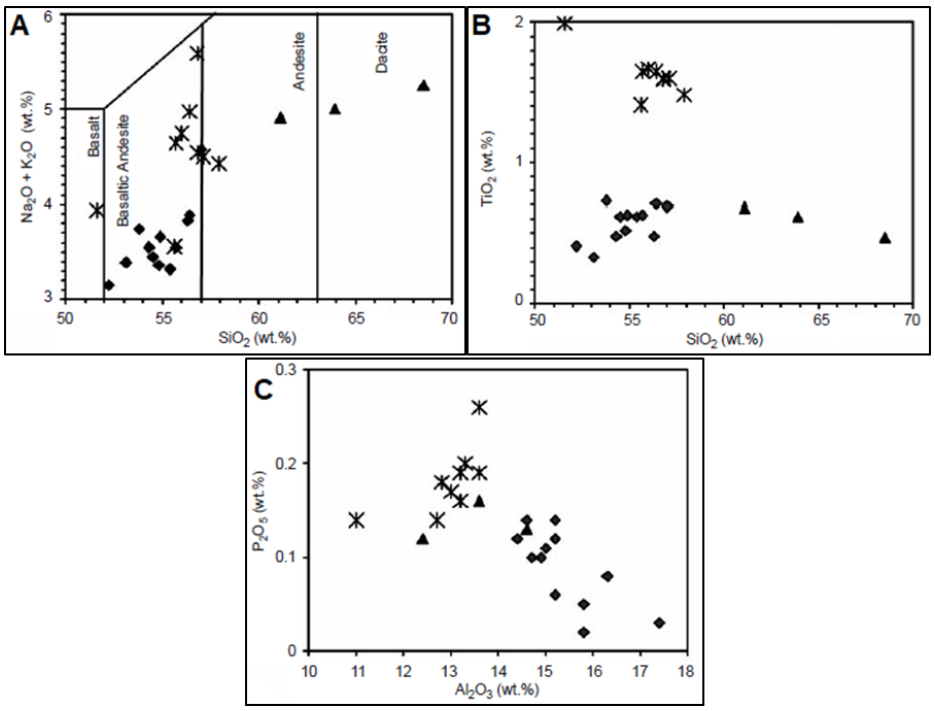

Figure 8.5: Dullstroom Formation major elements plots, (a) Classification system for Dullstroom Formation volcanic rocks based on SiO_2 (wt. %) vs $Na_2O + K_2O$ (wt. %) after Le Bas *et al* (1986). (b) SiO_2 (wt. %) vs TiO_2 (wt. %) and, (c) Al_2O_3 (wt. %) vs P_2O_5 (wt. %) for volcanic units of the Dullstroom Formation. High Ti rocks represented by asterisks, low Ti (filled diamonds), and high Mg felsic represented by filled triangles (all Figures from Buchanan *et al*., 1999)

8.2.4 Sr Isotopes of the Bushveld Complex, Waterberg Project and Dullstroom Formation

Mineral exploration in the Bushveld Complex mafic and ultramafic rocks has increased in recent years in the northern limb (Huthmann *et al*., 2017). As a result, academic research has focused on the area and several studies that were done by authors such as Roelofse and Ashwal (2012) and Mangwegape *et al* (2016) have included Sr isotope data. These results assist in understanding the petrogenetic evolution and highlight the similarities and differences between the northern limb and other limbs of the Bushveld Complex (Huthmann *et al*., 2017). Cawthorn *et al* (1985) and Barton *et al* (1986) were the first to analyse Sr isotopes of the PGE-rich samples of the northern limb. Cawthorn *et al* (1985) reported the initial $^{87}Sr/^{86}Sr$ ratios (Sri) of 0.7104 to 0.7227 with an average of 0.7160 for the Platreef and initial $^{87}Sr/^{86}Sr$ ratio (Sri) of 0.7079 for the overlying gabbro. Barton *et al* (1986) reported Sri ranging from 0.7107 to 0.7226 for Platreef samples overlying granite footwall and Sri ranging from 0.7054 to 0.7147 for Platreef overlying dolomitic footwall.

In the western limb, Kruger (1994) divided the Bushveld succession into two stages which are the integration and differentiation stages, based on the measured Sr isotopic composition. The integration stage includes the Lower Zone, Critical Zone and Lower Main Zone that display an irregular upward increase in Sri from 0.7047 to 0.7091 and it is interpreted to be the result of repeated influxes of magma (Kruger, 1994). The Main Zone and Upper Zone are a part of the differentiation stage and characterised by a constant Sri of 0.7083 up to the level of the pyroxenite marker where the values decrease to 0.7073 (Huthmann *et al*., 2017). Latest isotope analysis techniques such as in-situ laser ablation multi-collector ICPMS are increasingly applied (Huthmann *et al*., 2017) and more efficient because inclusions in plagioclase grains can be avoided during analysis.

Mangwegape *et al* (2016) analysed 27 samples using in situ LA-ICPMS, covering the entire stratigraphy of the northern limb of the Bushveld Complex. Thirteen polished thick sections were prepared from samples of BV-1 and 14 from MO-1 drill holes (Figure 8.6 shows BV-1 and MO-1 locations; cropped from Roelofse, 2010). The data shows that the Lower Main Zone has an average initial $^{87}Sr/^{86}Sr$ ratio (Sri) of 0.7088 with individual values ranging from 0.7075 to 0.7106, in line with values published by Roelofse and Ashwal (2012). The Upper Main Zone has an average Sri of 0.7070 (0.7069 – 0.7087) and the Upper Zone has an average Sri of 0.7073 with values ranging from 0.7063 to 0.7079 (Mangwegape *et al*., 2016).

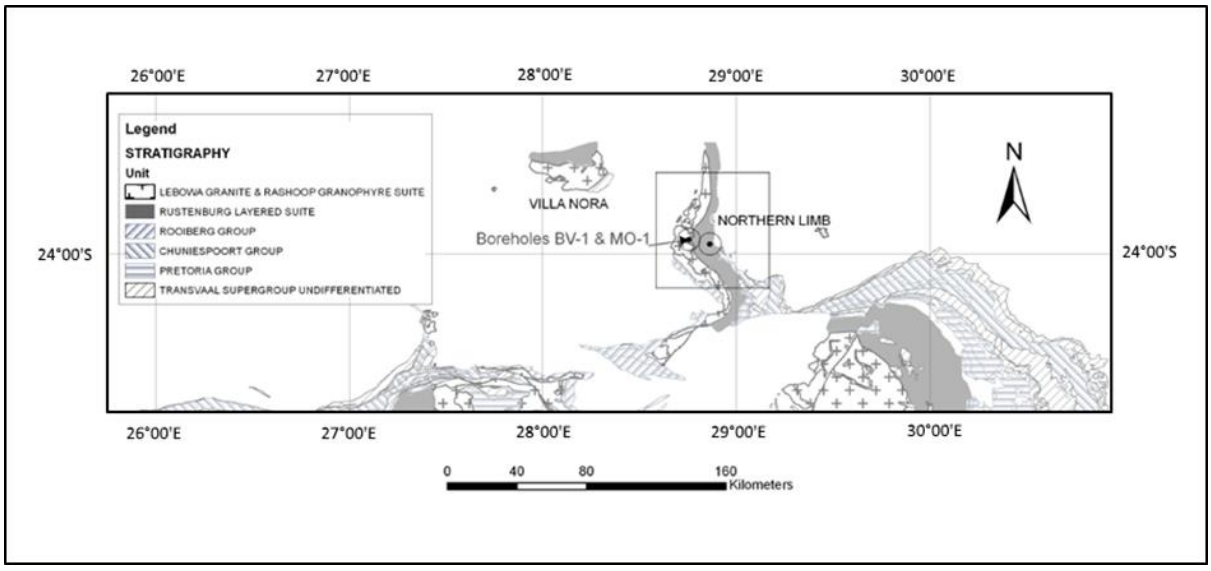

Figure 8.6: Geological map showing the locations of borehole BV-1 and MO-1 (cropped from Roelofse, 2010)

The mafic to ultramafic rocks and the associated PGE deposits of the Waterberg Project, located far north of the Bushveld Complex northern limb (Figure 8.7a; Kinnaird *et al*., 2017), were discovered in 2011 and have not previously been investigated in any detail (Huthmann *et al*., 2017). Huthmann *et al* (2017) provided the in situ Sr isotopic data for plagioclase grains of these Bushveld-age rocks located immediately north of what has previously been regarded as the northern limit of the northern limb, the Hout River Shear Zone. The Waterberg Project lithology includes Waterberg group sedimentary rocks, Upper Zone, Troctolite-Gabbronorite-Anorthosite (TSA) sequence and the Ultramafic sequence (Figure 8.7b; Huthmann *et al*., 2017).

The Upper Zone (magnetite-bearing gabbro and gabbronorite) plagioclase grains have an average initial $^{87}Sr/^{86}Sr$ ratio of 0.7069 and range from 0.7063 to 0.7075 (Huthmann *et al*., 2017). A feldspathic pyroxenite sample hosting the T zone mineralisation has initial $^{87}Sr/^{86}Sr$ ratio values ranging between 0.7063 – 0.7069 (average 0.7066), while the mineralised gabbronorites below the T zone have values ranging from 0.7066 – 0.7072 (average 0.7069) (Huthmann *et al*., 2017). Gabbronorites and norites of the upper part of the TGA (Troctolite-Gabbronorite-Anorthosite) sequence have an initial $^{87}Sr/^{86}Sr$ ratio range of 0.7061 – 0.7074, and an average of 0.7069 (Huthmann *et al*., 2017). The lower part of the TGA sequence consists of troctolite with 0.7068 – 0.7079 initial $^{87}Sr/^{86}Sr$ ratio range and an average of 0.7072 (Huthmann *et al*., 2017). A harzburgite sample from the Ultramafic Sequence has an initial $^{87}Sr/^{86}Sr$ ratio ranging from 0.7068 – 0.7076 with an average of 0.7072 (Huthmann *et al*., 2017).

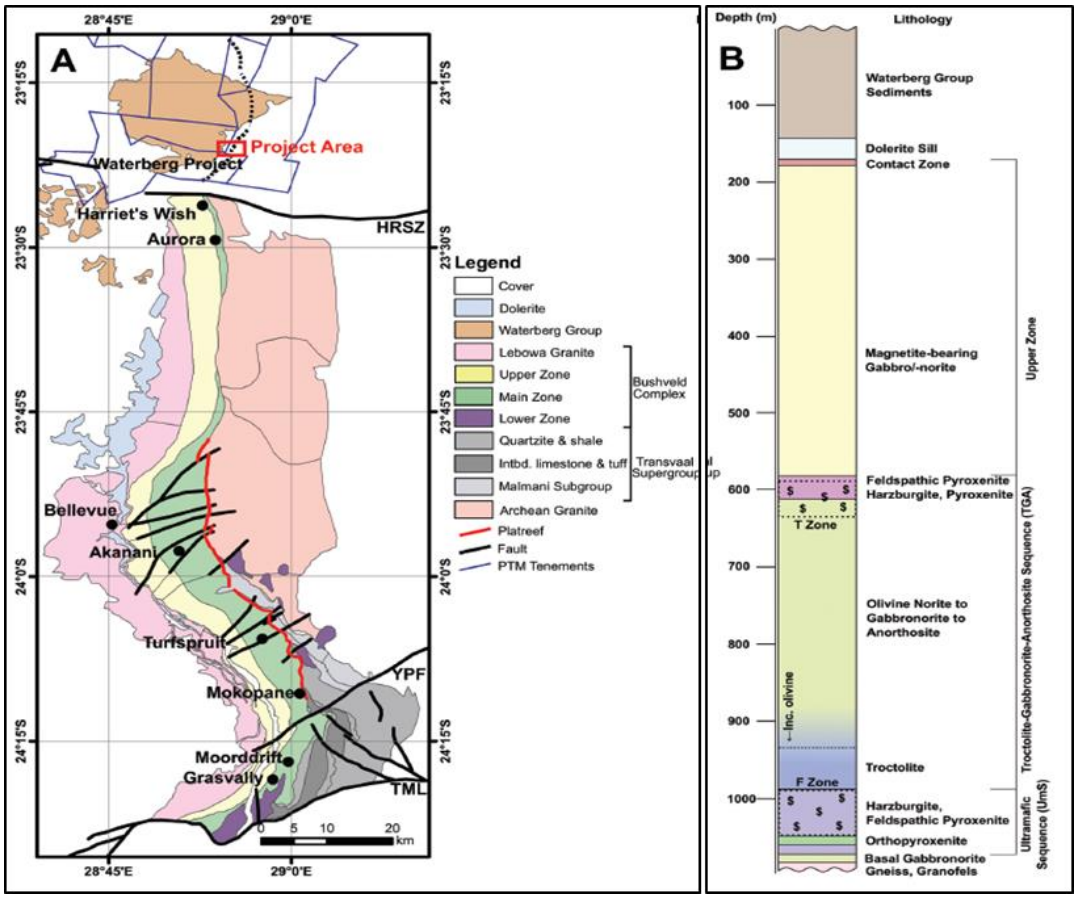

Figure 8.7: Geology of the northern limb of the Bushveld Complex, (a) Map showing the Waterberg Project location. HRSZ = Hout River Shear Zone, PYF = Planknek-Ysterberg Fault, TML = Thabazimbi-Murchison Lineament. (b) Stratigraphy of the Waterberg Project area (from Kinnaird *et al*., 2017)

Kinnard *et al* (2017) concluded that the Waterberg succession (north of Hout River Shear Zone) has unique features which do not directly correlate with those of the northern limb south of the Hout River Shear Zone. These features include the presence of minor anorthosite layers together with harzburgite at the top of the TGA, which is the Main Zone equivalent, and the absence of magnetite layers in the Upper Zone (Kinnaird *et al*., 2017). These same features are identified in the NP1 core, also located north of the Hout River Shear Zone. However, several anorthosite and magnetite layers occur in the Upper Zone south of the northern limb, in the western and eastern limbs as well as in the Villa Nora fragment also south of the Hout River Shear Zone (Van der Merwe, 1976; von Gruenewaldt *et al*., 1985). The occurrence of minor anorthosite layers and absence of magnetite layers north of the Hout River Shear Zone, as well as the presence of several anorthosite and magnetite layers south of the Hout River Shear Zone confirm the lack of stratigraphic connection between rocks north and rocks south of the Shear Zone as stated by Huthmann *et al* (2017).

Buchanan *et al* (2004) analysed 34 samples of volcanic rocks from the Rooiberg Group for Rb-Sr isotopic compositions, with 21 of the 34 samples representing the Dullstroom Formation. $^{87}Sr/^{86}Sr$ isotopic ratios for standards and samples were measured by thermal ionisation mass spectrometry at the Hugh Allsopp Laboratory, Economic Geology Research Institute, University of the Witwatersrand, Johannesburg in South Africa (Buchanan *et al*., 2004). The initial Sr ratio for the Dullstroom Formation from these results ranges from 0.7052 to 0.7083.

8.2.5 A comparison of the NP1 Results with those of the northern limb, the Waterberg Project and the Dullstroom Formation

8.2.5.1 Petrology and Petrography

The NP1 core was logged from 1070 m to the end of hole at 2500 m. It is made up of Waterberg sedimentary rocks, dolerite sills, gabbronorites, olivine-rich gabbroic rocks, mottled anorthosite, xenoliths and monzodiorites. The core does not have any magnetite layers but multiple undulating coarse-grained feldspar-magnetite veins, and a few subvertical feldspar-quartz-magnetite veins, feldspar veins, plagioclase veins, and granitic veins. The veins cross-cut the gabbronorite rocks indicating that they are younger. Quartz-feldspathic xenoliths, first identified at 1842.2 m during core logging, as well as shale to hornfels xenoliths were identified. Olivine concentration increases downhole from a depth of 2158 m. From 2158 m, apatite and magnetite concentration also increase downhole (Figure 8.8). A downhole increase in olivine is not consistent with the recognised olivine enrichment in the upper part of the Upper Zone elsewhere in the Bushveld Complex, as stated by von Gruenewaldt (1978) and Ashwal *et al* (2005). This therefore suggests that the upper part of the NP1 sequence, consisting of fine-grained gabbronorites from 1318 m to 2158 m, is not a component of the Upper Zone.

Volcanic units (basaltic andesites, basalts, and andesites) of the Dullstroom Formation are moderately metamorphosed and consist of a fine-grained groundmass with variable minor proportions of phenocrysts, porphyroblasts and zoned amygdales (Buchanan *et al*., 1999). The rock types of the NP1 gabbronorite package and the known Dullstroom Formation rocks are not similar except for the porphyritic texture with plagioclase phenocrysts. NP1 fine-grained gabbronorite were formerly basalts and have been metamorphosed by the Bushveld intrusion and recrystallised. The shale to hornfels interval on the NP1 core is evidence of metamorphism. Quartz-feldspathic xenoliths show a granoblastic texture (Figure 8.9) which is also evidence of metamorphism. From petrographic observations, plagioclase phenocrysts within gabbronorites are relics from basalts. A whole rock geochemical comparison further correlates the NP1 gabbronorite package with the Dullstroom Formation rocks (section 8.2.5.2).

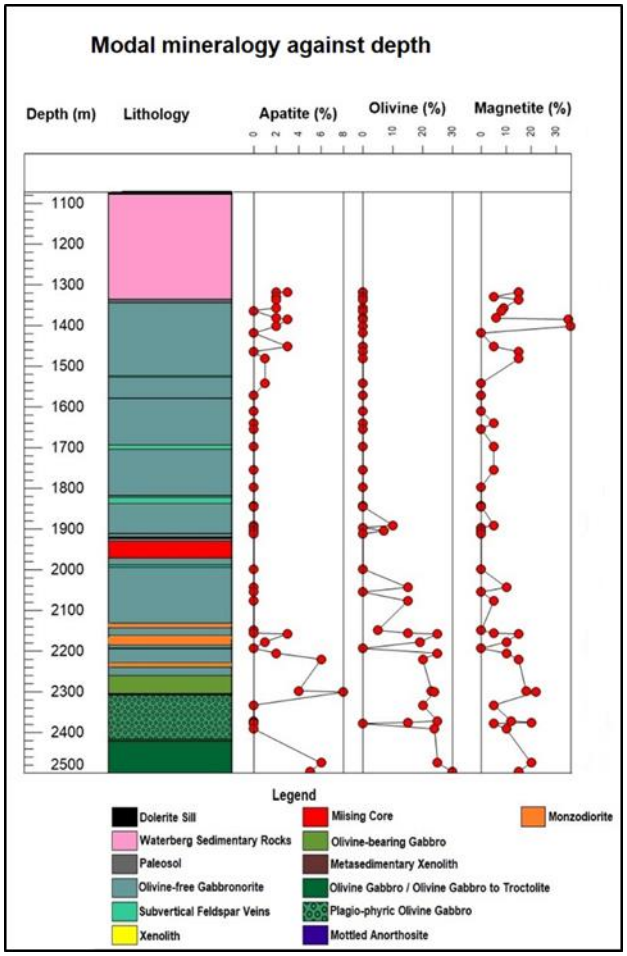

Figure 8.8: NP1 stratigraphy plotted against olivine, apatite and magnetite modal mineralogy which shows an increase in concentration of these minerals from 2158 m to the base of the core (2 500 m)

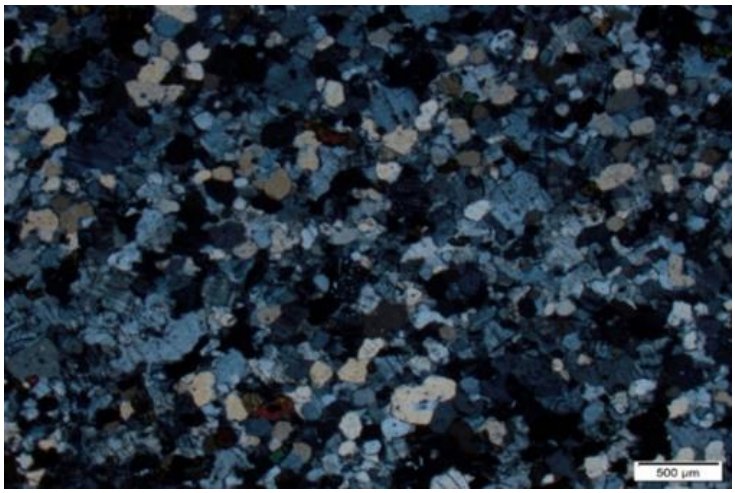

Figure 8.9: Thin section image of a metamorphosed quartz-feldspathic xenolith showing a granoblastic texture, sample 1844.4

8.2.5.2 Whole rock geochemistry

Whole rock trace and major element results indicate the elemental distribution through the entire NP1 core. The NP1 fine-grained gabbronorite package is enriched in SiO_2 and depleted in Fe whereas the Upper Zone olivine gabbroic rocks are richer in Fe and P, and poorer in SiO_2. The enrichment of NP1 Upper Zone olivine-rich gabbroic rocks in Fe and P is directly linked to an increase in olivine ($(Mg,Fe)_2SiO_4$) and apatite ($Ca_5(PO_4)_3(OH,F,Cl)$) concentrations respectively in that section of the core. With regards to major elements, the NP1 gabbronorites have the following ranges in concentration: SiO_2 ranges from 51.94 – 72.71 wt.%, Fe_2O_3 from 5.12 – 13.28 wt.%, P_2O_5 from 0.05 – 0.45 wt.%, TiO_2 from 0.34 – 1.19 wt.% and MgO from 0.06 – 6.46 wt.%. The Upper Zone olivine-rich gabbroic sequence has the following concentration ranges: SiO_2 ranges from 37.32 – 49.57 wt.%, Fe_2O_3 from 18.69 – 37.06 wt.%, P_2O_5 from 0.22 – 2.12 wt.%, TiO_2 from 1.19 – 5.53 wt.% and MgO from 0.85 – 3.11 wt.%.

In terms of trace element analysis of the NP1 samples, the gabbronorite package is richer in Co, Cr, Ni, V and Pb whereas Upper Zone olivine-rich gabbroic rocks package is poorer in these elements. For gabbronorites, Cr concentrations range from 1.25 – 221.12 ppm, Co from 1.42 – 41.26 ppm, Ni from 1.69 – 105.53 ppm, V from 120.61 – 162.85 ppm, Pb from 6.33 – 20.57 ppm. Most of the Upper Zone gabbroic rocks samples have Cr concentrations ranging between 0.75 – 9.16 ppm and only one sample at 2205 m has a concentration of 50.63 ppm. Co ranges from 0.11 – 23.25 ppm and Pb from 0.94 – 10.25 ppm.

A comparison was made between major and trace elements of NP1 samples as well as samples from high and low Ti Dullstroom Formation volcanic rocks from the south-eastern Bushveld Complex analysed by Buchanan *et al* (1999). Four plots (Figure 8.10) were constructed with major element SiO_2 against MgO, Fe_2O_3, P_2O_5 and ($Na_2O + K_2O$) and three plots with trace element Cr against Co, Ni and V (Figure 8.11). Veins and xenoliths were excluded from the NP1 data, while amygdales, veins, and alteration areas were excluded from the Dullstroom Formation volcanic rocks sample collection. The geochemistry of the high and low Ti Dullstroom rocks (from Buchanan *et al*., 1999) which were used in major and trace element comparative plots is shown in Appendix G and Appendix H. On all the major and trace element comparison plots, the high and low Ti Dullstroom samples plot around the same areas as the NP1 fine-grained gabbronorites, indicating that they share similar characteristics and infer that the NP1 gabbronorites could belong to the Dullstroom Formation. The NP1 Upper Zone olivine-rich gabbro samples plot at different areas in all plots when compared to the high and low Ti Dullstroom samples indicating that they do not share similar characteristics.

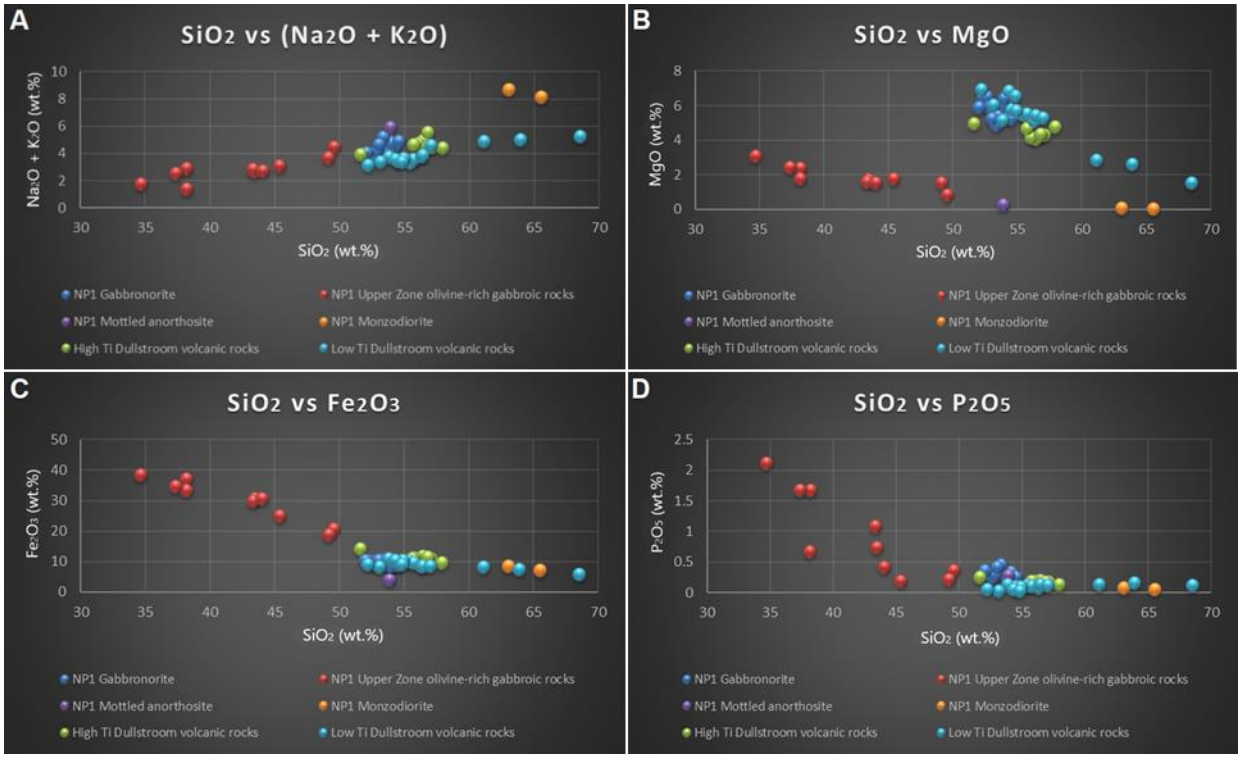

Figure 8.10: Major element comparison plots of NP1 gabbronorite, Upper Zone olivine-rich gabbro, mottled anorthosite and monzodiorite against low and high Ti Dullstroom rocks, (a) SiO_2 vs (Na_2O + K_2O), (b) SiO_2 vs MgO, (c) SiO_2 vs Fe_2O_3, (d) SiO_2 vs P_2O_5

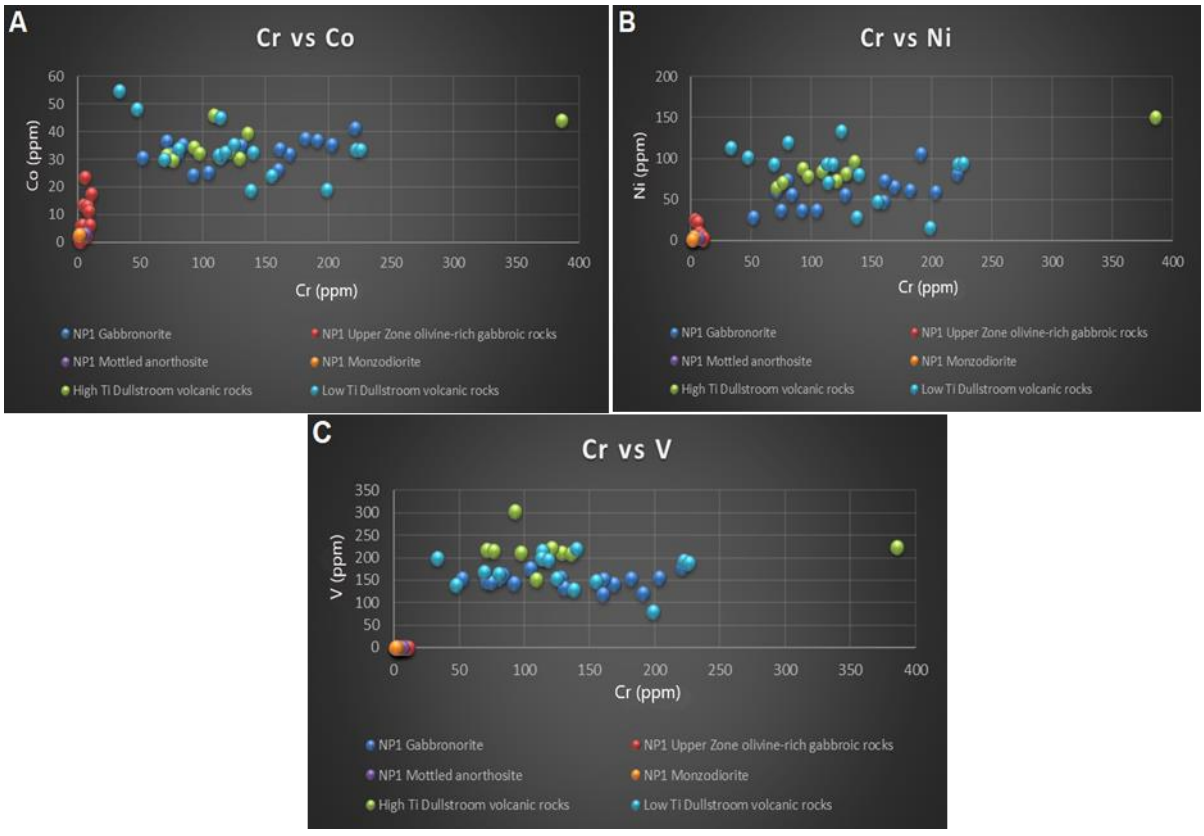

Figure 8.11: Trace element comparison plots of NP1 gabbronorite, Upper Zone olivine-rich gabbro, mottled anorthosite and monzodiorite against low and high Ti Dullstroom rocks, (a) Cr vs Co, (b) Cr vs Ni, (c) Cr vs V

8.2.5.3 Sr isotopes

NP1 initial Sr isotope data has been compared with Sr data from the Dullstroom Formation, Bushveld Complex northern limb Upper Zone and Waterberg Project below. Buchanan *et al* (2004) indicated the initial Sr ratio ranges of the Dullstroom Formation volcanic rocks to be from 0.7052 to 0.7083. Mangwegape *et al* (2016) indicated a range from 0.7063 to 0.7079 for the northern limb Upper Zone rocks, while Huthmann *et al* (2017) mentioned that initial Sr ratio of the far northern limb (Waterberg Project) Upper Zone rocks range from 0.7063 to 0.7075. Figure 8.12 represents a plotted diagram of NP1 initial Sr ratio against depth, with a contact marked in red separating NP1 gabbronorites and NP1 olivine-rich gabbroic rocks. The contact is placed at 2158 m where olivine was first identified during core logging. The change in initial Sr ratio below the 2158 m contact accommodates the 0.7063 – 0.7079 Bushveld northern limb Upper Zone initial Sr ratio range by Mangwegape *et al* (2016) and the range of 0.7063 – 0.7075 for the Upper Zone of the Waterberg Project (Huthmann *et al.,* 2017).

The initial Sr ratio of NP1 gabbronorites (0.7042 – 0.7066) is less radiogenic for the rocks at the top of the NP1 sequence. This upward decrease in Sr isotope composition within the NP1 core could be linked to the modifying effect of fluids related to metamorphism of the up-section of the sequence. The range in Sr isotope compositions from bulk rock samples of the Dullstroom Formation is larger compared to the Sr isotope data of plagioclase grains in the NP1 gabbronorites and this can be attributed to the fact that the gabbronorites have been recrystallised under Bushveld heat, and secondly that different analytical approaches were used to analyse the NP1 and Dullstroom samples. Buchanan *et al* (2004) analysed an entire sample using thermal ionisation mass spectrometry, whereas NP1 Sr data were obtained from plagioclase in situ analysis by LA-MC-ICPMS that permits avoiding altered and weathered grains and allows a visual control of any disturbance of isotopic systems during analysis. The green, orange, and blue arrows in Figure 8.12 represent the initial $^{87}Sr/^{86}Sr$ ratio ranges of the Dullstroom Formation volcanic rocks (Buchanan *et al*., 2004), Waterberg Project Upper Zone (Huthmann *et al*., 2017) and northern limb Upper Zone (Mangwegape *et al*., 2016) respectively.

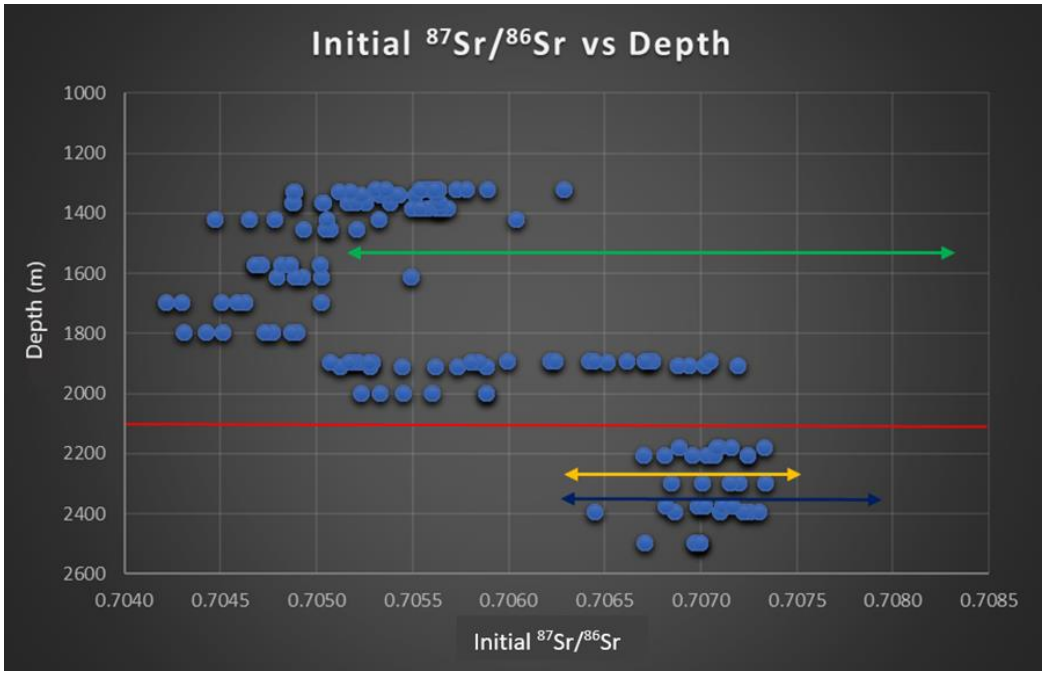

Figure 8.12: NP1 initial $^{87}Sr/^{86}Sr$ against depth in comparison with the initial Sr ratio ranges of Dullstroom Formation represented by a green arrow (0.7052-0.7083, Buchanan *et al*., 2004), Waterberg Project Upper Zone represented by an orange arrow (0.7065-0.7075, Huthmann *et al*., 2017) and northern limb Upper Zone represented by a blue arrow (0.7065-0.7079, Mangwegape *et al*., 2016)

8.3 Conclusion

The interconnection between the northern limb and the Villa Nora fragment of the Bushveld Complex was questioned since the discovery of the thick Bushveld sequence striking north-northeast on the Waterberg Project area (Huthmann *et al*., 2016; Kinnaird *et al*., 2017). Although the Bushveld sequence is confirmed to be present north of the Hout River Shear Zone, the Upper Zone magnetitite layers are absent at the Waterberg Project area (far northern limb). Magnetitite layers are persistently exposed through the northern limb and Villa Nora area, located south of the Hout River Shear Zone (Grobler and Whitfield, 1969).

This study aimed to describe the intersected sequence, logged as the Upper Zone by the Rand Mines Ltd exploration team, and substantiate its correlation with the Bushveld stratigraphic units. Methods used to collect data on the studied core were core logging, thin sections petrographic descriptions, whole rock geochemical analysis, and Sr isotopic analysis. The NP1 core is made up of Waterberg sedimentary rocks and dolerite sills from the surface to a depth of 1312 m. From 1312 m to 2158 m, a fine-grained olivine-free gabbronorite package occurs. The olivine-rich gabbroic rocks occur from 2158 m to the end of hole at 2500 m. "Olivine-rich gabbroic rocks" refers to the four (4) sub-units within that interval namely; olivine-bearing gabbro, plagio-phyric olivine gabbro, olivine gabbro and olivine gabbro to troctolite. Massive magnetitite layers are absent in the lower unit of NP1 core (olivine-rich gabbroic rocks), although disseminated magnetite can account for up to 20% modal mineralogy in this rock unit.

Whole rock geochemistry does not reveal the expected Si, Fe and P enrichment towards the top of the intersected sequence. It rather reveals an opposite trend consistent with the visible downhole increase in magnetite, fayalitic olivine and apatite contents towards the bottom part of the core. This constitution is not consistent with the Upper Zone compositional variations as seen in the eastern and western limbs by von Gruenewaldt (1973) and for the northern limb by Ashwal *et al* (2005). The high concentration in apatite was reached at approximately 1000 m below the roof contact in the eastern and western limbs (von Gruenewaldt, 1973) and at approximately 600 m below the contact in the northern limb of the Bushveld Complex (Ashwal *et al*., 2005). The major and trace element comparison plots in section 8.2.5.2 (SiO_2 vs Na_2O+K_2O, MgO, Fe_2O_3, P_2O_5 and Cr vs Co, Ni, and V) compared the NP1 results with the low and high Ti Dullstroom data and showed NP1 gabbronorites were compositionally similar to the low and high Ti Dullstroom samples. This indicates that these units share similar characteristics and that the NP1 fine-grained gabbronorite section belongs to the Dullstroom Formation and not the Upper Zone as initially logged by the Rand Mines Ltd exploration team.

Sr isotope analysis was carried out to verify the Upper Zone affiliation with the studied sequence. The Sr isotope composition of plagioclase from the upper unit (gabbronorites) is not consistent with the Upper Zone signature. The NP1 gabbronorite rocks initial $^{87}Sr/^{86}Sr$ ratio (Sri) range from 0.7042 to 0.7066 is distinctly different from the values of Upper Zone plagioclase in the northern limb, which range from 0.7063 to 0.7079 (Mangwegape *et al*., 2016) and Upper Zone plagioclase from the Waterberg Project, where values vary from 0.7065 to 0.7075 (Huthmann *et al*., 2017). However, the Sr isotope composition of plagioclase crystals from the NP1 olivine-rich gabbroic rocks is characterised by a relatively narrow range of Sri values between 0.7064 to 0.7073, consistent with northern limb Upper Zone Sri values ranging from 0.7063 to 0.7079 from Mangwegape *et al* (2016). This interpretation is also supported by the presence of apatite, magnetite, and olivine within the NP1 gabbroic rocks section, which are common minerals occurring in the Upper Zone, as confirmation that the NP1 olivine-rich gabbroic rocks section is the Upper Zone.

Field relations between the Bushveld Complex and Rooiberg Group whereby the unconformable emplacement of the RLS cross-cut the Rooiberg Group across the Bushveld Complex provides more evidence that the NP1 gabbronorites indeed belong to the Rooiberg Group. The RLS splits the Dullstroom Formation of the Rooiberg Group into upper and lower Dullstroom at Loskop Dam (Harmer and Farrow, 1995; Lenhardt and Eriksson, 2012), and split the Damwal Formation of the Rooiberg Group at the Stofberg area, southeast of the Bushveld Complex (Lenhardt and Eriksson, 2012). At the NP1 sequence, it is concluded that the RLS (Upper Zone) intruded the Dullstroom Formation, which forms the immediate roof of the RLS in the area. The intrusion of the RLS is supported by the evidence of metamorphism within the NP1 gabbronorite package by the fine-grained to granoblastic texture of the rocks and the presence of clinopyroxene, plagioclase and phlogopite phenocrysts. Granoblastic texture of the metamorphosed quartz-feldspathic xenoliths is also evidence of metamorphism, and the foliation texture in hornfels is likely related to metamorphism.

It is therefore concluded that the NP1 borehole intersected an earlier unseen top contact of the Bushveld Complex with the metamorphosed rocks of the Dullstroom Formation as illustrated in Figure 8.13. This correlation is consistent with the similarities in the mineral assemblages and the observed whole rock geochemical compositions. The correlation is also strongly supported by the relics of porphyritic texture in some rocks and by occurrence of the sedimentary xenoliths (at 1842.5 m and 2054.5 m), which are resembling the sedimentary layers known within the Dullstroom Formation.

The results of the study area confirm the existence of the Bushveld extensive magmatic basin north of the Hout River Shear Zone. However, the absence of magnetitite layers favour a provisional stratigraphic connection rather with the Waterberg Project area (located north of the Hout River Shear Zone as the NP1 sequence) than with the Villa Nora sequence and northern limb of the Bushveld Complex (both located south of the Hout River Shear Zone).

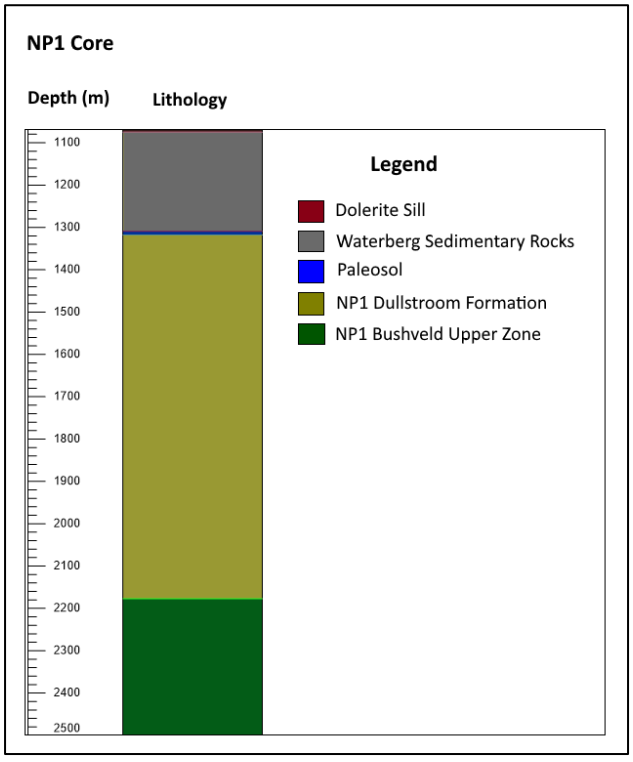

Figure 8.13: NP1 stratigraphic diagram illustrating a contact between Dullstroom Formation rocks and the Bushveld Upper Zone

8.4 Limitations

The study was conducted with the only available drill hole. If the study could be carried out with more drill holes, the data confidence could have been higher and better comparisons would have been carried out.

8.5 Recommendations

It is recommended that to have a better understanding regarding the sequence at the Non Parella farm, trace element data from ICP-MS whole rock analysis is needed to make the conclusion and comparisons be firmer. ICP-MS analytical technique is more accurate and has very low detection limits (ppb) for most elements, while XRF analytical technique has detection limits in ppm. In addition, more stratigraphic holes could be drilled, logged, sampled, and analysed to increase the data confidence of the area. In situ isotope analysis of plagioclase from basalt and basaltic andesite of the Dullstroom Formation could potentially add more confidence to the suggested hypothesis.

List of References

Ashwal, L.D., Webb, S.J., Knoper, M.W., 2005. Magmatic stratigraphy in the Bushveld Northern Lobe: continuous geophysical and mineralogical data from the 2950 m Bellevue drill core. South African Journal of Geology, 108, 199-232.

Barton, J.M., Cawthorn, R.G., White, J., 1986. The role of contamination in the evolution of the Platreef of the Bushveld Complex. Economic Geology, 81, 1096-1104.

Buchanan, P.C., 2006. The Rooiberg group. In: M.R., Anhaeusser, C.R., Thomas, R.J. (Eds), The Geology of South Africa. Geological Society of South Africa/Council for Geoscience, Johannesburg/Pretoria, 283-289.

Buchanan, P.C., Koeberl, C., Reimold, W.U., 1999. Petrogenesis of the Dullstroom Formation, Bushveld Magmatic Province, South Africa. Contributions to Mineralogy and Petrology, 137, 133-146.

Buchanan, P.C., Reimold, W.C., Koeberl, C., Kruger, F.J., 2004. Rb-Sr and Sm-Nd isotopic compositions of the Rooiberg Group, South Africa: early Bushveld-related volcanism. Lithos, 29, 373-388.

Cairncross, B., 2004. Field guide to rocks and minerals of Southern Africa.

Cameron, E.N., 1978. The Lower Zone of the Eastern Bushveld Complex in the Olifants River trough. Journal of Petrology, 19(3), 437-462.

Cawthorn, R.G., Barton, J.M., Viljoen, M.J., 1985. Interaction of floor rocks with the Platreef on Overysel, Portgietersrus, northern Transvaal. Economic Geology, 80, 988-1006.

Cawthorn, G.R., Eales, H.V., Walraven, F., Uken, R., Watkeys, M.K., 2006. The Bushveld Complex. In: Johnson, M.R., Ahaeusser, C.R. and Thomas, R.J (Eds), the Geology of South Africa. Geological Society of South Africa, Johannesburg/Council for Geoscience, Pretoria, 261-279.

Cheney, E.S., Twist, D., 1991. The conformable emplacement of the Bushveld mafic rocks along a regional unconformity in the Transvaal succession of South Africa. Precambrian Research, 52, 115-132.

Council for Geoscience., 1978. 1: 250 000 Geological maps (22528 Pretoria and 2428 Nylstroom sheets). Pretoria, South Africa.

Eales, H.V., and Cawthorn, R.G., 1996. The Bushveld Complex, in Cawthorn, R.G., ed., Layered intrusions: Amsterdam, Elsevier, 182-187.

Elston, W.E., 1992. Does the Bushveld-Vredefort system (South Africa) record the largest known terrestrial impact catastrophe? [abs]: International Conference on Large Meteorite Impacts and Planetary Evolution, Lunar Planet Institution Contribution, 790, 23-24. Abstracts.

Eriksson, P.G., Schreiber, U.M., Reczko, B.F.F., Snyman, C.P., 1994. Petrography and geochemistry of sandstone interbedded with the Rooiberg Felsite Group (Transvaal Sequence, South Africa): implications for provenance and tectonic setting. Journal of Sedimentary Research, A64, 836-846.

Finn, C.A., Bedrosia, P.A., Cole, J.A., Khoza, T.D., Webb, S.J., 2015. Mapping the 3D extent of the Northern Lobe of the Bushveld Layered mafic intrusion from geophysical data. Precambrian Research, 268, 279-294.

Grobler, N.J., and Whitfield, G.G., 1970. The olivine-apatite magnetitites and related rocks in the Villa Nora occurrence of the Bushveld. The Geological Society of South Africa, Special Publication, 208-225.

Harmer, R.E., Sharpe, M.R., 1985. Field relations and strontium isotope systematics on the marginal rocks of the eastern Bushveld Complex. Economic Geology, 80, 813-837.

Harmer, R.E., Farrow, D., 1995. An isotopic study on the volcanics of the Rooiberg Group: age implication and a potential exploration tool. Mineralium Deposita, 30, 188-195.

Hartzer, F.J., 1995. Transvaal Supergroup inliers: geology, tectonic development and relationship with the Bushveld Complex, South Africa. Journal of African Earth Science, 21, 521-547.

Huthmann, F.M., Yudovskaya, M.A., Frei, D., Kinnaird, J.A., 2016. Geochronological evidence for an extension of the Northern Lobe of the Bushveld Complex, Limpopo Province, South Africa. Precambrian Research, 280, 61-75.

Huthmann, F.M., Kinnaird, J.A., Yudovskaya, M.A., Elburg, M.A., 2017. The Sr isotopic stratigraphy of the far northern Bushveld Complex. South African Journal of Geology, 120.4, 499-510.

Kinnaird, J.A., 2005a. Geochemical evidence for multiphase emplacement in the Southern Platreef. Applied Earth Science, Transaction of the Institute of Mining and Metallurgy, 114, 225-241.

Kinnaird, J.A., 2005b. The Bushveld Large Igneous Province, http://www.largeigneousprovinces.org/LOM.htlm (accessed in June 2019).

Kinnaird, J.A., and McDonald, I., 2015. An introduction to mineralisation in the Northern Limb of the Bushveld Complex. Applied Earth Science, 114, 194-198.

Kinnaird, J.A., Yudovskaya, M., McCreesh, M., Huthmann, F., Botha, T.J., 2017. The Waterberg Platinum Group Element deposit: atypical mineralisation in mafic-ultramafic rocks of the Bushveld Igneous Complex, South Africa. Economic Geology, 112, 1-28.

Kruger, F.J., 1994. The Sr-isotopic stratigraphy of the western Bushveld Complex. South African Journal of Geology, 97, 393-398.

Kruger, F.J., 2005. Filling the Bushveld Complex magma chamber: Lateral expansion, roof and floor interaction, magmatic unconformities, and the formation of giant chromitite, PGE and Ti-V-magnetite deposits. Mineralium Deposita, 40, 451-472.

Le Bas, M.J., Le Maitre, R.W., Streckeise, A., Zanettin., 1986. A chemical classification of volcanic rocks based on the total alkali-silica diagram. Journal of Petrology, 27, 745-750.

Le Maitre, R.W., 2002. Igneous rocks, a classification and glossary of terms. Second edition.

Lenhardt, N., and Eriksson, P.G., 2012. Volcanism of the Palaeoproterozoic Bushveld Large Igneous Province: The Rooiberg Group, Kaapvaal Craton, South Africa. Precambrian Research, 214-215, 82-94.

Maier, W.D., Arndt, N.T., Curl, E.A., 2000. Progressive crustal contamination of the Bushveld Complex: evidence from Nd isotopic analysis of the cumulate rocks. Contributions to Mineralogy and Petrology, 140, 316-327.

Mangwegape, M., Roelofse, F., Mock, T., Carlson, R.W., 2016. The Sr-isotopic stratigraphy of the Northern Limb of the Bushveld Complex, South Africa. Journal of African Earth Sciences, 113, 95-100.

McDonald, I., Harmer, R.E.J., Holwell, D.A., Hughes, H.S.R., Boyce, A.J., 2017. Cu-Ni-PGE mineralisation at the Aurora project and potential for a new PGE province in the Northern Bushveld Main Zone. Ore Geology Reviews, 80, 1135-1159.

Mitchell, A.A., 1990. The stratigraphy, petrography and mineralogy of the Main Zone of the North-western Bushveld Complex. South African Journal of Geology, 93, 818-831.

Molyneux, T.G., 1970. A geological investigation of the Bushveld Complex in Sekhukhune land and part of the Steelpoort Valley, Eastern Transvaal, with particular reference to the oxide minerals. D.Sc. Thesis (Unpublished) University of Pretoria, p123.

Molyneux, T.G., 1974. A geological investigation of the Bushveld Complex in Sekhukhune land and part of the Steelpoort Valley: Transaction of the Geological Society of South Africa, 77, 329-338.

Nebel, O., Scherer, E. E., Mezger, K., 2011. Evaluation of the ^{87}Rb decay constant by age comparison against the U-Pb system. Earth and Planetary Science Letters, 301,1-8.

Rhodes, R.C., 1975. New evidence for impact origin of the Bushveld Complex, South Africa. South African Journal of Geology, 3, 549-554.

Roelofse, F., 2010. Constraints on the magmatic evolution of the Lower Main Zone platreef on the northern limb of the Bushveld Complex as inferred from the Moordekopje drill core. PhD thesis, University of the Witwatersrand, Johannesburg, South Africa, p2.

Roelofse, F., and Ashwal, L.D., 2012. The Lower Main Zone in the Northern Limb of the Bushveld Complex a > 1.3 km thick sequence of intruded and variably contaminated crystal mushes. Journal of Petrology, 53, 1449-1476.

SACS (South African Committee for Stratigraphy), 1980. In: Kent, L.E. (Ed). Stratigraphy of South Africa. Part 1: Lithostratigraphy of the Republic of South Africa, South West Africa/Namibia and the Republics of Bophuthatswana, Transkei, and Venda. Handbook Geological Survey of South Africa, Pretoria, South Africa.

Salminen, R., (Chief ed) et al., 2005. Geochemical Atlas of Europe, Part 1 – Background information, methodology and maps. Geological Survey of Finland, Otamedia Oy, Espoo, 121-395.

Schweitzer, J.K., Hatton, C.J., de Waal, S.A., 1995. Regional lithochemical stratigraphy of the Rooiberg Group, upper Transvaal Supergroup: a proposed new submission. South African Journal of Geology, 98, 254-255.

Streckeisen, A., 1976. To each plutonic rock its proper name. Earth Science Reviews, 12(1), 1-33.

Teigler, B., 1990. Mineralogy, petrology and geochemistry of the Lower Critical Zone, Northwestern Bushveld Complex. Unpublished PhD thesis, Rhodes University, Grahamstown.

The analytical X-ray company., 2009. Axios max [online]. The Netherlands: PANanalytical B.V. [Accessed in 22 December 2019]

Twist, D., 1985. Geochemical evolution of the Rooiberg silicic lavas in the Loskop Dam area, Southeastern Bushveld. Economic Geology, 80, 1153-1165.

van der Merwe, M.J., 1976. The layered sequence of the Potgietersrus limb of the Bushveld Complex. Economic Geology, 71(7), 1337-1351.

van der Merwe, M.J., 1978. The geology of the basic and ultramafic rocks of the Potgietersrus limb of the Bushveld Complex. Unpublished PhD dissertation, University of the Witwatersrand, Johannesburg, South Africa.

Vermaak, C.F., and von Gruenewaldt, G., 1986. Introduction to the Bushveld Complex, in: Anhaeusser, C.R., Maske, S. (Eds), Mineral Deposit of South Africa. The Geological Society of South Africa, 1021-1029.

von Gruenewaldt, G., 1973. The Main and Upper Zones of the Bushveld Complex in the Rossenekal area eastern Transvaal: Geological Society of South Africa Transactions, 76, 207-227.

von Gruenewaldt, G., Sharpe, M.R., Hatton, C.J., 1985. The Bushveld Complex; Introduction and review. Economic Geology, 80, 803-812.

Walraven, F., 1982. Textural, geochemical and genetical aspect of the granophyric rocks of the Bushveld Complex. PhD thesis, University of the Witwatersrand, Johannesburg, South Africa.

Walraven, F., Hattingh, E., 1993. Geochronology of the Nebo Granite, Bushveld Complex. South African Journal of Geology, 96, 31-41.

Walraven, F., Armstrong, R.A., Kruger, F.J., 1990. A chrono-stratigraphic framework for the north-central Kaapvaal craton, the Bushveld Complex and the Vredefort structure. Tectonophysics, 171, 23-48.

Yudovskaya, M.A., Kinnaird, J.A., Grobler, D.F., Costin, G., Abramova, V.D., Dunnet, T., and Barnes, S.J., 2017. Zonation of Merensky-style platinum mineralisation in Turfspruit thick reef facies (northern limb of the Bushveld Complex). Economic Geology, 112, 1333-1365.

Yudovskaya, M.A., Kinnaird, J.A., Sobolev, A.V., Kuzmin, D.V., McDonald, I., Wilson, A.H., 2013. Petrogenesis of the Lower Zone olivine-rich cumulates beneath the Platreef and their correlation with recognised occurrences in the Bushveld Complex. Economic Geology, 108, 1923-1952.

Zeh, A., Ovtcharova, M., Wilson, A.H., Schaltergger, U., 2015. The Bushveld Complex was emplaced and cooled in less than one million years – results of zirconology, and geotectonic implications. Earth and Planetary Science Letters, 418, 103-114.

Appendices

Appendix A: Hand specimen descriptions of the samples from core NP1 used in this thesis

Sample Number	Major Minerals	Minor Minerals	Colour & Texture	Grain Size	Mineral Proportion	Rock Name	Sample Picture
1318.3 - 1318.5	Plagioclase Clinopyroxene Orthopyroxene Orthoclase	Magnetite Phlogopite Quartz	Grey	Fine with coarse-grained veins	**Coarse-grained**: Plagioclase= 70% Magnetite= 7% Quartz= 10% Orthoclase= 13% **Fine-grained**: Clinopyroxene=30% Orthopyroxene= 20% Plagioclase= 47% Phlogopite= 3%	Gabbronorite with cross-cutting quartz-feldspar coarse-grained vein	
1328.5	Orthopyroxene Clinopyroxene Plagioclase	Magnetite Phlogopite	Grey	Fine-grained	Orthopyroxene= 26% Clinopyroxene= 20% Plagioclase= 48% Magnetite= 4% Phlogopite= 2%	Gabbronorite	
1336	Plagioclase Alkali feldspar	Magnetite Phlogopite Quartz	Light-grey	Coarse-grained	Plagioclase= 50% Alkali feldspar=23% Quartz= 15% Magnetite= 10% Phlogopite= 2%	Quartz-feldspar-magnetite vein	

1356.3	Plagioclase Clinopyroxene Orthopyroxene	Magnetite Phlogopite	Grey	Fine-grained	Plagioclase= 50% Clinopyroxene= 25% Orthopyroxene= 20% Magnetite= 3% Phlogopite= 2%	Gabbronorite	
1363.35 – 1363.5	Plagioclase Clinopyroxene Orthopyroxene Orthoclase	Phlogopite Magnetite	Grey colour & Porphyritic texture (Fine-grained part)	Fine-grained matrix cross-cut by coarse-grained vein	**Fine-grained**: Plagioclase= 50% Clinopyroxene= 20% Orthopyroxene= 25% Phlogopite=5% **Coarse-grained**: Plagioclase= 70% Magnetite= 2% Phlogopite= 1% Orthoclase= 27%	Gabbronorite	
1381.7	Plagioclase Clinopyroxene Orthopyroxene Orthoclase	Phlogopite Magnetite Alkali feldspar	Grey	Fine-grained matrix cross-cut by coarse-grained vein	**Fine-grained**: Plagioclase = 50% Clinopyroxene= 18% Orthopyroxene= 14% Alkali feldspar= 8% Phlogopite= 6% Magnetite= 4% **Coarse-grained**: Plagioclase= 70% Clinopyroxene= 11% Orthoclase= 19%	Gabbronorite	

1385.3 – 1385.5	Plagioclase Clinopyroxene Orthopyroxene Magnetite		Grey	Fine-grained (cross-cut by coarse-grained vein)	Plagioclase= 53% Clinopyroxene = 20% Orthopyroxene =15% Magnetite= 12%	Gabbronorite (with cross-cutting Feldspar-magnetite vein)	
1401.5	Magnetite Plagioclase Alkali feldspar Clinopyroxene	Quartz	Whitish-grey to grey	Coarse-grained	Plagioclase= 40% Magnetite= 30% Alkali feldspar= 12% Clinopyroxene= 10% Quartz= 8%	Feldspar-magnetite vein	
1418.5	Plagioclase Orthopyroxene Clinopyroxene	Phlogopite	Grey	Fine-grained matrix with plagioclase phenocrysts	Plagioclase= 60% Orthopyroxene= 20% Clinopyroxene= 15% Phlogopite= 5%	Gabbronorite	
1451.5	Plagioclase Clinopyroxene Orthopyroxene	Phlogopite	Grey	Fine to medium-grained	Plagioclase= 60% Clinopyroxene= 20% Orthopyroxene= 15% Phlogopite= 10%	Phlogopite Gabbronorite	

1464.2	Plagioclase Magnetite Alkali feldspar Phlogopite Clinopyroxene		Whitish-grey to grey	Coarse grained	Plagioclase= 45% Magnetite= 20% Alkali feldspar= 10% Phlogopite= 5% Clinopyroxene= 20%	Feldspar-magnetite vein	
1481.5	Plagioclase Alkali feldspar Clinopyroxene Magnetite Quartz	Phlogopite	Light-grey	Coarse-grained	Plagioclase= 45% Alkali feldspar= 15% Clinopyroxene= 15% Magnetite= 10% Quartz= 10% Phlogopite= 5%	Quartz-feldspar vein	
1541.5	Plagioclase Clinopyroxene Orthopyroxene	Phlogopite Pyrite	Grey colour & Porphyritic texture	Fine-grained ground mass & medium-grained crystals	Plagioclase= 50% Orthopyroxene= 25% Clinopyroxene= 20% Phlogopite= 4% Pyrite= 1%	Gabbronorite	
1570.5	Plagioclase Clinopyroxene Orthopyroxene	Phlogopite	Grey	Fine-grained	Plagioclase= 50% Clinopyroxene= 25% Orthopyroxene= 20% Phlogopite= 5%	Gabbronorite	

1609.8	Plagioclase Clinopyroxene Orthopyroxene	Phlogopite Pyrite	Grey colour & Porphyritic texture	Fine-grained ground mass & medium-grained crystals	Plagioclase= 49% Clinopyroxene= 23% Orthopyroxene= 20% Phlogopite= 5% Pyrite= 3%	Gabbronorite	
1640	Alkali feldspar Plagioclase Quartz	Magnetite Phlogopite Orthopyroxene	Brownish-grey	Coarse-grained	Alkali feldspar= 30% Plagioclase= 40% Quartz= 20% Magnetite= 5% Phlogopite= 2% Orthopyroxene= 3%	Quartz-feldspar veins	
1654	Plagioclase Clinopyroxene Orthopyroxene	Pyrite	Grey colour & Porphyritic texture	Fine-grained	Plagioclase= 50% Orthopyroxene= 25% Clinopyroxene= 20% Pyrite= 5%	Gabbronorite	
1696.5	Plagioclase Clinopyroxene Orthopyroxene	Magnetite Phlogopite	Grey colour & Oikocryst texture	Fine to medium-grained	Plagioclase= 45% Orthopyroxene= 25% Clinopyroxene= 20% Magnetite= 5% Phlogopite= 5%	Gabbronorite	

1755	Alkali feldspar Plagioclase Quartz	Magnetite Phlogopite	Brownish-grey	Coarse-grained	Alkali feldspar= 50% Plagioclase= 20% Quartz= 20% Magnetite= 7% Phlogopite= 3%	Quartz-feldspar vein	
1796.6	Plagioclase Clinopyroxene Orthopyroxene	Phlogopite	Grey	Fine-grained	Plagioclase= 45% Orthopyroxene= 25% Clinopyroxene= 20% Phlogopite= 10%	Gabbronorite	
1842.5	Alkali feldspar Quartz Plagioclase		Golden brown	Medium-grained	Alkali feldspar= 55% Quartz = 35% Plagioclase= 10%	Metamorphosed quartz-feldspathic xenolith	
1843.5	Alkali feldspar Quartz Plagioclase	Magnetite	Golden brown	Coarse-grained	Alkali feldspar= 50% Quartz= 35% Plagioclase= 10% Magnetite= 5%	Metamorphosed quartz-feldspathic xenolith	

1844.4	Quartz Alkali feldspar Clinopyroxene	Plagioclase	Golden brown	Medium-grained	Quartz= 40% Alkali feldspar= 40% Clinopyroxene= 15% Plagioclase= 5%	Shale to hornfels xenolith	
1890.5	Plagioclase Clinopyroxene Orthopyroxene	Magnetite Olivine	Grey	Fine-grained matrix with cross-cutting coarse-grained vein	Plagioclase= 55% Clinopyroxene= 20% Orthopyroxene= 15% Magnetite= 5% Olivine= 5%	Gabbronorite with cross-cutting feldspar-magnetite vein	
1896.5	Plagioclase Clinopyroxene Orthopyroxene	Phlogopite	Grey colour & Porphyritic texture	Fine-grained ground mass & medium-grained grains	Plagioclase= 50% Clinopyroxene= 25% Orthopyroxene= 20% Phlogopite= 5%	Gabbronorite	
1904.5	Plagioclase Alkali feldspar Quartz	Olivine Clinopyroxene Orthopyroxene Magnetite	Light- grey	Coarse-grained	Plagioclase= 30% Alkali feldspar= 30% Quartz= 14% Clinopyroxene= 8% Orthopyroxene= 8% Olivine= 7% Magnetite= 3%	Quartz-feldspar-plagioclase vein	

1911.7	Plagioclase Clinopyroxene Orthopyroxene Phlogopite		Grey	Fine-grained	Plagioclase= 40% Clinopyroxene= 25% Orthopyroxene= 20% Phlogopite= 15%	Phlogopite Gabbronorite	
1998	Plagioclase Orthopyroxene Clinopyroxene	Phlogopite	Grey	Fine-grained	Plagioclase= 48% Orthopyroxene= 25% Clinopyroxene= 20% Phlogopite= 7%	Gabbronorite	
2043	Alkali feldspar Plagioclase Quartz	Magnetite Clinopyroxene Phlogopite	Brownish-grey	Coarse-grained	Alkali feldspar= 40% Plagioclase= 20% Quartz= 20% Magnetite= 10% Clinopyroxene= 8% Phlogopite= 2%	Monzodiorite	
2054.5	Alkali feldspar Quartz Plagioclase	Orthopyroxene Clinopyroxene	Grey colour & Oikocrystic pyroxenes	Fine-grained mass & medium- grained pyroxenes	Alkali feldspar= 30% Plagioclase= 30% Quartz= 30% Clinopyroxene= 5% Orthopyroxene= 5%	Pyroxene granite or migmatised sediments	

2076.8	Alkali feldspar Quartz Plagioclase Olivine	Magnetite	Grey	Medium-grained	Alkali feldspar= 40% Quartz= 30% Olivine= 15% Plagioclase= 10% Magnetite= 5%	Monzodiorite	
2148.5	Alkali feldspar Quartz Clinopyroxene Plagioclase	Orthopyroxene Olivine	Grey	Fine-grained	Alkali feldspar= 20% Plagioclase= 20% Quartz= 30% Clinopyroxene= 20% Orthopyroxene= 5% Olivine= 5%	Pyroxene granite or migmatised sediments	
2155.6	Alkali feldspar Quartz Olivine Plagioclase	Magnetite Clinopyroxene	Brownish-grey	Medium to coarse-grained	Plagioclase= 20% Quartz= 37% Alkali feldspar= 18% Olivine= 15% Magnetite= 5% Clinopyroxene= 5%	Pyroxene granite or migmatised hornfels	
2157.5	Alkali feldspar Olivine Quartz Magnetite Clinopyroxene Plagioclase		Light-grey	Medium to coarse-grained	Alkali feldspar= 20% Olivine= 25% Quartz= 10% Magnetite= 15% Clinopyroxene= 10% Plagioclase= 20%	Olivine-bearing cross-cutting Quartz-Plagioclase vein with fayalitic olivine veinlets	

2177.2	Plagioclase Olivine Magnetite Clinopyroxene		Brownish-grey	Medium to coarse-grained	Plagioclase= 55% Olivine= 25% Magnetite= 10% Clinopyroxene= 10%	Olivine-bearing gabbro	
2193.2	Iron oxides and graphite Clinopyroxene Orthopyroxene Alkali feldspar Plagioclase	Phlogopite	Brown	Fine-grained	Iron oxides and graphite= 40% Clinopyroxene= 25% Alkali feldspar= 5% Plagioclase= 15% Orthopyroxene= 10% Phlogopite= 5%	Hornfels	
2205	Plagioclase Olivine Clinopyroxene Magnetite	Orthopyroxene	Brownish-grey colour & Porphyritic texture (Plagioclase)	Medium to coarse-grained	Plagioclase= 45% Olivine= 25% Clinopyroxene= 15% Magnetite= 10% Orthopyroxene= 5%	Plagio-phyric Olivine gabbro	
2220	Plagioclase Olivine Clinopyroxene Magnetite	Orthopyroxene	Brownish-grey colour & Porphyritic texture (Plagioclase)	Medium to coarse-grained	Plagioclase= 45% Olivine= 25% Clinopyroxene= 15% Magnetite= 10% Orthopyroxene= 5%	Plagio-phyric Olivine gabbro	

2297.2	Plagioclase Olivine Clinopyroxene Magnetite	Orthopyroxene	Brownish-grey colour & Porphyritic texture (Plagioclase)	Medium to coarse-grained	Plagioclase= 35% Olivine= 30% Clinopyroxene= 15% Orthopyroxene= 5% Magnetite= 15%	Plagio-phyric Olivine gabbro	
2300.5	Plagioclase Olivine Magnetite Clinopyroxene	Orthopyroxene	Brownish-grey	Medium to coarse-grained	Plagioclase= 30% Olivine= 30% Magnetite= 15% Clinopyroxene= 20% Orthopyroxene= 5%	Olivine-magnetite gabbro	
2332.5	Plagioclase Olivine Magnetite Clinopyroxene	Orthopyroxene	Brownish-grey	Medium to coarse-grained	Plagioclase= 30% Olivine= 30% Magnetite= 15% Clinopyroxene= 20% Orthopyroxene= 5%	Olivine-magnetite gabbro	
2371.3	Plagioclase Olivine Magnetite Clinopyroxene	Orthopyroxene	Brownish-grey	Medium to coarse-grained	Plagioclase= 30% Olivine= 30% Magnetite= 15% Clinopyroxene= 20% Orthopyroxene= 5%	Olivine-magnetite gabbro	

2374.9	Plagioclase Magnetite Olivine	Orthopyroxene	Whitish-grey	Coarse-grained	Plagioclase= 60% Magnetite= 20% Olivine= 15% Orthopyroxene= 5%	Mottled Anorthosite with magnetite & olivine	
2377.8	Plagioclase Clinopyroxene	Magnetite Phlogopite Orthopyroxene	Whitish-grey	Coarse-grained	Plagioclase= 70% Clinopyroxene= 15% Magnetite= 5% Phlogopite= 5% Orthopyroxene= 5%	Mottled Anorthosite with magnetite	
2391	Plagioclase Olivine Magnetite Clinopyroxene	Orthopyroxene	Brownish - grey	Medium to coarse-grained	Plagioclase= 30% Olivine= 30% Magnetite= 15% Clinopyroxene= 20% Orthopyroxene= 5%	Olivine-magnetite gabbro	
2474.5	Plagioclase Olivine Magnetite Clinopyroxene	Orthopyroxene	Brownish-grey	Medium to coarse-grained	Plagioclase= 30% Olivine= 30% Magnetite= 15% Clinopyroxene= 20% Orthopyroxene = 5%	Olivine-magnetite gabbro	

2496.1	Plagioclase Olivine Magnetite Clinopyroxene	Orthopyroxene	Brownish-grey	Medium to coarse-grained	Plagioclase= 30% Olivine= 30% Magnetite= 15% Clinopyroxene= 20% Orthopyroxene= 5%	Olivine-magnetite gabbro	

Appendix B: Petrography and modal mineralogy of selected samples from core NP1

Sample number and Rock name	Major minerals	Minor minerals	Mineral proportion	Grain size	Texture(s)	Sample picture
1318.35 **Quartz-feldspar-magnetite vein**	Plagioclase Alkali feldspar Magnetite Quartz	Apatite Zircon Clinopyroxene Phlogopite	Plagioclase = 40% Alkali feldspar = 15% Quartz = 15% Magnetite = 15% Phlogopite = 5% Zircon = 4% Clinopyroxene = 3% Apatite = 3%	Coarse-grained	Equigranular and locally granophyric	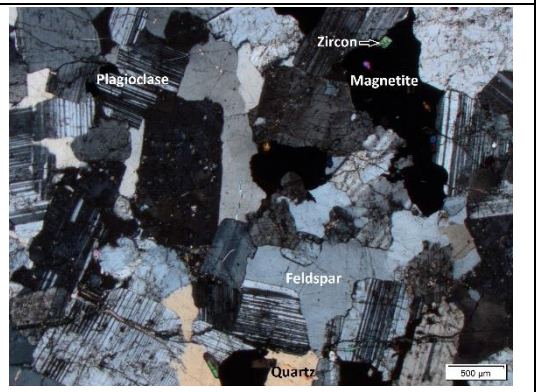
1318.45 **Olivine-free Gabbronorite** **(Contact)**	Plagioclase Magnetite	Phlogopite Hornblende Clinopyroxene Orthopyroxene Apatite Zircon	Plagioclase = 55% Magnetite = 15% Hornblende = 9% Phlogopite = 8% Zircon = 5% Apatite = 2% Clinopyroxene = 4% Orthopyroxene = 2%	Fine - grained matrix host the 1318.35 vein	Intergranular to subophitic	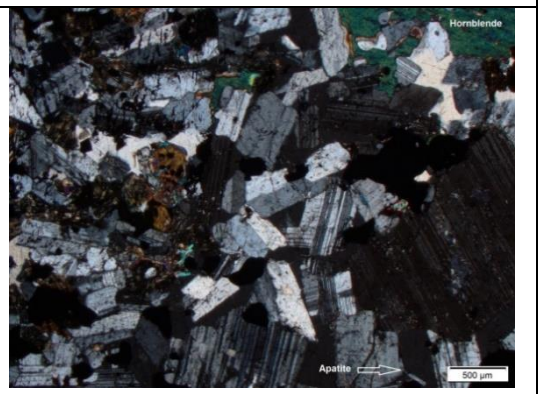

1328.5 **Olivine-free Gabbronorite**	Plagioclase Orthopyroxene Clinopyroxene	Magnetite Phlogopite Apatite	Plagioclase = 49% Orthopyroxene = 25% Clinopyroxene = 15% Magnetite = 5% Phlogopite = 4% Apatite = 2%	Fine-grained	Intergranular	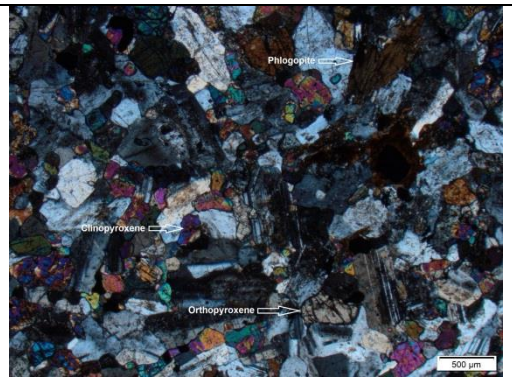
1336 **Cross-cutting Feldspar-magnetite rich vein**	Plagioclase Magnetite Alkali feldspar Quartz Phlogopite	Zircon Apatite	Plagioclase = 40% Alkali feldspar = 18% Magnetite = 15% Quartz = 10% Phlogopite = 10% Zircon = 5% Apatite = 2%	Coarse-grained	Equigranular	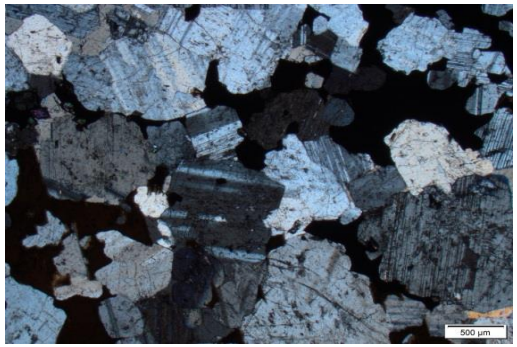
1356.3 **Olivine-free Gabbronorite**	Plagioclase Clinopyroxene Orthopyroxene	Magnetite Phlogopite Apatite	Plagioclase = 48% Clinopyroxene = 16% Orthopyroxene = 16% Magnetite = 9% Phlogopite = 9% Apatite = 2%	Fine-grained	Intergranular	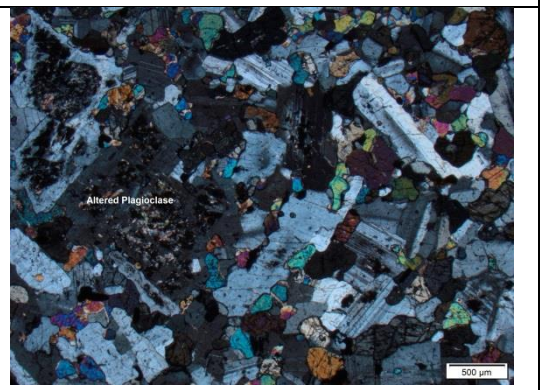

1363.45 **Olivine-free Gabbronorite**	Plagioclase Clinopyroxene Orthopyroxene	Magnetite Phlogopite Apatite	Plagioclase = 52% Orthopyroxene = 16% Clinopyroxene = 14% Magnetite = 8% Phlogopite = 7% Zircon = 3%	Fine to Coarse-grained (Contact)	Glomerophyric	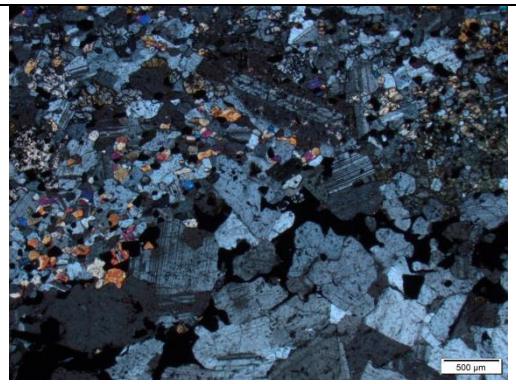
1381.7 **Olivine-free Gabbronorite** **(with cross-cutting feldspar-quartz-magnetite vein)**	Plagioclase Clinopyroxene Orthopyroxene Phlogopite	Magnetite Zircon Apatite Hornblende	Plagioclase = 41% Orthopyroxene = 20% Clinopyroxene = 10% Phlogopite = 10% Hornblende = 8% Magnetite = 6% Zircon = 3% Apatite = 2%	Fine to coarse-grained	Intergranular	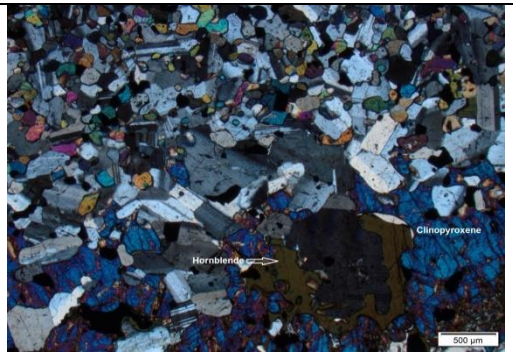
1385.3 **Feldspar-magnetite vein**	Magnetite Plagioclase Orthopyroxene	Zircon Apatite Alkali feldspar	Magnetite = 35% Plagioclase = 25% Orthopyroxene = 25% Zircon = 7% Alkali feldspar = 5% Apatite = 3%	Coarse-grained	Equigranular with perthitic feldspar	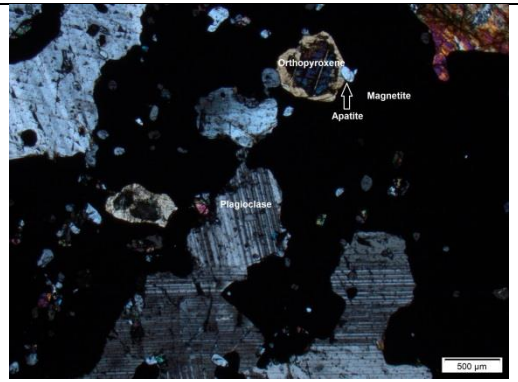

1401.5 **Feldspar-magnetite vein**	Magnetite Plagioclase	Alkali feldspar Phlogopite Zircon Clinopyroxene Orthopyroxene Apatite	Magnetite = 36% Plagioclase = 35% Alkali feldspar = 8% Phlogopite = 6% Zircon = 5% Clinopyroxene = 4% Orthopyroxene = 4% Apatite = 2%	Coarse-grained	Equigranular with perthitic feldspar	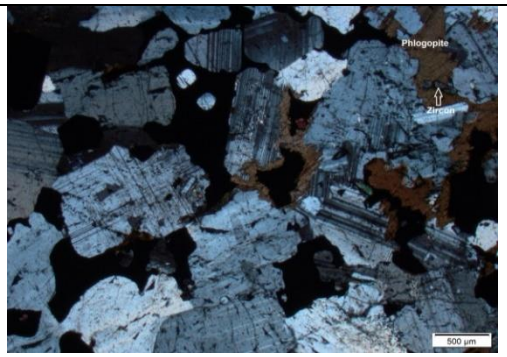
1418.5 **Olivine-free Gabbronorite**	Plagioclase Clinopyroxene Orthopyroxene	Opaques Phlogopite	Plagioclase = 55% Clinopyroxene = 20% Orthopyroxene = 15% Opaques = 5% Phlogopite = 5%	Fine-grained	Intergranular	
1451.5 **Olivine-free Gabbronorite**	Plagioclase Clinopyroxene Orthopyroxene Phlogopite	Magnetite Apatite	Plagioclase = 52% Clinopyroxene = 15% Orthopyroxene = 15% Phlogopite = 10% Magnetite = 5% Apatite = 3%	Fine to medium-grained	Intergranular	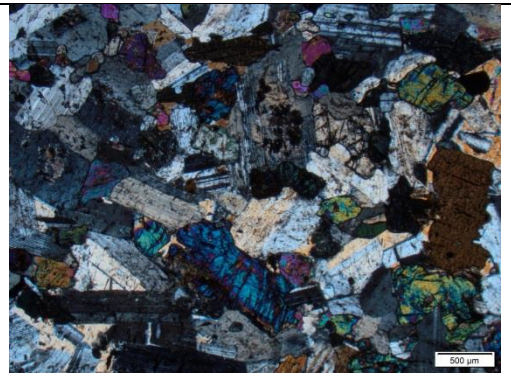

1464.2 **Feldspar-magnetite vein**	Plagioclase Magnetite Alkali feldspar Quartz Phlogopite	Orthopyroxene Zircon	Plagioclase = 45% Magnetite = 15% Alkali feldspar = 10% Quartz = 10% Phlogopite = 10% Orthopyroxene =7% Zircon = 3%	Coarse-grained	Equigranular to poikilitic with perthitic Feldspar	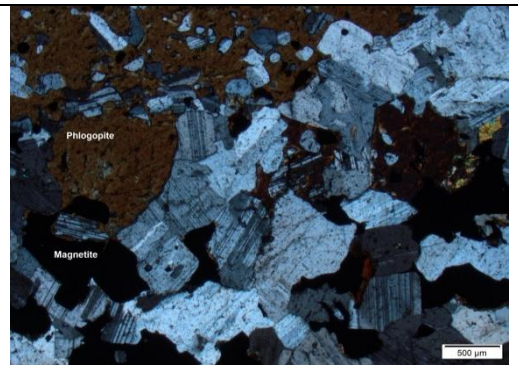
1481.5 **Feldspar vein**	Plagioclase Magnetite Alkali feldspar Phlogopite	Quartz Hornblende Orthopyroxene Zircon Apatite	Plagioclase = 40% Magnetite = 15% Phlogopite = 15% Alkali feldspar = 10% Quartz = 6% Orthopyroxene = 5% Hornblende = 5% Zircon = 3% Apatite = 1%	Coarse-grained	Hypidiomorphic	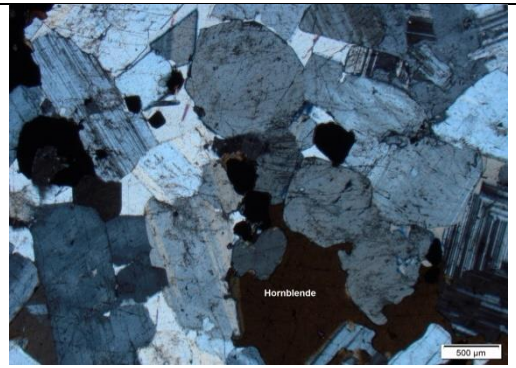
1541.5 **Olivine-free Gabbronorite**	Plagioclase Orthopyroxene Clinopyroxene	Phlogopite Opaques Apatite	Plagioclase = 50% Clinopyroxene = 20% Orthopyroxene = 20% Phlogopite = 6% Opaques = 3% Apatite = 1%	Fine-grained	Ophitic to poikilitic and hypidiomorphic	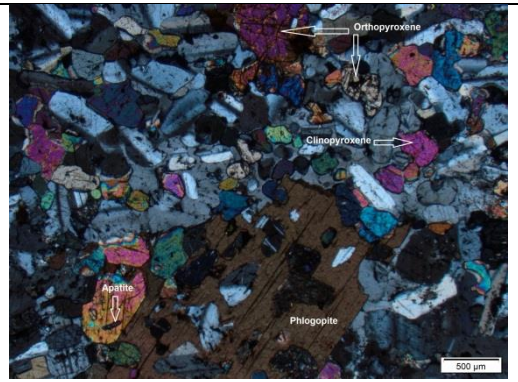

1570.5 **Olivine-free Gabbronorite**	Plagioclase Clinopyroxene Orthopyroxene	Phlogopite Opaques	Plagioclase = 45% Clinopyroxene = 23% Orthopyroxene = 20% Phlogopite = 7% Opaques = 5%	Fine-grained	Intergranular to subophitic	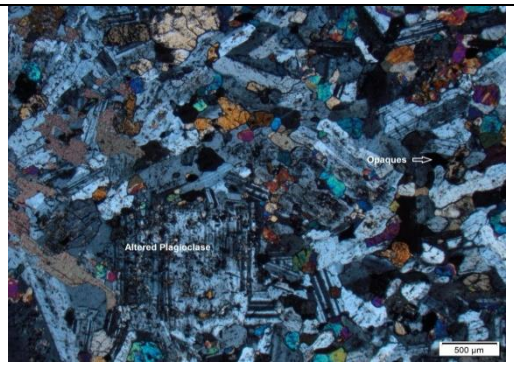
1609.8 **Olivine-free Gabbronorite**	Plagioclase Clinopyroxene Orthopyroxene	Phlogopite Opaques Pyrite	Plagioclase = 45% Orthopyroxene = 23% Clinopyroxene = 22% Phlogopite = 5% Opaques = 3% Pyrite = 2%	Fine-grained	Ophitic	
1640 **Feldspar vein**	Alkali feldspar Plagioclase Quartz	Magnetite Hornblende Phlogopite Orthopyroxene Zircon	Alkali feldspar = 40% Plagioclase = 25% Quartz = 15% Magnetite = 5% Phlogopite = 5% Hornblende = 5% Orthopyroxene = 3% Zircon = 2%	Coarse-grained	Hypidiomorphic with perthitic Feldspar	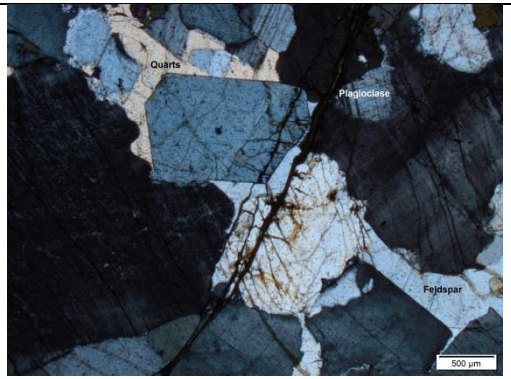

1654 **Olivine-free Gabbronorite**	Plagioclase Clinopyroxene Orthopyroxene	Opaques Phlogopite	Plagioclase = 45% Clinopyroxene = 23% Orthopyroxene =22% Opaques = 5% Phlogopite = 5%	Fine-grained	Intergranular to subophitic	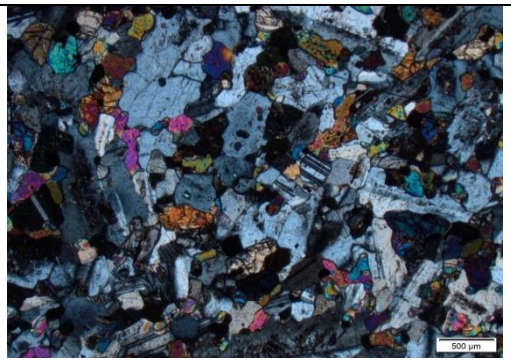
1696.5 **Olivine-free Gabbronorite**	Plagioclase Clinopyroxene Orthopyroxene Phlogopite	Magnetite	Plagioclase = 42% Orthopyroxene = 23% Clinopyroxene = 20% Phlogopite = 10% Magnetite = 5%	Fine-grained	Intergranular to ophitic	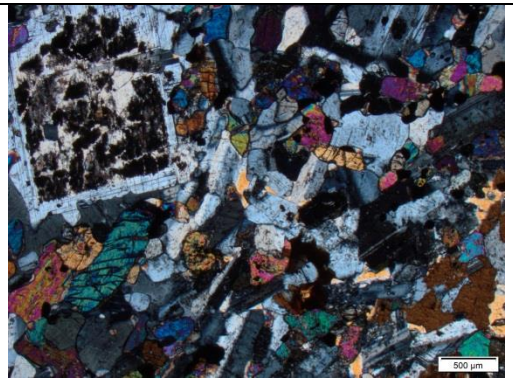
1755 **Quartz-feldspar vein**	Alkali feldspar Plagioclase Quartz Hornblende	Magnetite Phlogopite	Alkali feldspar = 40% Plagioclase = 20% Quartz = 15% Hornblende = 10% Phlogopite = 5% Magnetite = 5% Orthopyroxene = 5%	Coarse-grained	Hypidiomorphic with perthitic feldspar	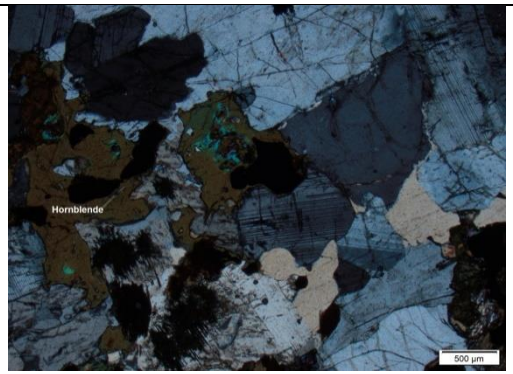

1796.6 **Olivine-free Gabbronorite**	Plagioclase Clinopyroxene Orthopyroxene	Phlogopite Opaques	Plagioclase = 45% Clinopyroxene = 22% Orthopyroxene =20% Phlogopite = 8% Opaques = 5%	Fine-grained	Subophilitic to porphyric	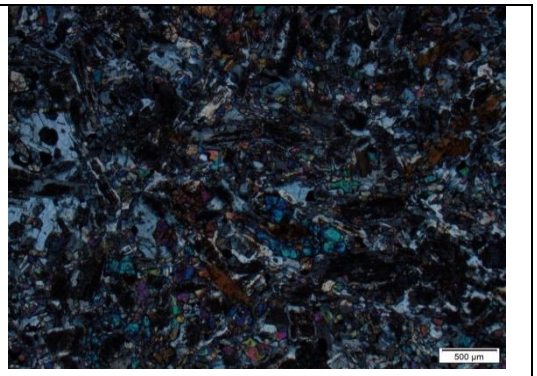
1842.5 **Metamorphosed quartz-feldspathic xenolith**	Alkali feldspar Quartz Plagioclase		Alkali feldspar = 55% Quartz = 35% Plagioclase = 10%	Coarse-grained	Equigranular to granophyric	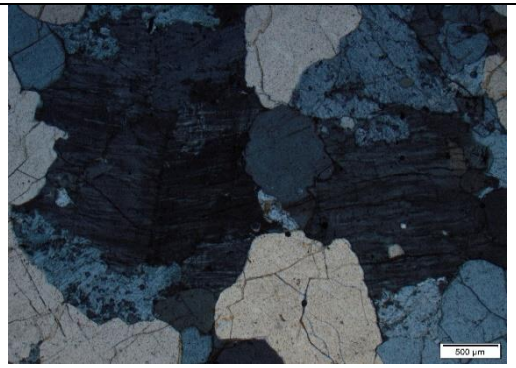
1843.5 **Metamorphosed quartz-feldspathic xenolith**	Quartz Alkali feldspar	Plagioclase Opaques Phlogopite Zircon	Quartz = 55% Alkali feldspar = 25% Opaques = 7% Plagioclase = 5% Phlogopite = 5% Zircon = 3%	Coarse-grained	Equigranular	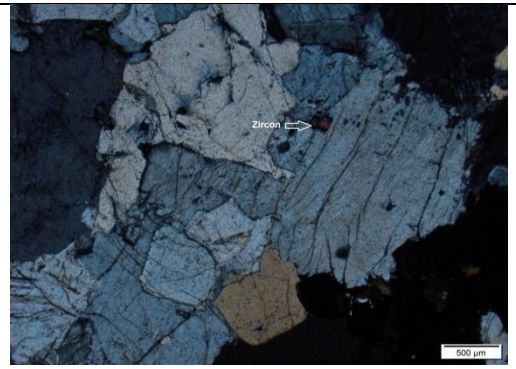

1844.4 **Metamorphosed xenolith of argillite**	Quartz Alkali feldspar	Clinopyroxene Orthopyroxene Opaques Plagioclase	Quartz = 42% Alkali feldspar = 38% Clinopyroxene = 8% Orthopyroxene = 7% Opaques = 3% Plagioclase = 2%	Fine-grained	Granoblastic	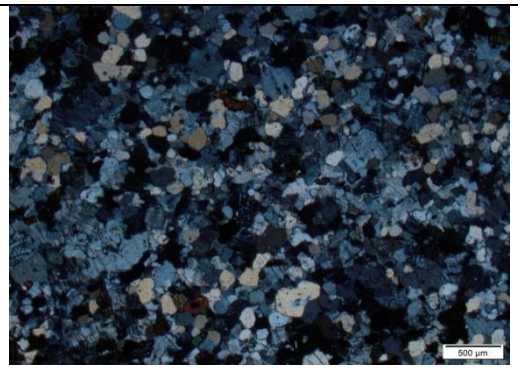
1890.5 **Feldspar-magnetite vein**	Plagioclase Alkali feldspar Olivine	Magnetite	Plagioclase = 50% Alkali feldspar = 35% Olivine = 10% Magnetite = 5%	Coarse-grained	Hypidiomorphic to granophyric	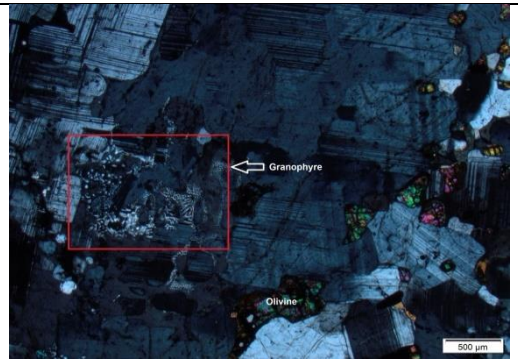
1896.5 **Olivine-free Gabbronorite**	Plagioclase Clinopyroxene Orthopyroxene	Opaques Phlogopite	Plagioclase = 55% Clinopyroxene = 20% Orthopyroxene = 15% Opaques = 5% Phlogopite = 5%	Fine to Coarse-grained	Intergranular to ophitic and porphyric	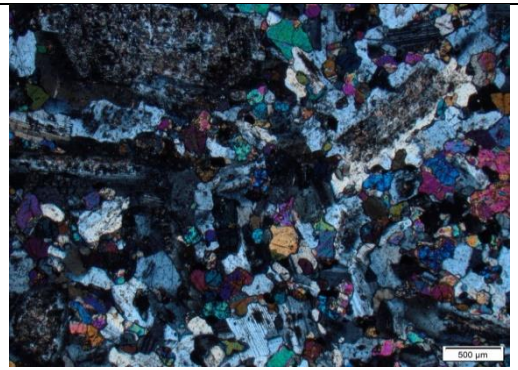

1904.5 **Quartz-feldspar-plagioclase vein**	Plagioclase Alkali feldspar Quartz	Clinopyroxene Orthopyroxene Olivine Zircon	Plagioclase = 30% Alkali feldspar =38% Quartz = 13% Clinopyroxene = 6% Orthopyroxene = 4% Olivine = 7% Zircon = 2%	Coarse-grained	Hypidiomorphic to granophyric with perthitic feldspar	
1911.7 **Phlogopite Olivine-free Gabbronorite**	Plagioclase Clinopyroxene Orthopyroxene Phlogopite	Opaques	Plagioclase = 35% Clinopyroxene= 25% Orthopyroxene = 20% Phlogopite = 15% Opaques = 5%	Fine to Coarse-grained	Subophilitic	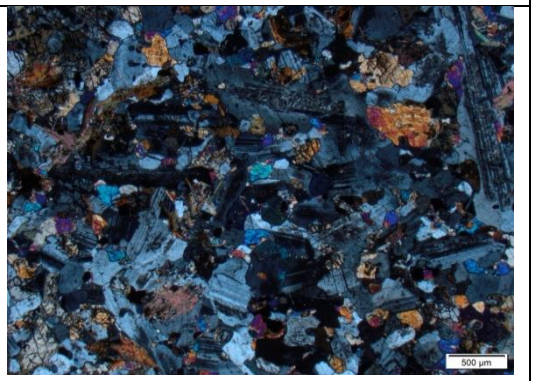
1998 **Olivine-free Gabbronorite**	Plagioclase Clinopyroxene Orthopyroxene Phlogopite	Opaques	Plagioclase = 45% Clinopyroxene =20% Orthopyroxene = 20% Phlogopite = 10% Opaques = 5%	Fine to medium-grained	Subophilitic to ophitic	

2043 **Monzodiorite**	Alkali feldspar Plagioclase Olivine Quartz Magnetite	Clinopyroxene Zircon	Alkali feldspar = 40% Plagioclase = 15% Olivine = 15% Magnetite = 10% Quartz = 10% Clinopyroxene = 8% Zircon = 2%	Coarse-grained	Hypidiomorphic to perthite and Granophyric textures	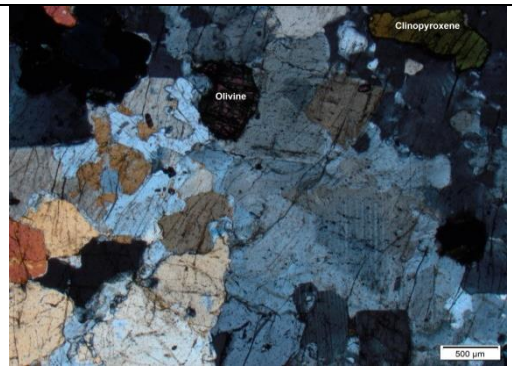
2054.5 **Pyroxene granite or migmatised sediments**	Alkali feldspar Quartz Clinopyroxene	Orthopyroxene Opaques Plagioclase	Alkali feldspar = 40% Quartz = 32% Clinopyroxene = 14% Orthopyroxene = 6% Opaques = 5% Plagioclase = 3%	Fine-grained	Granoblastic	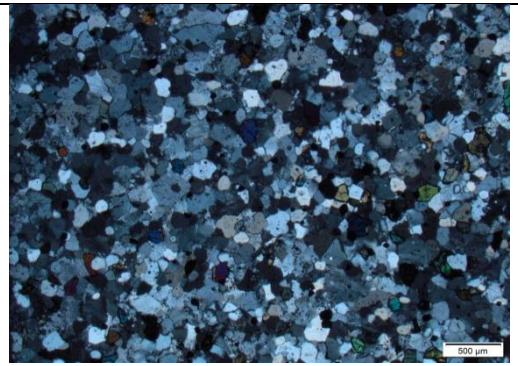
2076.8 **Monzodiorite**	Alkali feldspar Quartz Olivine	Plagioclase Clinopyroxene Magnetite Zircon	Alkali feldspar = 45% Quartz = 20% Olivine = 15% Plagioclase = 8% Clinopyroxene = 6% Magnetite = 5% Zircon = 1%	Coarse-grained	Hypidiomorphic to granophyric with perthitic feldspar	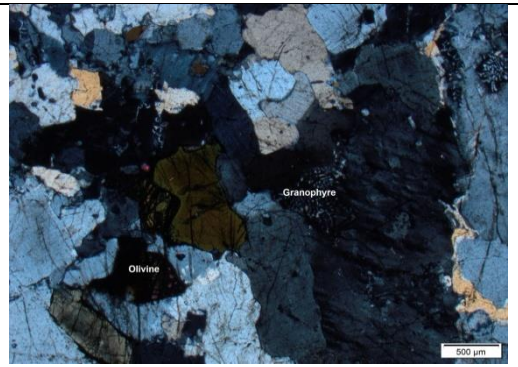

2148.5 **Pyroxene granite or migmatised sediments**	Alkali feldspar Quartz Clinopyroxene	Plagioclase Olivine Opaques Orthopyroxene	Alkali feldspar = 40% Quartz = 30% Clinopyroxene = 15% Opaques = 5% Olivine = 5% Orthopyroxene = 3% Plagioclase = 2%	Fine grained	Granoblastic	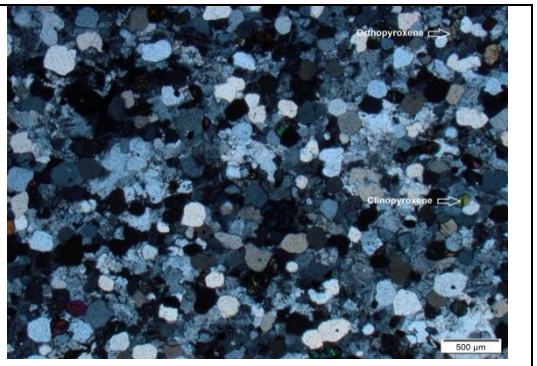
2155.6 **Quartz-feldspar vein or pyroxene granite**	Alkali feldspar Quartz Olivine	Magnetite Clinopyroxene Plagioclase	Alkali feldspar = 38% Quartz = 37% Olivine = 15% Magnetite = 5% Clinopyroxene = 3% Plagioclase = 2%	Coarse-grained	Hypidiomorphic to perthite and Granophyric textures	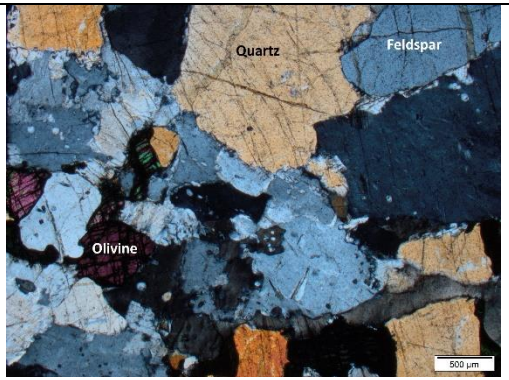
2157.5 **Olivine-bearing quartz-feldspar vein**	Alkali feldspar Quartz Olivine Magnetite	Plagioclase Clinopyroxene Apatite Zircon	Alkali feldspar = 25% Olivine = 25% Quartz = 20% Magnetite = 15% Plagioclase = 5% Clinopyroxene = 5% Apatite = 3% Zircon = 2%	Coarse-grained	Hypidiomorphic with perthitic feldspar	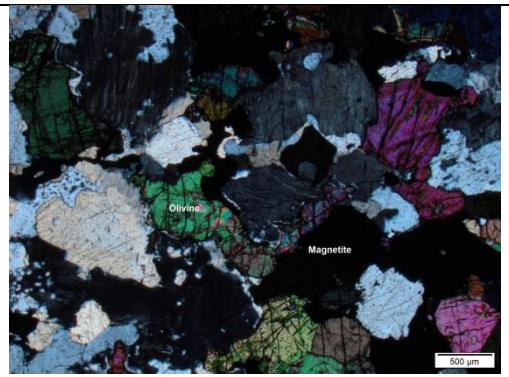

2177.2 **Olivine-bearing Gabbro**	Plagioclase Olivine Magnetite	Clinopyroxene Apatite	Plagioclase = 65% Olivine = 19% Clinopyroxene = 5% Magnetite = 10% Apatite = 1%	Coarse-grained	Hypidiomorphic	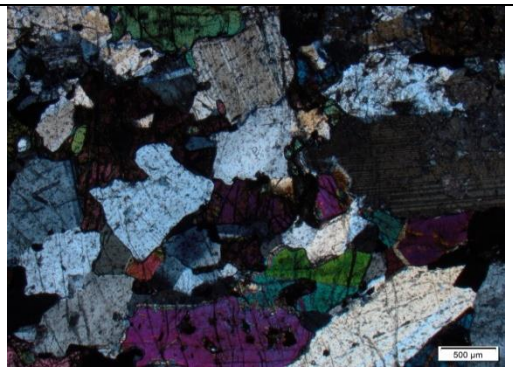
2193.2 **Hornfels after magnetite-rich shales**	Iron Oxides Clinopyroxene Orthopyroxene Alkali feldspar	Phlogopite	Iron oxides = 40% Clinopyroxene = 25% Alkali feldspar = 20% Orthopyroxene = 10% Phlogopite = 5%	Fine-grained	Granoblastic to lepidoblastic	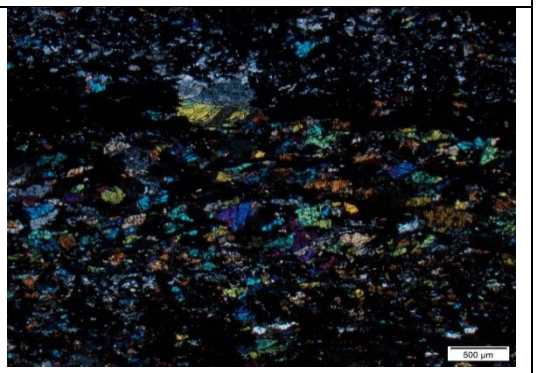
2205 **Plagio-phyric Olivine-magnetite Gabbro**	Plagioclase Olivine Clinopyroxene Magnetite	Apatite	Plagioclase = 50% Olivine = 25% Clinopyroxene = 13% Magnetite = 10% Apatite = 2%	Coarse-grained	Intergranular to porphyric and glomeroporphyritic	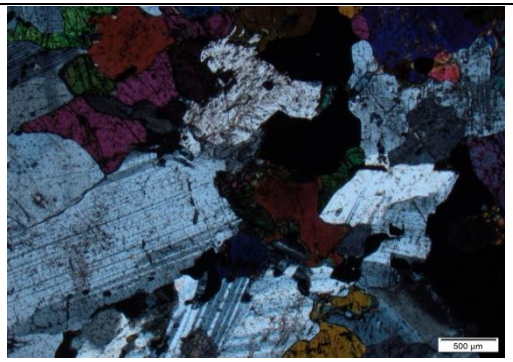

2220 **Plagio-phyric Olivine-magnetite Gabbro**	Plagioclase Olivine Clinopyroxene Magnetite	Apatite Orthopyroxene Zircon	Plagioclase = 39% Olivine = 20% Clinopyroxene = 15% Magnetite = 15% Apatite = 6% Orthopyroxene = 4% Zircon = 1%	Coarse-grained	Intergranular to equigranular	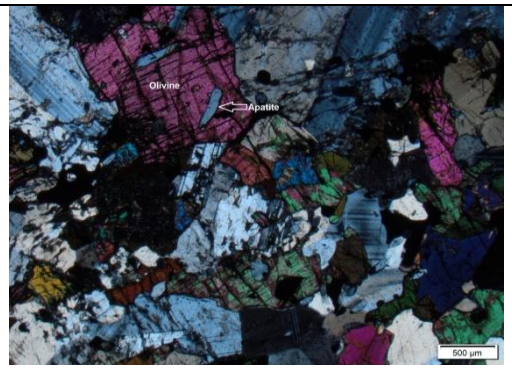
2297.2 **Plagio-phyric Olivine-magnetite Gabbro**	Plagioclase Olivine Magnetite Clinopyroxene	Orthopyroxene Apatite	Plagioclase = 35% Olivine = 23% Magnetite = 18% Clinopyroxene = 16% Orthopyroxene = 4% Apatite = 4%	Coarse-grained	Intergranular to equigranular	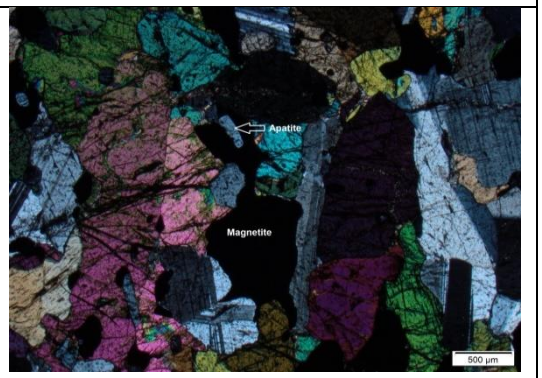
2300.5 **Olivine-magnetite Gabbro**	Plagioclase Olivine Magnetite Clinopyroxene	Apatite Orthopyroxene	Plagioclase = 31% Olivine = 24% Magnetite = 22% Clinopyroxene = 10% Apatite = 8% Orthopyroxene = 5%	Coarse-grained	Intergranular to equigranular	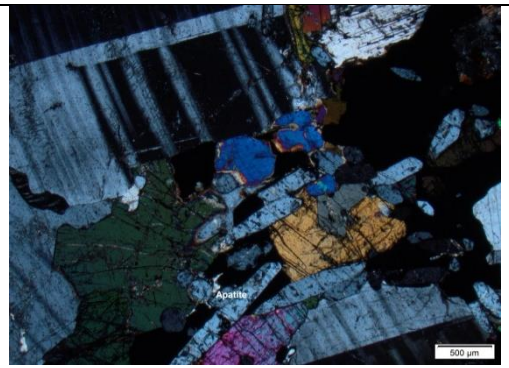

2332.5 **Olivine-magnetite Gabbro**	Plagioclase Olivine Clinopyroxene	Magnetite Orthopyroxene	Plagioclase = 53% Olivine = 20% Clinopyroxene = 17% Magnetite = 5% Orthopyroxene = 5%	Coarse-grained	Intergranular	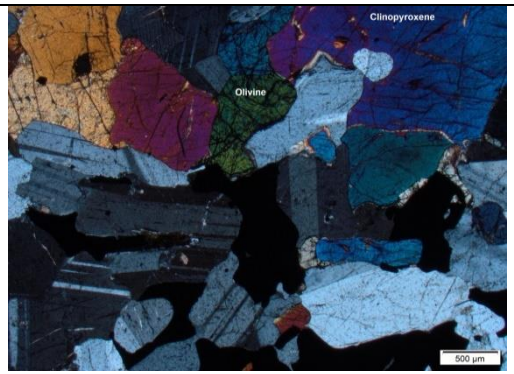
2371.3 **Olivine-magnetite Gabbro**	Plagioclase Olivine Clinopyroxene Magnetite	Alkali feldspar Orthopyroxene	Plagioclase = 43% Olivine = 25% Clinopyroxene = 15% Magnetite = 12% Orthopyroxene = 5%	Coarse-grained	Intergranular to equigranular	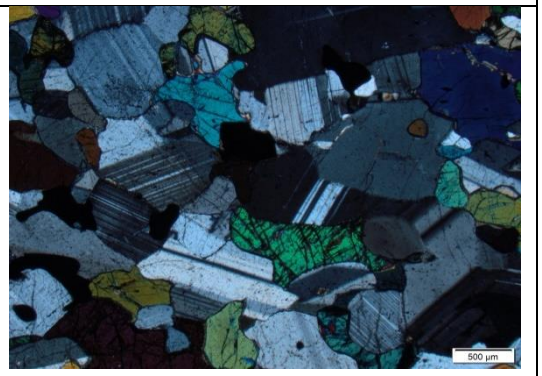
2374.9 **Mottled Anorthosite**	Plagioclase Magnetite Olivine	Orthopyroxene Clinopyroxene	Plagioclase = 58% Magnetite = 20% Olivine = 15% Clinopyroxene = 2% Orthopyroxene = 5%	Coarse-grained	Equigranular	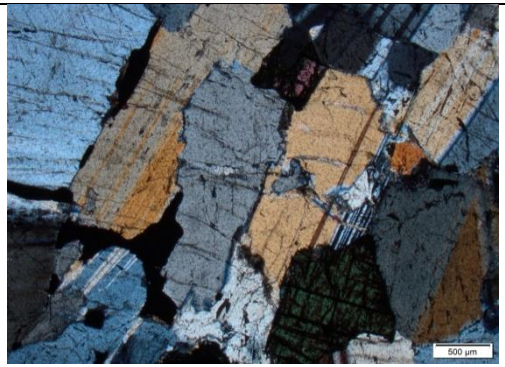

2377.8 **Mottled Anorthosite**	Plagioclase Clinopyroxene	Magnetite Phlogopite Orthopyroxene	Plagioclase = 70% Clinopyroxene = 15% Magnetite = 5% Phlogopite = 5% Orthopyroxene = 5%	Coarse-grained	Equigranular to poikilitic	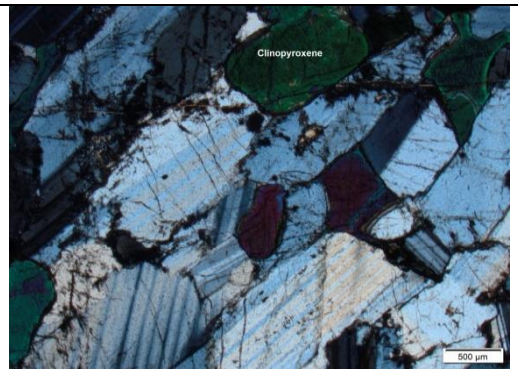
2391 **Olivine Gabbro to Troctolite**	Plagioclase Olivine Clinopyroxene Magnetite	Orthopyroxene	Plagioclase = 46% Olivine = 24% Clinopyroxene = 15% Magnetite = 10% Orthopyroxene = 5%	Coarse-grained	Intergranular to equigranular	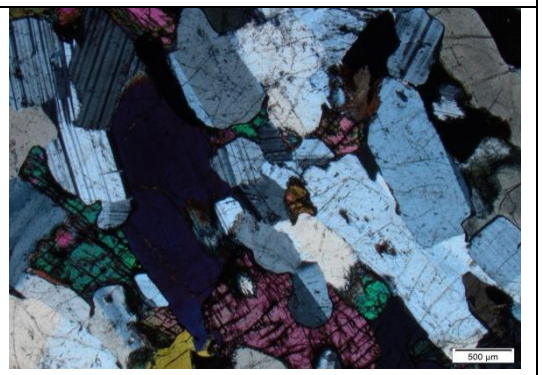
2474.5 **Olivine Gabbro to Troctolite**	Plagioclase Olivine Magnetite	Clinopyroxene Apatite Zircon	Plagioclase = 38% Olivine = 25% Magnetite = 20% Clinopyroxene = 8% Apatite = 6% Zircon = 3%	Coarse-grained	Intergranular to equigranular	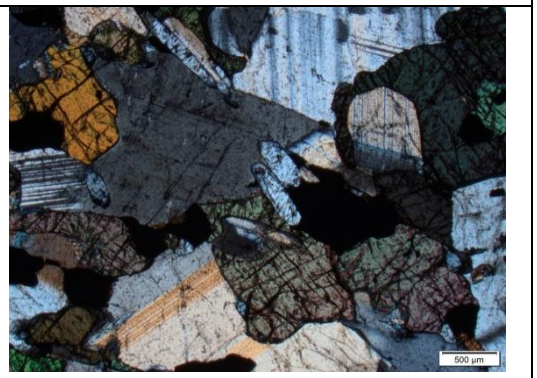

2496.1 **Olivine Gabbro to Troctolite**	Plagioclase Olivine Magnetite	Clinopyroxene Apatite	Plagioclase = 42% Olivine = 30% Magnetite = 15% Clinopyroxene = 8% Apatite = 5%	Coarse-grained	Intergranular to subophitic and equigranular	

Appendix C: NP1 Whole rock geochemistry results

Table C.1: Trace element data

Sample	Rock Name	Sc (ppm)	V (ppm)	Cr (ppm)	Co (ppm)	Ni (ppm)	Cu (ppm)	Zn (ppm)	Ga (ppm)	Rb (ppm)	Sr (ppm)	Y (ppm)	Zr (ppm)	Nb (ppm)	Mo (ppm)	Ba (ppm)	Pb (ppm)	Th (ppm)	U (ppm)
1318.35	FQMV	24.05	144.51	92.29	24.31	36.96	48.04	149.92	26.99	20.52	482.78	41.93	735.58	5.61	1.84	747.07	14.13	1.8	d.l.
1318.45	OFG	30.48	176.5	104.39	25.35	36.7	50.49	167.26	21.3	15.2	476.02	42.03	134.51	4.86	1.31	1800.3	10.36	d.l.	d.l.
1328.5	OFG	24.45	155.63	128.08	34.36	55.95	55.97	89.54	19.94	7.97	526.11	23.85	170.47	7.49	1.32	1477.75	9.34	0.83	d.l.
1336	FMV	9.01	88.85	9.28	25.14	28.64	24.12	205.53	38.3	33.54	613.09	14.3	2236.59	11.93	6.35	1365.04	14.78	14.9	d.l.
1356.3	OFG	28.26	142.1	168.88	31.97	65.77	49.43	103.83	20.13	13.92	520.74	24.36	171.12	8.11	1.01	1185.43	10.72	1.89	d.l.
1363.35	OFG	23.42	133.59	130.74	35.04	83	45.74	87.92	18.45	4.85	507.34	22.39	177.72	6.32	0.62	856.17	9.65	d.l.	0.09
1385.3	FMV	27.41	155.47	138.75	37.22	76.32	51.07	113.01	20.06	4.6	540.87	28.89	203.15	8.89	2.09	785.13	8.75	2.04	d.l.
1418.5	OFG	25.59	154.78	80.26	31.96	73.73	52.57	106.8	18.92	8.82	565.69	27.33	197.15	9.41	0.53	1223.01	13.86	1.93	d.l.
1451.5	OFG	29.79	151.41	161.06	33.61	73.46	53.16	84.23	19.49	15.58	537.67	25.36	149.5	9.83	0.83	584.64	9.96	4.49	d.l.
1481.5	FV	5.95	64.19	7.25	19.15	37.48	30.92	191.77	32.06	27.17	581.36	31.45	1514.16	31.29	5.54	1233.26	15.18	18.61	d.l.
1541.5	OFG	29.3	162.85	83.65	35.19	56.01	64.34	90.8	18.94	8.48	538.09	23.56	98.37	6.18	0.48	785.69	7.71	3.03	d.l.
1570.5	OFG	27.87	148.64	71.13	36.66	60.28	55.78	95.01	19.1	10.28	502.63	27.91	149.34	7.67	d.l.	887.22	9.48	5.42	d.l.
1609.8	OFG	33.45	154.59	181.9	37.65	61.6	60.64	89.07	16.38	6.52	552	21.83	94.22	2.57	0.23	729.39	6.33	d.l.	d.l.
1640	FV	6.99	d.l.	2.44	5.62	6.12	17.65	75.9	20.38	49.2	341.08	17.1	901.48	9.1	3.28	4731.47	9.55	d.l.	d.l.
1654	OFG	25.85	156.45	203.02	35.22	58.71	55.87	105.72	16.66	8.69	474.6	29.27	187.44	4.24	0.49	1115.23	10.54	d.l.	d.l.
1696.5	OFG	26.31	179.12	221.12	41.26	81.98	54.84	109.54	19.51	10.56	556.39	31.04	188.76	6.62	1.85	828.87	8.58	0.83	d.l.
1755	FV	4.56	5.09	4.02	3.4	15.21	12.97	121.94	26.83	92.59	520.89	21.76	806.07	9.56	2.55	9828.48	20.2	3.78	d.l.
1796.6	OFG	19.74	120.61	190.97	36.76	105.53	47.31	85.08	17.4	35.17	472.55	21.01	170.82	6.98	1.63	782.15	15.03	1.34	0.26
1842.5	Xeno	0.31	d.l.	1.28	5.31	3.47	7.1	24.37	13.79	43.65	133.19	5.81	50.61	0.85	1.4	2029.98	14.78	d.l.	d.l.
1843.5	Xeno	0.03	d.l.	6.68	2.69	3.16	11.48	69.17	16.05	63.81	168.82	13.23	487.33	7.33	1.04	2602.8	13.97	3.17	d.l.
1896.5	OFG	28.49	118	160.15	26.09	47.3	47.14	87.42	17.58	20.35	434.58	26.55	178.85	7.92	1.47	1115.82	11.93	4.91	d.l.
1904.5	FV	5.59	1.39	2.18	0.04	1.17	15.88	104.59	25.89	71.73	603.32	21.43	717.99	2.28	1.93	12680.99	12.86	8.99	d.l.
1911.7	OFG	25.53	154.76	52.13	30.56	28.36	45.01	109.22	18.49	18.52	488.93	27.57	212.7	9.45	0.72	1302.73	10.09	2.91	d.l.

1998	OFG	25.78	145.14	74.66	31.83	36.66	57.59	106.89	19.92	15.49	535.84	26.96	198.14	9	0.69	1691.18	9.49	2.76	d.l.
2043	MD	4.94	d.l.	2.34	2.71	4.07	24.58	115.57	23.8	58.77	454.27	32.73	821.03	12.71	3.3	6283.02	21.07	6.99	d.l.
2054.5	PG or MS	5.73	d.l.	1.25	1.42	1.69	14.65	95.01	18.86	116.59	102.25	30.97	339.66	8.62	3.11	1251.3	20.21	2.09	d.l.
2076.8	MD	8.78	d.l.	1.35	2.58	0.67	25.63	134.26	23.27	59.67	472.41	29.4	863.8	15.15	1.91	6699.22	14.77	3.74	d.l.
2148.5	PG or MS	6.55	d.l.	2.9	2.67	2	9.79	86.65	18.61	73.08	116.95	29.89	343.69	5.88	2.66	1408.99	16.62	0.58	d.l.
2155.6	OBG to OG	5	d.l.	d.l.	1.59	2.05	15.99	108.29	20.29	81.98	295.3	27.47	167.93	8.71	2.08	4598.55	20.57	2.69	d.l.
2177.2	OBG to OG	41.69	d.l.	0.75	0.11	0.66	53.43	270.3	29.09	6.92	462.71	46.75	87.53	33.17	2.58	660.52	10.75	d.l.	d.l.
2205	OBG to OG	80.36	d.l.	50.63	5.81	25.13	83.52	215.74	20.34	2.18	318.74	34.01	44.71	6.1	3.98	263.67	5.38	d.l.	d.l.
2220	OBG to OG	76.9	d.l.	0.79	6.2	6.15	90.94	215.59	24.27	3.5	321.27	46.2	48.26	10.03	3.08	333.01	4.15	d.l.	d.l.
2297.2	OBG to OG	107.66	d.l.	6.72	13.22	23.07	35.71	213.49	17.44	0.66	197	25.61	40.75	7.12	1.36	114.99	3.7	d.l.	d.l.
2300.5	OBG to OG	58.86	d.l.	8.16	23.25	22.37	51.88	242.46	18.11	1.83	244.81	58.35	55.98	12.35	1.88	162.48	7.13	d.l.	d.l.
2332.5	OBG to OG	100.59	d.l.	6.19	2.06	8.95	32.69	160.24	18.08	0.6	278.03	21.76	29.3	5.65	1.23	213.9	6.81	d.l.	d.l.
2371.3	OBG to OG	85.52	d.l.	1.18	13.18	3.3	29.41	167.43	23.4	3.14	362.07	12.71	34.24	4.33	3.14	257.98	3.28	d.l.	d.l.
2377.8	MA	21.77	d.l.	6.25	2.98	2.43	9.07	50.34	33.39	6.29	679.72	10.2	21.91	d.l.	1.44	354.91	3.98	d.l.	d.l.
2391	OBG to OG	74.94	d.l.	9.16	11.28	6.18	29.76	120.18	27.32	3.7	429.94	17.13	30.85	1.32	1.3	274.29	4.8	d.l.	d.l.
2474.5	OBG to OG	25.53	d.l.	7.09	6.2	0.32	66.84	180.46	25.68	3.61	364.38	26.96	25.08	2.16	1.96	191.38	0.94	d.l.	d.l.
2496.1	OBG to OG	46.81	d.l.	2.07	17.5	2.76	79.46	208.76	23.5	1.5	307.7	27.52	26.93	3.48	3.95	154.57	1.37	d.l.	d.l.

*OFG – Olivine-free gabbronorite

*OBG to OG – Olivine-bearing gabbro to Olivine gabbro

*MD – Monzodiorite

*MA – Mottled anorthosite

*Xeno – Xenolith

*FQMV – Feldspar-quartz-magnetite vein

*FMV – Feldspar-magnetite vein

*FV – Feldspar vein

*PG or MS – Pyroxenite granite or migmatised sediments

Table C.2: Major element data

Sample	Rock Name	SiO_2 (Wt.%)	Al_2O_3 (Wt.%)	Fe_2O_3 (Wt.%)	MnO (Wt.%)	MgO (Wt.%)	CaO (Wt.%)	Na_2O (Wt.%)	K_2O (Wt.%)	TiO_2 (Wt.%)	P_2O_5 (Wt.%)	Cr_2O_3 (Wt.%)	NiO (Wt.%)	LOI	Total
1318.35	FQMV	51.94	15.72	13.28	0.17	3.57	8.50	3.50	1.12	1.05	0.32	0.02	0.01	0.65	99.84
1318.45	OFG	52.10	14.69	12.31	0.23	4.67	9.83	3.14	1.30	0.94	0.35	0.03	0.01	0.49	100.10
1328.5	OFG	53.84	15.38	9.61	0.16	5.63	9.09	3.47	1.04	0.87	0.29	0.03	0.01	0.34	99.76
1336	FMV	48.69	18.64	18.37	0.09	0.45	5.09	4.20	1.84	2.72	0.13	0.01	0.00	-0.07	100.15
1356.3	OFG	53.96	15.85	9.27	0.16	5.34	9.17	3.50	1.31	0.81	0.27	0.04	0.01	0.23	99.91
1363.35	OFG	53.75	15.92	9.29	0.15	5.91	8.77	3.65	0.81	0.87	0.26	0.03	0.01	0.45	99.86
1385.3	FMV	53.38	15.65	10.21	0.16	5.57	8.78	3.63	0.83	1.04	0.36	0.03	0.01	0.10	99.75
1418.5	OFG	53.45	15.47	10.42	0.15	5.44	8.62	3.55	1.13	1.07	0.36	0.03	0.01	0.07	99.77
1451.5	OFG	54.11	15.62	8.95	0.14	6.01	9.31	3.35	0.97	0.89	0.34	0.03	0.01	0.20	99.92
1481.5	FV	52.78	18.86	12.63	0.11	1.06	5.66	4.34	1.63	2.57	0.24	0.01	0.01	0.12	100.00
1541.5	OFG	52.34	15.50	10.21	0.16	6.46	10.20	3.07	0.68	0.85	0.29	0.02	0.01	0.12	99.89
1570.5	OFG	53.81	15.22	9.86	0.15	6.04	9.46	3.35	0.89	0.81	0.26	0.02	0.01	0.10	99.98
1609.8	OFG	52.63	15.77	9.24	0.16	6.52	10.52	3.07	0.64	0.75	0.25	0.03	0.01	0.34	99.93
1640	FV	66.02	14.11	7.66	0.17	0.19	2.94	2.93	4.47	0.66	0.09	0.01	0.00	0.23	99.49
1654	OFG	52.81	15.32	10.14	0.16	5.90	9.67	3.25	0.92	0.83	0.29	0.04	0.01	0.55	99.90
1696.5	OFG	52.02	15.75	10.48	0.16	5.91	9.84	3.25	0.80	1.01	0.36	0.04	0.01	0.22	99.84
1755	FV	60.45	17.17	6.87	0.08	0.51	2.75	3.44	6.10	0.60	0.10	0.00	0.00	0.35	98.42
1796.6	OFG	53.94	15.93	8.58	0.13	6.43	8.77	3.39	1.38	0.73	0.26	0.04	0.01	0.35	99.94
1842.5	Xeno	80.93	9.38	1.48	0.02	0.03	0.90	2.26	3.89	0.05	0.01	0.00	0.00	0.20	99.15
1843.5	Xeno	72.17	12.46	4.24	0.07	0.06	1.47	3.06	5.05	0.34	0.04	0.00	0.00	0.33	99.28
1896.5	OFG	54.51	15.73	8.85	0.14	5.25	9.06	3.82	1.08	0.79	0.26	0.04	0.01	0.27	99.81
1904.5	FV	61.98	17.23	6.89	0.08	0.51	2.77	3.45	6.12	0.60	0.10	0.00	0.00	-0.02	99.71
1911.7	OFG	53.30	15.11	10.56	0.16	4.86	8.66	3.81	1.36	1.19	0.45	0.01	0.00	0.37	99.82
1998	OFG	53.01	15.60	10.46	0.17	5.27	9.30	3.44	1.24	1.11	0.41	0.02	0.01	0.02	100.06
2043	MD	65.52	14.19	7.24	0.14	0.05	3.03	4.11	4.06	0.70	0.06	0.00	0.00	0.02	99.11
2054.5	PG or MS	72.71	11.52	5.12	0.08	0.07	1.39	3.26	4.57	0.34	0.04	0.00	0.00	0.34	99.43

2076.8	MD	63.06	14.53	8.59	0.16	0.07	3.49	4.02	4.71	0.78	0.08	0.00	0.00	-0.04	99.44
2148.5	PG or MS	71.76	11.49	5.68	0.09	0.07	1.63	3.13	4.55	0.34	0.05	0.00	0.00	0.39	99.19
2155.6	OBG to OG	69.66	12.53	5.99	0.11	0.06	1.91	3.19	4.91	0.40	0.05	0.00	0.00	0.28	99.09
2177.2	OBG to OG	49.57	15.12	20.72	0.42	0.85	7.98	3.72	0.78	1.84	0.36	0.01	0.00	-0.91	100.45
2205	OBG to OG	43.42	11.04	30.69	0.52	1.75	9.58	2.33	0.33	2.12	0.73	0.02	0.00	-1.76	100.77
2220	OBG to OG	43.29	11.13	29.83	0.49	1.57	9.54	2.47	0.39	2.55	1.09	0.02	0.01	-1.76	100.61
2297.2	OBG to OG	38.15	6.79	37.06	0.56	2.38	10.90	1.24	0.15	4.90	0.67	0.02	0.01	-2.17	100.65
2300.5	OBG to OG	34.66	8.17	38.58	0.52	3.11	8.71	1.59	0.20	5.53	2.12	0.02	0.01	-2.52	100.72
2332.5	OBG to OG	44.03	10.94	30.75	0.54	1.56	10.24	2.44	0.29	1.32	0.41	0.01	0.00	-1.93	100.60
2371.3	OBG to OG	45.36	13.59	25.13	0.40	1.80	9.66	2.74	0.32	2.40	0.19	0.02	0.00	-1.15	100.46
2377.8	MA	53.87	24.31	4.07	0.06	0.29	9.71	5.23	0.68	0.56	0.28	0.00	0.00	0.64	99.69
2391	OBG to OG	49.13	16.06	18.69	0.31	1.56	10.52	3.30	0.38	1.19	0.22	0.01	0.00	-0.97	100.42
2474.5	OBG to OG	38.18	13.44	33.28	0.47	1.77	7.29	2.58	0.31	3.95	1.68	0.01	0.00	-2.47	100.48
2496.1	OBG to OG	37.32	11.63	34.85	0.50	2.45	7.95	2.26	0.29	3.84	1.67	0.01	0.00	-2.38	100.39

*OFG – Olivine-free gabbronorite

*OBG to OG – Olivine-bearing gabbro to Olivine gabbro

*MD – Monzodiorite

*MA – Mottled anorthosite

*Xeno – Xenolith

*FQMV – Feldspar-quartz-magnetite Vein

*FMV – Feldspar-magnetite vein

*FV – Feldspar vein

*PG or MS – Pyroxenite granite or migmatised sediments

Appendix D: NP1 Binary plots of SiO_2 against other major elements

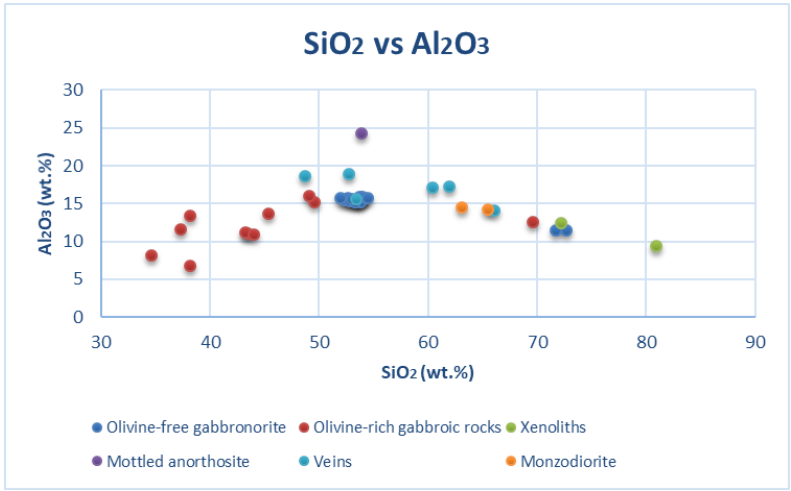

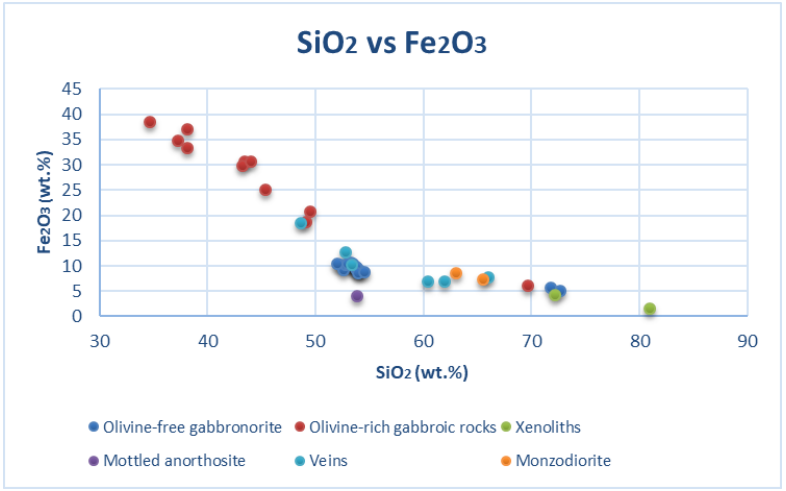

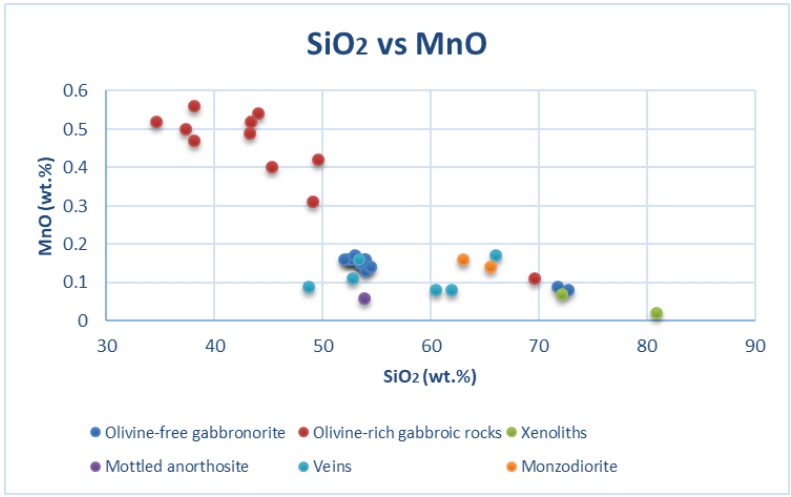

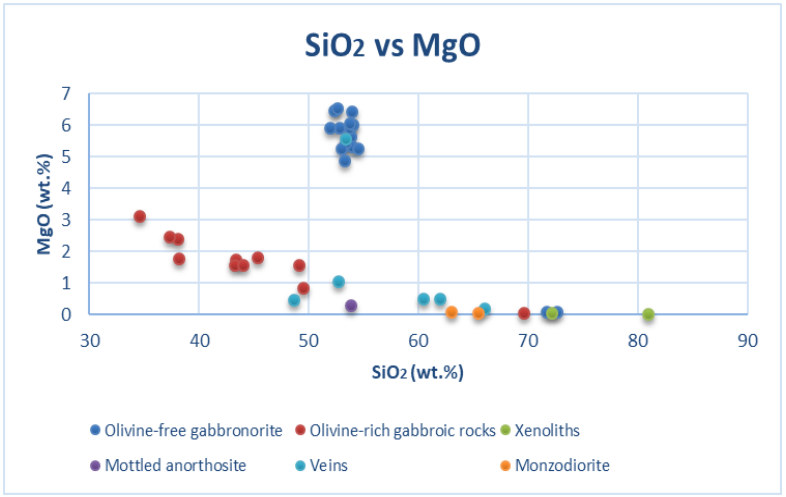

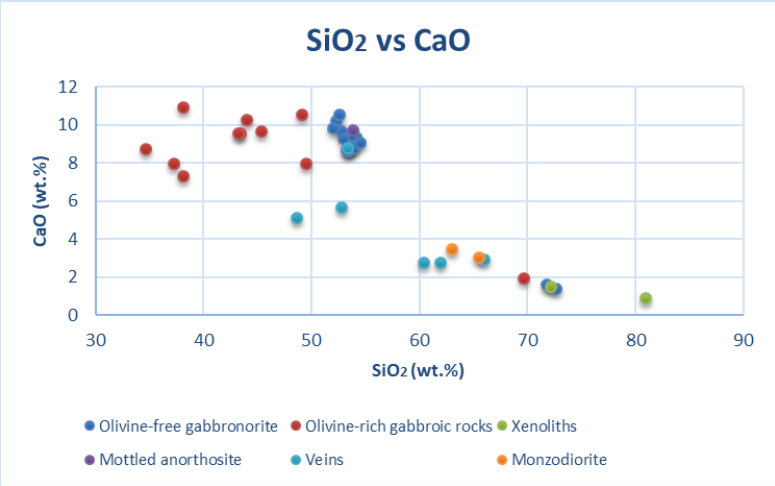
SiO2 vs CaO
CaO (wt.%)
SiO2 (wt.%)
Olivine-free gabbronorite
Olivine-rich gabbroic rocks
Xenoliths
Mottled anorthosite
Veins
Monzodiorite

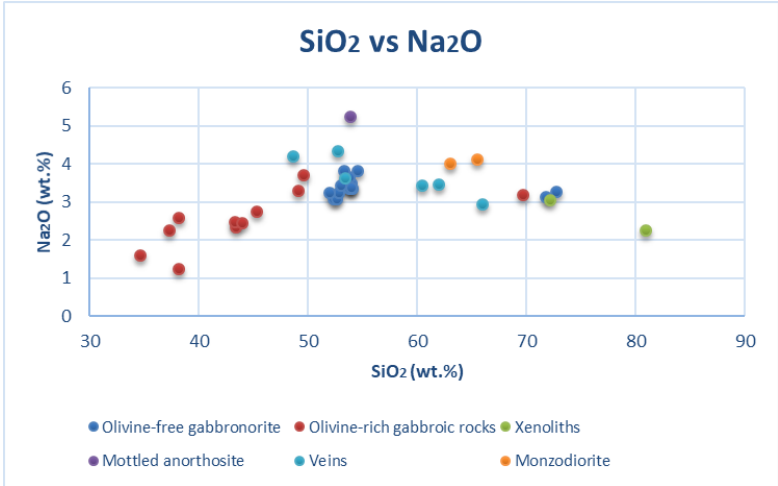
SiO2 vs Na2O
Na2O (wt.%)
SiO2 (wt.%)
Olivine-free gabbronorite
Olivine-rich gabbroic rocks
Xenoliths
Mottled anorthosite
Veins
Monzodiorite

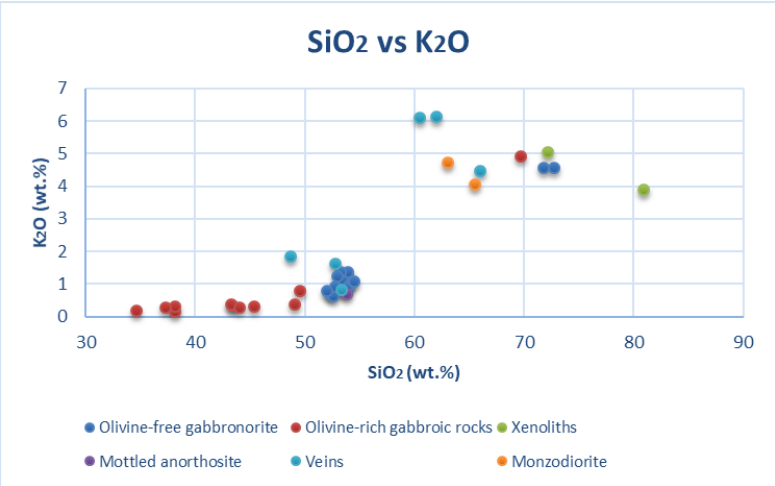
SiO2 vs K2O
K2O (wt.%)
SiO2 (wt.%)
Olivine-free gabbronorite
Olivine-rich gabbroic rocks
Xenoliths
Mottled anorthosite
Veins
Monzodiorite

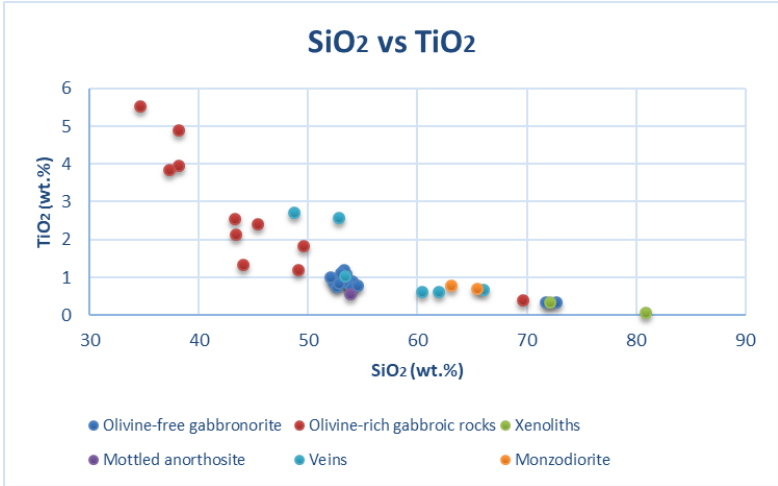
SiO2 vs TiO2
TiO2 (wt.%)
SiO2 (wt.%)
Olivine-free gabbronorite
Olivine-rich gabbroic rocks
Xenoliths
Mottled anorthosite
Veins
Monzodiorite

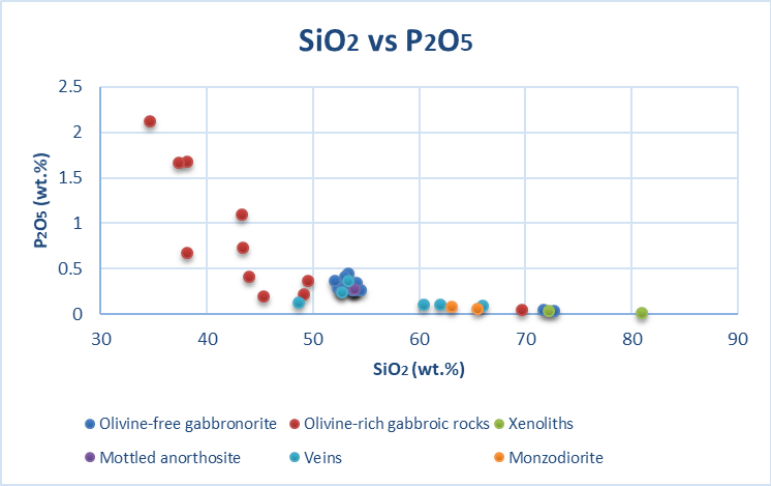
SiO2 vs P2O5
2.5
2
1.5
1
0.5
0
P2O5 (wt.%)
30
40
50
60
70
80
90
SiO2 (wt.%)
Olivine-free gabbronorite
Olivine-rich gabbroic rocks
Xenoliths
Mottled anorthosite
Veins
Monzodiorite

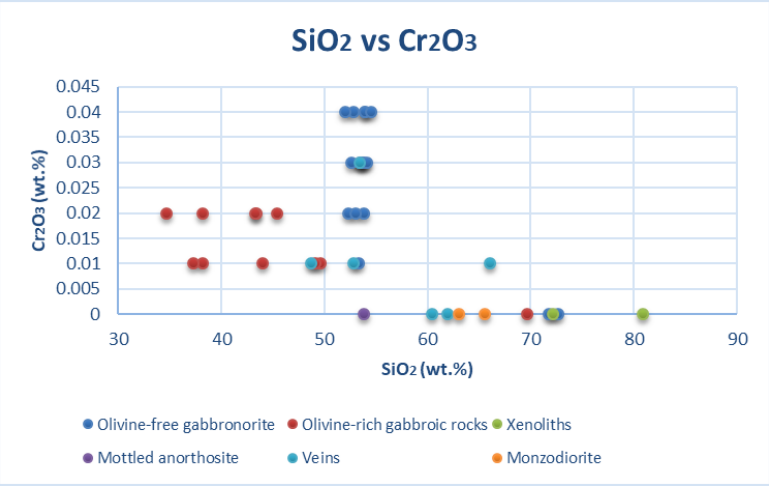
SiO2 vs Cr2O3
0.045
0.04
0.035
0.03
0.025
0.02
0.015
0.01
0.005
0
Cr2O3 (wt.%)
30
40
50
60
70
80
90
SiO2 (wt.%)
Olivine-free gabbronorite
Olivine-rich gabbroic rocks
Xenoliths
Mottled anorthosite
Veins
Monzodiorite

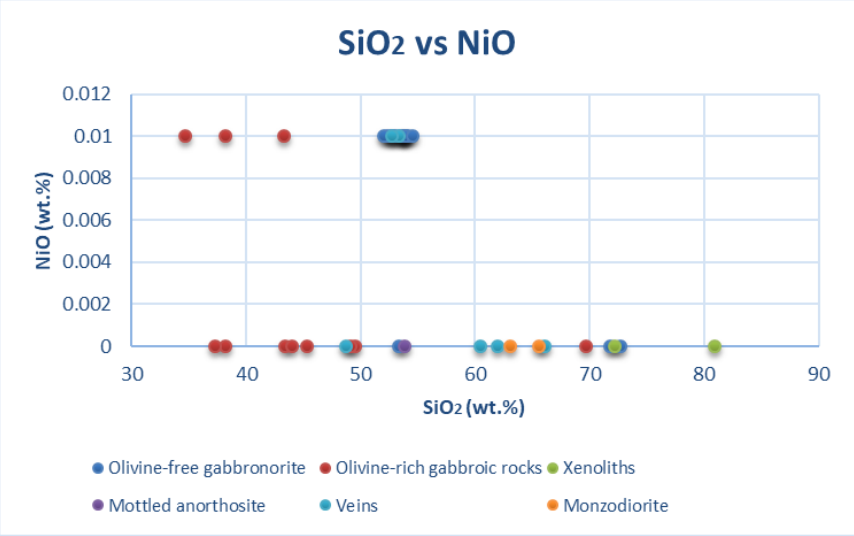
SiO2 vs NiO
0.012
0.01
0.008
0.006
0.004
0.002
0
NiO (wt.%)
30
40
50
60
70
80
90
SiO2 (wt.%)
Olivine-free gabbronorite
Olivine-rich gabbroic rocks
Xenoliths
Mottled anorthosite
Veins
Monzodiorite

Appendix E: NP1 Binary plots of MgO against other major elements

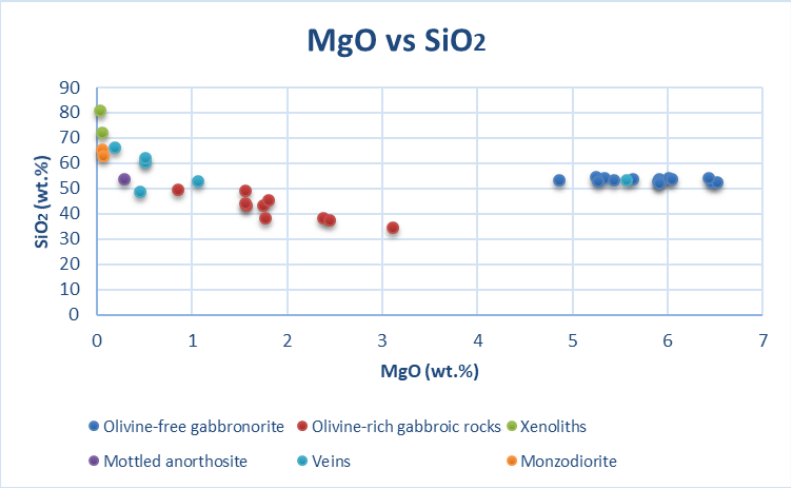

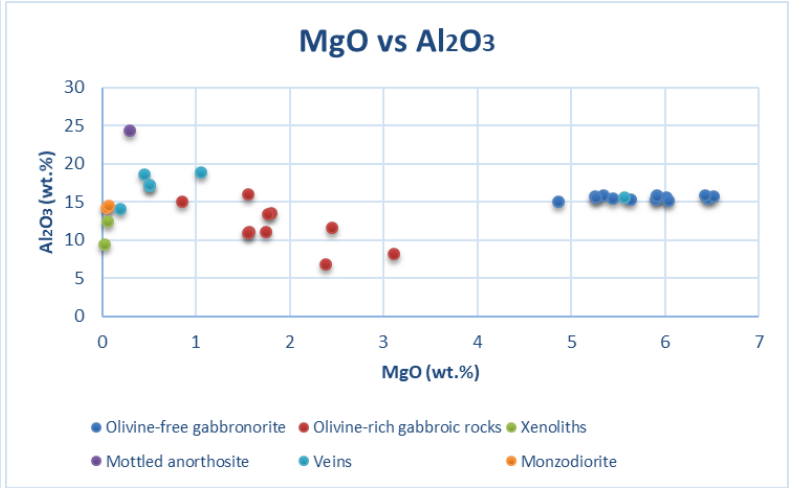

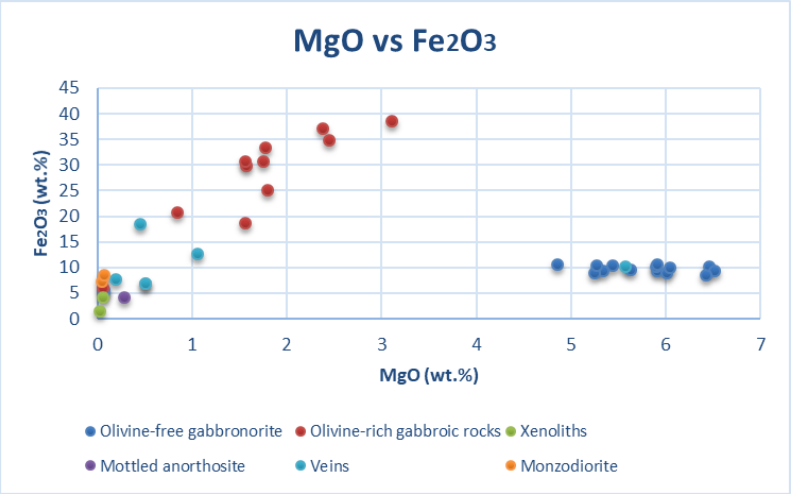

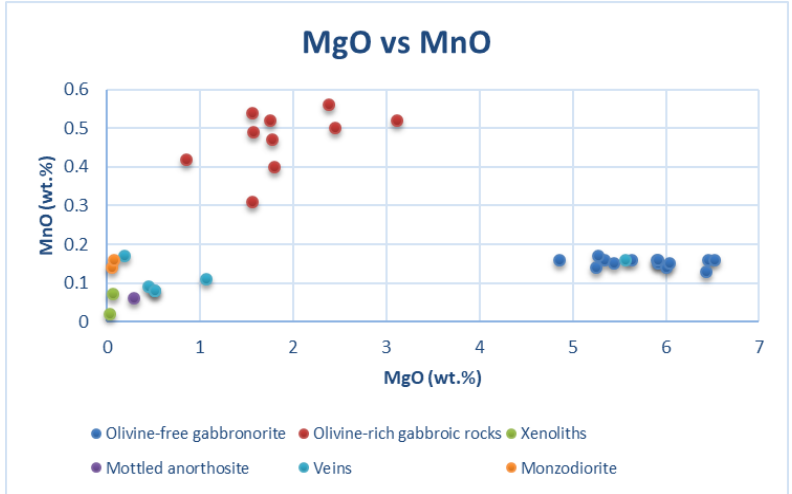

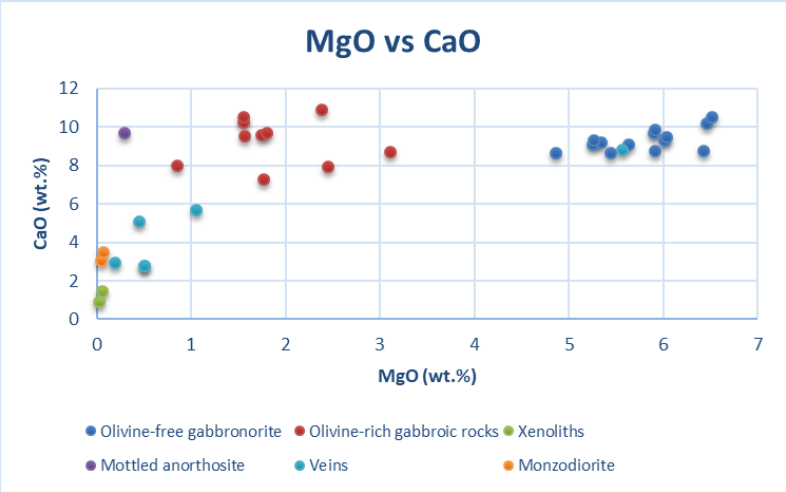
MgO vs CaO
CaO (wt.%)
MgO (wt.%)
Olivine-free gabbronorite
Olivine-rich gabbroic rocks
Xenoliths
Mottled anorthosite
Veins
Monzodiorite

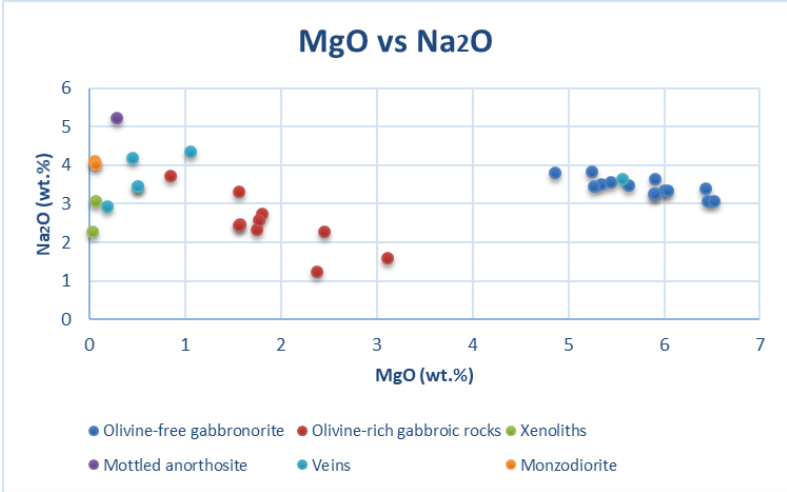
MgO vs Na2O
Na2O (wt.%)
MgO (wt.%)
Olivine-free gabbronorite
Olivine-rich gabbroic rocks
Xenoliths
Mottled anorthosite
Veins
Monzodiorite

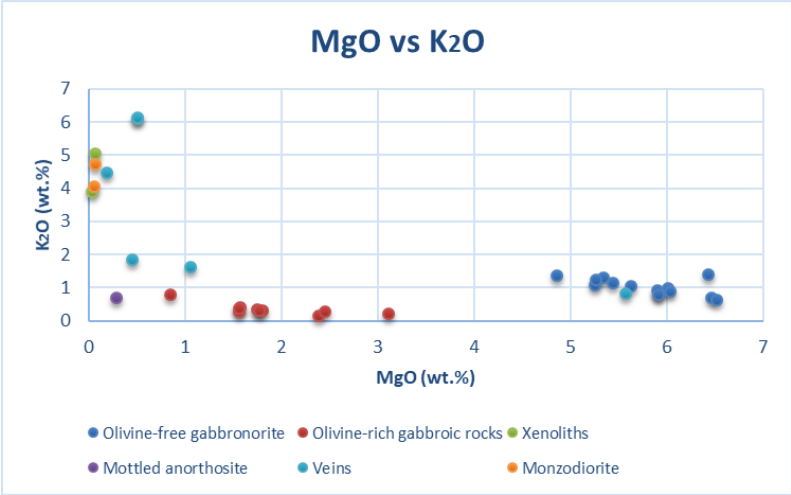
MgO vs K2O
K2O (wt.%)
MgO (wt.%)
Olivine-free gabbronorite
Olivine-rich gabbroic rocks
Xenoliths
Mottled anorthosite
Veins
Monzodiorite

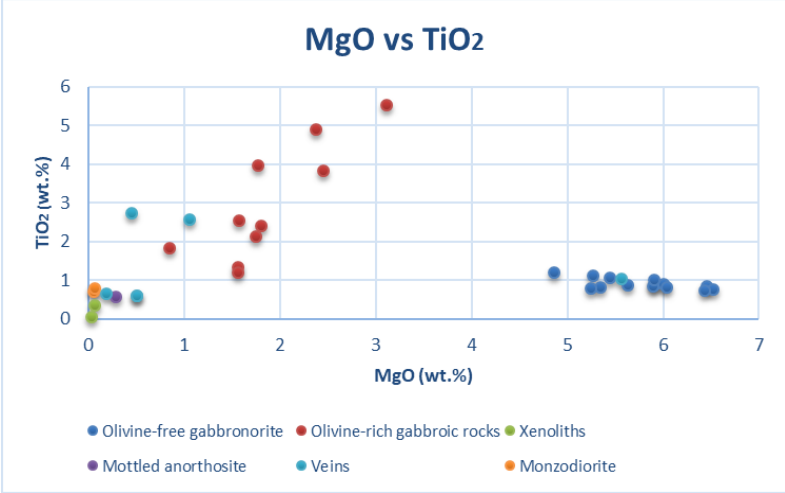
MgO vs TiO2
TiO2 (wt.%)
MgO (wt.%)
Olivine-free gabbronorite
Olivine-rich gabbroic rocks
Xenoliths
Mottled anorthosite
Veins
Monzodiorite

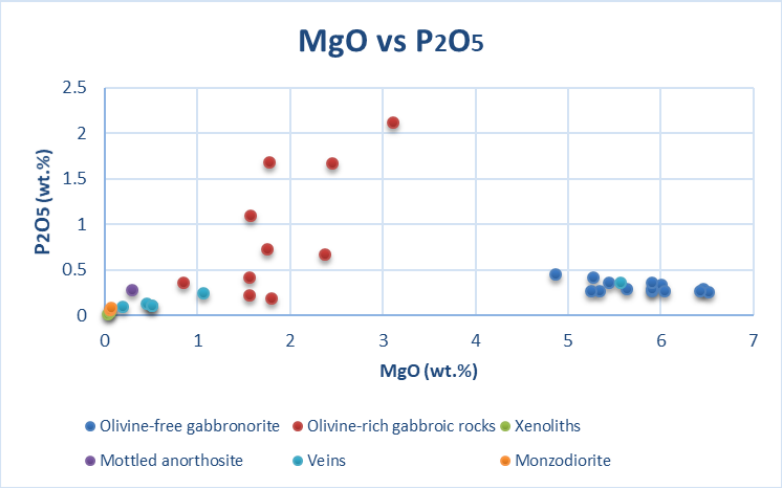
MgO vs P2O5
P2O5 (wt.%)
2.5
2
1.5
1
0.5
0
0
1
2
3
4
5
6
7
MgO (wt.%)
Olivine-free gabbronorite
Olivine-rich gabbroic rocks
Xenoliths
Mottled anorthosite
Veins
Monzodiorite

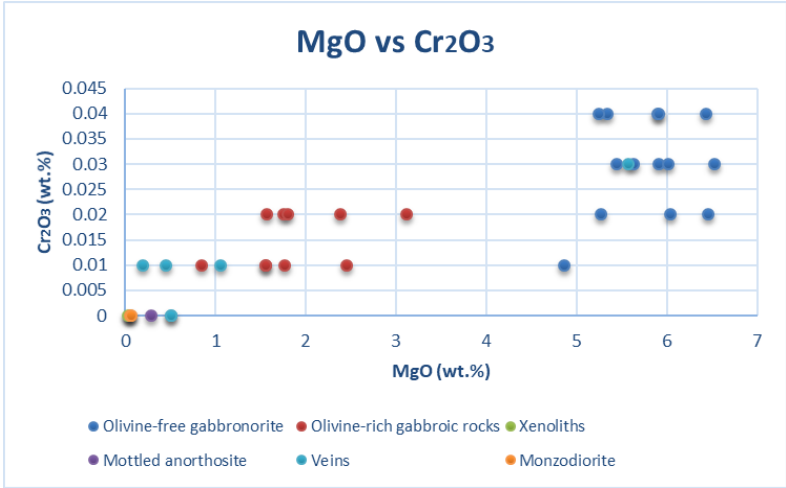
MgO vs Cr2O3
Cr2O3 (wt.%)
0.045
0.04
0.035
0.03
0.025
0.02
0.015
0.01
0.005
0
0
1
2
3
4
5
6
7
MgO (wt.%)
Olivine-free gabbronorite
Olivine-rich gabbroic rocks
Xenoliths
Mottled anorthosite
Veins
Monzodiorite

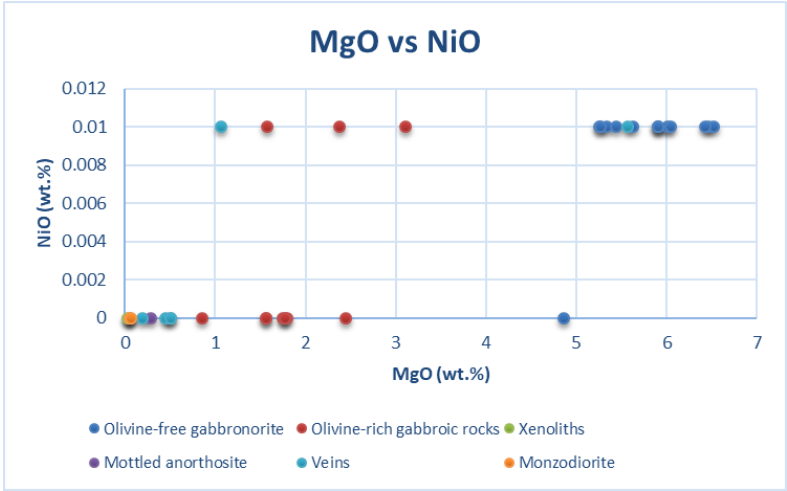
MgO vs NiO
NiO (wt.%)
0.012
0.01
0.008
0.006
0.004
0.002
0
0
1
2
3
4
5
6
7
MgO (wt.%)
Olivine-free gabbronorite
Olivine-rich gabbroic rocks
Xenoliths
Mottled anorthosite
Veins
Monzodiorite

Appendix F: NP1 Sr and Rb isotope results

Sample Number	Rock Name	Number of analyses	initial $^{87}Sr/^{86}Sr$	Corrected $^{87}Sr/^{86}Sr$	Corrected $^{87}Rb/^{86}Sr$
1318.35	Quartz-feldspar-magnetite vein	1	0.7059	0.7061	0.00561
1318.35	Quartz-feldspar-magnetite vein	2	0.7063	0.7065	0.00707
1318.35	Quartz-feldspar-magnetite vein	3	0.7056	0.7057	0.00306
1318.35	Quartz-feldspar-magnetite vein	4	0.7056	0.7056	0.00100
1318.35	Quartz-feldspar-magnetite vein	5	0.7056	0.7056	0.00311
1318.35	Quartz-feldspar-magnetite vein	6	0.7053	0.7055	0.00585
1318.35	Quartz-feldspar-magnetite vein	7	0.7057	0.7059	0.00524
1318.35	Quartz-feldspar-magnetite vein	8	0.7058	0.7060	0.00880
1318.35	Quartz-feldspar-magnetite vein	9	0.7055	0.7056	0.00314
1318.35	Quartz-feldspar-magnetite vein	10	0.7054	0.7056	0.00745
1318.35	Quartz-feldspar-magnetite vein	11	0.7056	0.7058	0.00549
1328.5	Gabbronorite	1	0.7052	0.7056	0.01412
1328.5	Gabbronorite	2	0.7053	0.7055	0.00687
1328.5	Gabbronorite	3	0.7049	0.7051	0.00611
1328.5	Gabbronorite	4	0.7051	0.7057	0.01994
1328.5	Gabbronorite	5	0.7049	0.7051	0.00807
1336	Feldspar-magnetite vein	1	0.7056	0.7058	0.00752
1336	Feldspar-magnetite vein	2	0.7054	0.7055	0.00378
1336	Feldspar-magnetite vein	3	0.7054	0.7055	0.00406
1336	Feldspar-magnetite vein	4	0.7054	0.7056	0.00492
1336	Feldspar-magnetite vein	5	0.7052	0.7053	0.00323
1336	Feldspar-magnetite vein	6	0.7053	0.7056	0.00825
1336	Feldspar-magnetite vein	7	0.7055	0.7056	0.00471
1363.45	Gabbronorite	1	0.7052	0.7052	0.00110
1363.45	Gabbronorite	2	0.7050	0.7051	0.00209
1363.45	Gabbronorite	3	0.7054	0.7062	0.02741

1363.45	Gabbronorite	4	0.7049	0.7051	0.00615
1363.45	Gabbronorite	5	0.7049	0.7050	0.00380
1363.45	Gabbronorite	6	0.7056	0.7057	0.00086
1363.45	Gabbronorite	7	0.7053	0.7053	0.00256
1363.45	Gabbronorite	8	0.7050	0.7053	0.01002
1363.45	Gabbronorite	9	0.7052	0.7053	0.00264
1381.7	Gabbronorite	1	0.7056	0.7057	0.00578
1381.7	Gabbronorite	2	0.7057	0.7060	0.01049
1381.7	Gabbronorite	3	0.7055	0.7055	0.00157
1381.7	Gabbronorite	4	0.7055	0.7056	0.00208
1381.7	Gabbronorite	5	0.7056	0.7057	0.00133
1381.7	Gabbronorite	6	0.7056	0.7057	0.00164
1381.7	Gabbronorite	7	0.7057	0.7062	0.02004
1418.5	Gabbronorite	1	0.7048	0.7050	0.00866
1418.5	Gabbronorite	2	0.7047	0.7051	0.01391
1418.5	Gabbronorite	3	0.7060	0.7078	0.06214
1418.5	Gabbronorite	4	0.7051	0.7060	0.03268
1418.5	Gabbronorite	5	0.7045	0.7047	0.00800
1418.5	Gabbronorite	6	0.7053	0.7060	0.02384
1451.5	Gabbronorite	1	0.7049	0.7050	0.00163
1451.5	Gabbronorite	2	0.7051	0.7052	0.00587
1451.5	Gabbronorite	3	0.7051	0.7051	0.00142
1451.5	Gabbronorite	4	0.7052	0.7053	0.00205
1570.5	Gabbronorite	1	0.7049	0.7053	0.01602
1570.5	Gabbronorite	2	0.7047	0.7049	0.00815
1570.5	Gabbronorite	3	0.7047	0.7052	0.01645
1570.5	Gabbronorite	4	0.7050	0.7060	0.03330
1570.5	Gabbronorite	5	0.7048	0.7054	0.01934
1570.5	Gabbronorite	6	0.7049	0.7055	0.02253
1570.5	Gabbronorite	7	0.7047	0.7051	0.01476

1609.8	Gabbronorite	1	0.7049	0.7050	0.00100
1609.8	Gabbronorite	2	0.7055	0.7055	0.00148
1609.8	Gabbronorite	3	0.7049	0.7049	0.00085
1609.8	Gabbronorite	4	0.7050	0.7053	0.00783
1609.8	Gabbronorite	5	0.7048	0.7049	0.00257
1696.5	Gabbronorite	1	0.7050	0.7054	0.01350
1696.5	Gabbronorite	2	0.7046	0.7047	0.00281
1696.5	Gabbronorite	3	0.7042	0.7043	0.00360
1696.5	Gabbronorite	4	0.7046	0.7047	0.00455
1696.5	Gabbronorite	5	0.7045	0.7046	0.00451
1696.5	Gabbronorite	6	0.7043	0.7046	0.00901
1796.6	Gabbronorite	1	0.7045	0.7057	0.04033
1796.6	Gabbronorite	2	0.7049	0.7052	0.01145
1796.6	Gabbronorite	3	0.7048	0.7062	0.04767
1796.6	Gabbronorite	4	0.7047	0.7058	0.03717
1796.6	Gabbronorite	5	0.7044	0.7070	0.08991
1796.6	Gabbronorite	6	0.7043	0.7073	0.10184
1796.6	Gabbronorite	7	0.7049	0.7074	0.08844
1890.5	Feldspar-magnetite vein	1	0.7062	0.7062	0.00098
1890.5	Feldspar-magnetite vein	2	0.7064	0.7066	0.00617
1890.5	Feldspar-magnetite vein	3	0.7060	0.7061	0.00371
1890.5	Feldspar-magnetite vein	4	0.7062	0.7063	0.00252
1890.5	Feldspar-magnetite vein	5	0.7066	0.7067	0.00128
1890.5	Feldspar-magnetite vein	6	0.7064	0.7065	0.00345
1890.5	Feldspar-magnetite vein	7	0.7068	0.7069	0.00389
1890.5	Feldspar-magnetite vein	8	0.7067	0.7070	0.01095
1890.5	Feldspar-magnetite vein	9	0.7067	0.7069	0.00501
1890.5	Feldspar-magnetite vein	10	0.7071	0.7073	0.00759
1896.5	Gabbronorite	1	0.7053	0.7055	0.00804
1896.5	Gabbronorite	2	0.7052	0.7054	0.00542

1896.5	Gabbronorite	3	0.7065	0.7077	0.03975
1896.5	Gabbronorite	4	0.7052	0.7061	0.03299
1896.5	Gabbronorite	5	0.7053	0.7060	0.02426
1896.5	Gabbronorite	6	0.7058	0.7064	0.02081
1896.5	Gabbronorite	7	0.7058	0.7068	0.03342
1896.5	Gabbronorite	8	0.7052	0.7061	0.03322
1896.5	Gabbronorite	9	0.7051	0.7055	0.01452
1904.5	Quartz-feldspar-plagioclase vein	1	0.7069	0.7070	0.00186
1904.5	Quartz-feldspar-plagioclase vein	2	0.7069	0.7071	0.00604
1904.5	Quartz-feldspar-plagioclase vein	3	0.7070	0.7071	0.00255
1904.5	Quartz-feldspar-plagioclase vein	4	0.7072	0.7072	0.00157
1911.7	Gabbronorite	1	0.7059	0.7069	0.03646
1911.7	Gabbronorite	2	0.7053	0.7076	0.08109
1911.7	Gabbronorite	3	0.7056	0.7072	0.05466
1911.7	Gabbronorite	4	0.7051	0.7057	0.02046
1911.7	Gabbronorite	5	0.7054	0.7077	0.07922
1911.7	Gabbronorite	6	0.7057	0.7071	0.04542
1998	Gabbronorite	1	0.7055	0.7055	0.00281
1998	Gabbronorite	2	0.7056	0.7057	0.00462
1998	Gabbronorite	3	0.7059	0.7060	0.00419
1998	Gabbronorite	4	0.7053	0.7054	0.00256
1998	Gabbronorite	5	0.7052	0.7053	0.00385
1998	Gabbronorite	6	0.7059	0.7063	0.01270
2177.2	Olivine gabbro	1	0.7069	0.7075	0.020113
2177.2	Olivine gabbro	2	0.7071	0.7073	0.007023
2177.2	Olivine gabbro	3	0.7071	0.7073	0.009052
2177.2	Olivine gabbro	4	0.7073	0.7077	0.011177
2177.2	Olivine gabbro	5	0.7072	0.7074	0.008751
2205	Olivine gabbro	1	0.7070	0.7073	0.009388
2205	Olivine gabbro	2	0.7071	0.7072	0.00474

2205	Olivine gabbro	3	0.7072	0.7076	0.011106
2205	Olivine gabbro	4	0.7072	0.7073	0.002859
2205	Olivine gabbro	5	0.7068	0.7072	0.012543
2205	Olivine gabbro	6	0.7067	0.7074	0.023634
2205	Olivine gabbro	7	0.7070	0.7077	0.025161
2297.2	Olivine gabbro	1	0.7072	0.7075	0.011976
2297.2	Olivine gabbro	2	0.707	0.7073	0.009671
2297.2	Olivine gabbro	3	0.7072	0.7074	0.010147
2297.2	Olivine gabbro	4	0.7073	0.7076	0.009159
2297.2	Olivine gabbro	5	0.7069	0.7071	0.010372
2374.9	Mottled anorthosite	1	0.7070	0.7071	0.002028
2374.9	Mottled anorthosite	2	0.7070	0.7072	0.007067
2374.9	Mottled anorthosite	3	0.7070	0.7072	0.005364
2374.9	Mottled anorthosite	4	0.7068	0.7069	0.002027
2374.9	Mottled anorthosite	5	0.7071	0.7072	0.003715
2374.9	Mottled anorthosite	6	0.7072	0.7072	0.001916
2391	Olivine gabbro	1	0.7064	0.7069	0.014464
2391	Olivine gabbro	2	0.7069	0.7070	0.004955
2391	Olivine gabbro	3	0.7071	0.7075	0.012869
2391	Olivine gabbro	4	0.7073	0.7074	0.004666
2391	Olivine gabbro	5	0.7073	0.7075	0.005457
2391	Olivine gabbro	6	0.7072	0.7075	0.009275
2496.1	Olivine gabbro	1	0.7070	0.7073	0.008952
2496.1	Olivine gabbro	2	0.7070	0.7073	0.009931
2496.1	Olivine gabbro	3	0.7067	0.7071	0.012296
2496.1	Olivine gabbro	4	0.7070	0.7072	0.008332
2496.1	Olivine gabbro	5	0.7070	0.7075	0.015632

Appendix G: Low and High Ti Dullstroom Formation rocks major element data from literature (Buchanan *et al*., 1999)

Table G.1: High Ti Dullstroom Formation rocks major element compositions determined by XRF and INAA (Instrumental Neutron Activation Analysis) (Buchanan *et al*., 1999)

Sample	SiO_2 (wt.%)	TiO_2 (wt.%)	Al_2O_3 (wt.%)	Fe_2O_3 (wt.%)	MnO (wt.%)	MgO (wt.%)	CaO (wt.%)	Na_2O (wt.%)	K_2O (wt.%)	P_2O_5 (wt.%)	LOI	Total
kk11	51.6	1.99	13.6	14.3	0.18	4.95	10	3.57	0.37	0.26	N.D	100.9
kk24	56.4	1.65	13.3	11.7	0.14	4.07	6.93	3.34	1.63	0.2	0.72	100.1
kk25	56	1.67	13.6	10.9	0.13	4.17	7.03	3.18	1.56	0.19	1.06	99.5
kk26	57.1	1.6	13	10.9	0.13	4.31	7.44	2.97	1.53	0.17	0.8	99.9
kk27	55.7	1.65	13.2	11.3	0.12	4.67	7.67	2.95	1.69	0.19	0.58	99.7
kk28	56.8	1.6	13.2	10.9	0.15	4.3	7.16	2.69	1.85	0.16	1.27	100.1
kk31	57.9	1.48	12.7	9.6	0.2	4.77	7.68	2.22	2.2	0.14	0.89	100.5
kk32	56.8	1.59	12.8	11.6	0.15	4.34	6.79	3.86	1.73	0.18	0.63	98.1
kk33	55.6	1.41	11	11.1	0.23	5.43	8.96	2.41	1.15	0.14	0.53	99.7

Table G.2: Low Ti and high Mg Dullstroom Formation rocks major element determined by XRF and INAA (Instrumental Neutron Activation Analysis) (Buchanan *et al*., 1999)

Sample	SiO_2 (wt.%)	TiO_2 (wt.%)	Al_2O_3 (wt.%)	Fe_2O_3 (wt.%)	MnO (wt.%)	MgO (wt.%)	CaO (wt.%)	Na_2O (wt.%)	K_2O (wt.%)	P_2O_5 (wt.%)	LOI	Total
kk10	53.8	0.73	15.2	11	0.2	5.15	9.15	2.8	0.94	0.14	0.56	99.7
kk12-1	55.4	0.62	15.2	10.1	0.16	5.48	8.63	2.16	1.16	0.12	0.46	99.5
kk12-2	54.5	0.62	14.7	9.86	0.17	5.75	8.83	2.2	1.25	0.1	1.27	99.2
kk12-3	55.7	0.63	15	9.77	0.15	5.55	8.72	2.42	1.13	0.11	0.56	99.7
kk13	53.1	0.33	17.4	8.25	0.15	6.03	11.6	2.9	0.49	0.03	N.D	100.3
kk14	54.9	0.63	14.9	10.5	0.18	5.72	8.81	2.42	1.24	0.1	1.16	100.5
kk15	56.3	0.48	16.3	8.62	0.13	5.12	9.21	2.62	1.21	0.08	N.D	100
kk16	54.3	0.48	15.2	10.5	0.18	6.86	9.23	2.64	0.91	0.06	N.D	100.4
kk17	54.8	0.52	15.8	9.01	0.16	6.58	9.9	2.44	0.92	0.02	N.D	100.1
kk18	52.2	0.41	15.8	9.06	0.18	6.94	10.8	2.39	0.76	0.05	N.D	98.5
kk29	56.4	0.71	14.6	8.53	0.14	5.44	8.01	2.58	1.31	0.14	1.45	99.3
kk30	57	0.69	14.4	8.63	0.13	5.3	7.17	3.23	1.34	0.12	1.76	99.8
kk22	68.5	0.47	12.4	5.73	0.05	1.54	4.03	2.1	3.15	0.12	1.36	99.4
kk23	63.9	0.62	13.6	7.53	0.11	2.62	5.47	2.99	2.01	0.16	0.74	99.7
kk34	61.1	0.68	14.6	8.3	0.12	2.85	6.43	3.53	1.38	0.13	0.91	100

Appendix H: Low and High Ti Dullstroom Formation rocks trace element data from literature (Buchanan *et al*., 1999)

Table H.1: High Ti Dullstroom Formation rocks trace element compositions determined by XRF and INAA (Instrumental Neutron Activation Analysis) (Buchanan *et al*., 1999)

Sample	**kk11**	**kk24**	**kk25**	**kk26**	**kk27**	**kk28**	**kk31**	**kk32**	**kk33**
Sc (ppm)	30.1	22.8	23.1	24.7	25.2	23.9	17.6	21.2	21.4
V (ppm)	304	217	216	211	221	212	209	152	224
Cr (ppm)	92.8	71	76.3	129	121	97.5	136	109	386
Co (ppm)	34.5	31.4	29.7	30.3	32.7	32.1	39.4	45.9	44.1
Ni (ppm)	88	64	71	81	73	78	96	85	151
Cu (ppm)	30	127	83	125	154	169	40	228	18
Zn (ppm)	70	100	98.5	124	117	120	88.5	125	116
Rb (ppm)	7.3	81.3	53	79.5	61.2	83.8	94.8	71.7	34.4
Sr (ppm)	429	400	417	422	446	383	370	376	334
Y (ppm)	29	27	33	31	28	39	34	27	25
Zr (ppm)	221	201	206	201	198	193	174	220	156
Nb (ppm)	14	15	16	15	15	15	14	19	12
Cs (ppm)	0.24	2.01	0.95	1.68	1.19	2.81	2.13	1.39	1.14
Ba (ppm)	146	300	294	213	324	423	454	342	365
La (ppm)	22.2	28.9	33.1	33.5	28.9	34.6	28.2	32.2	24.2
Ce (ppm)	47.5	59.9	60.8	63.2	59.9	58.8	57.3	63.9	48.5
Nd (ppm)	27.9	32.2	34.9	37.6	35.8	38.2	30.9	34	26.4
Sm (ppm)	6.43	6.65	7.45	7.52	7.01	7.95	7.02	6.95	6.22
Eu (ppm)	1.78	1.68	1.96	1.87	1.79	2.26	1.89	2.27	1.81
Gd (ppm)	7.6	6.46	7.05	6.42	6.2	8.26	7.63	6.09	6.16
Tb (ppm)	1.14	0.99	1.08	0.92	0.84	1.24	1.11	1.04	0.79
Tm (ppm)	0.51	0.45	0.52	0.41	0.38	0.48	0.41	0.46	0.42
Yb (ppm)	3.22	2.65	2.77	2.56	2.36	3.32	2.59	2.7	2.53
Lu (ppm)	0.49	0.43	0.38	0.33	0.37	0.41	0.33	0.38	0.31
Hf (ppm)	5.55	4.88	4.56	4.91	5.05	4.97	3.37	5.03	3.75
Ta (ppm)	0.61	0.61	0.75	0.62	0.73	0.68	0.84	0.91	0.79
Th (ppm)	0.77	5.94	5.97	5.96	6.62	5.75	5.62	5.99	4.68
U (ppm)	0.15	0.91	1.27	1.34	1.44	1.57	1.09	1.32	1.32

Table H.2: Low Ti and high Mg Dullstroom Formation rocks trace element determined by XRF and INAA (Instrumental Neutron Activation Analysis) (Buchanan *et al*., 1999)

Sample	kk10	kk12-1	kk12-2	kk12-3	kk13	kk14	kk15	kk16	kk17	kk18	kk29	kk30	kk22	kk23	kk34
Sc (ppm)	38.6	28.9	34.6	34.3	34.5	37.9	29.9	31.6	31.8	32.9	52.1	23.1	14.1	22.5	N.D
V (ppm)	216	200	199	194	140	220	168	198	165	153	192	188	79	129	147
Cr (ppm)	114	114	113	118	47.4	140	69.3	33.3	80.6	125	222	226	199	138	155
Co (ppm)	30.5	44.9	31.6	32.6	48.1	32.6	30.1	54.7	33.7	35.4	33.4	33.5	19.1	18.6	24
Ni (ppm)	71	93	93	93	102	80	93	113	120	133	93	94	16	28	47
Cu (ppm)	25	54	60	28	45	33	50	46	65	68	64	61	56	21	20
Zn (ppm)	111	116	127	101	74.6	82.5	87.5	91.2	88.5	77.5	88	109	91.5	93	115
Rb (ppm)	23.8	45.4	49.2	26.5	15.2	25	29.3	28.8	22.2	18.2	50.4	64.8	128	27.8	58
Sr (ppm)	304	275	232	261	254	276	224	211	228	240	254	240	218	230	297
Y (ppm)	17	16	16	17	8	16	15	13	12	10	22	20	24	23	24
Zr (ppm)	127	103	104	115	42	101	85	75	70	47	120	131	183	180	165
Nb (ppm)	8	13	7	8	10	7	7	11	7	6	8	9	11	10	15
Cs (ppm)	0.63	1.99	1.86	2.07	0.65	1.17	0.46	0.85	0.81	0.52	1.68	1.31	1.02	1.72	N.D
Ba (ppm)	338	382	406	355	156	430	225	236	288	243	422	351	752	523	280
La (ppm)	20.8	18	21.1	10.4	8.73	18.3	16.4	14	15.2	12.2	20.4	21.3	38.9	34.7	N.D
Ce (ppm)	39.7	38.6	41.1	37.4	17.3	36.4	31.9	27.7	27.5	22.6	36.7	37.7	79.3	67.1	N.D
Nd (ppm)	17.5	20.5	19.7	18.5	7.34	19.5	16.9	12.3	13.1	12.2	18.8	20.2	38.3	30.1	N.D
Sm (ppm)	3.78	3.33	3.73	3.69	1.99	3.41	2.92	2.54	2.58	2.24	4.01	4.23	6.21	4.92	N.D
Eu (ppm)	1.11	1.02	0.99	0.91	0.83	0.99	0.79	0.97	0.76	0.72	0.92	1.09	1.06	1.02	N.D
Gd (ppm)	3.7	3.05	4.15	3.62	2.38	3.4	3.3	2.42	2.6	2.7	4.41	4.25	3.87	3.57	N.D
Tb (ppm)	0.59	0.57	0.72	0.55	0.41	0.51	0.49	0.44	0.39	0.41	0.64	0.61	0.65	0.57	N.D
Tm (ppm)	0.26	0.29	0.28	0.24	0.22	0.28	0.22	0.24	0.21	0.22	0.32	0.34	0.34	0.35	N.D
Yb (ppm)	1.92	1.86	1.87	1.63	1.37	1.73	1.53	1.77	1.31	1.43	2.02	2.16	2.26	2.36	N.D
Lu (ppm)	0.27	0.29	0.24	0.22	0.21	0.2	0.24	0.27	0.22	0.19	0.26	0.27	0.31	0.33	N.D
Hf (ppm)	3.02	2.68	2.66	2.77	0.99	2.32	2.19	2.08	2.12	1.51	2.69	2.78	5.04	4.32	N.D
Ta (ppm)	0.23	0.27	0.23	0.29	0.34	0.35	0.39	0.24	0.32	0.18	0.25	0.41	0.51	0.41	N.D
Th (ppm)	3.02	3.71	4.37	4.07	1.81	3.04	3.04	3.84	4.01	2.96	4.83	4.91	11.2	9.86	N.D
U (ppm)	0.89	0.57	0.82	0.75	0.37	0.44	0.44	0.53	0.67	0.51	0.87	0.95	2.58	1.86	N.D